13:54:46 OCA PAD AMENDMENT - PROJECT HEADER INFORMATION 02/20/92

Active

Project #: E-25-M79 Cost share #: E-25-354 Rev #: 7
Center # : R6728-0A0 Center shr #: 10/22-1-F6728-0A0 OCA file #:
Work type : RES
Contract#: N00014-89-J-1839 Mod #: P00004 Document : GRANT
Prime #: Contract entity: GTRC

Subprojects ? : N CFDA: 12.AAA
Main project #: PE #:

Project unit: MECH ENGR Unit code: 02.010.126
Project director(s):
ZHOU J-X MECH ENGR (404)894-6793
ZHOU J MECH ENGR (404)-

Sponsor/division names: NAVY / OFC OF NAVAL RESEARCH
Sponsor/division codes: 103 / 025

Award period: 890415 to 920930 (performance) 920930 (reports)

Sponsor amount	New this change	Total to date
Contract value	0.00	419,069.00
Funded	40,000.00	419,069.00
Cost sharing amount		60,443.00

Does subcontracting plan apply ?: N

Title: EFFECT OF SOLITARY WAVES ON LOW-FREQUENCY ACOUSTIC PROPAGATION SHALLOW WATER

PROJECT ADMINISTRATION DATA

OCA contact: E. Faith Gleason 894-4820

Sponsor technical contact

DR. MARSHALL ORR, CODE 1125
(202)696-6994

OFFICE OF NAVAL RESEARCH
800 NORTH QUINCY STREET
ARLINGTON, VA 22217-5000

Sponsor issuing office

GLYNIS M. FISHER
(202)696-4508

OFFICE OF NAVAL RESEARCH
800 NORTH QUINCY STREET
ARLINGTON, VA 22217-5000

Security class (U,C,S,TS) : U ONR resident rep. is ACO (Y/N): Y
Defense priority rating : N/A ONR supplemental sheet
Equipment title vests with: Sponsor GIT X

Administrative comments -
MODIFICATION NO. P00004 PROVIDES FINAL INCREMENT OF $40,000.
NOTE: PROJECT DIRECTOR IS CHANGED FROM PETER ROGERS TO JI-XUN ZHOU.

GEORGIA INSTITUTE OF TECHNOLOGY
OFFICE OF CONTRACT ADMINISTRATION

NOTICE OF PROJECT CLOSEOUT

Closeout Notice Date 12/17/92

Project No. E-25-M79 Center No. R6728-0A0

Project Director ZHOU J-X School/Lab MECH ENGR

Sponsor NAVY/OFC OF NAVAL RESEARCH

Contract/Grant No. N00014-89-J-1839 Contract Entity GTRC

Prime Contract No.

Title EFFECT OF SOLITARY WAVES ON LOW-FREQUENCY ACOUSTIC PROPAGATION SHALLOW WA

Effective Completion Date 920930 (Performance) 920930 (Reports)

Closeout Actions Required:	Y/N	Date Submitted
Final Invoice or Copy of Final Invoice	Y	
Final Report of Inventions and/or Subcontracts	Y	
Government Property Inventory & Related Certificate	N	
Classified Material Certificate	N	
Release and Assignment	Y	
Other	N	

CommentsEFFECTIVE DATE 4-15-89. CONTRACT VALUE $419,069.

Subproject Under Main Project No.

Continues Project No.

Distribution Required:

Project Director	Y
Administrative Network Representative	Y
GTRI Accounting/Grants and Contracts	Y
Procurement/Supply Services	Y
Research Property Managment	Y
Research Security Services	N
Reports Coordinator (OCA)	Y
GTRC	Y
Project File	Y
Other HARRY VANN-FMD	Y
FRED CAIN-OOD	Y

NOTE: Final Patent Questionnaire sent to PDPI.

E-25-M79

TITLE : Effect of Solitary Waves on Low-frequency Acoustic Propagation in Shallow Water

INVESTIGATORS : J. X. Zhou, P. H. Rogers and X. Z. Zhang
School of Mechanical Engineering
Georgia Institute of Technology
Atlanta, Georgia 30332–0405
(404)894–6793 or (404)894–3235

OBJECTIVE : To investigate the interaction between internal wave solitons and low-frequency acoustic waves in the coastal zone as a possible explanation to the anomalous, anisotropic and time-varying frequency response of shallow-water sound propagation which is often observed in the Summer.

BACKGROUND : **1.** Internal solitary waves have been frequently observed in many coastal areas such as the Massachusetts Bay, the New York Bight and the Gulf of California, using shipboard echo-sounding, thermistor chains, XBT profiling and SAR images from satellite. They are different from open sea internal waves which are best described as a stochastic phenomenon with a 8wide band frequency-wave number spectrum. They typically have deterministic packets with well-defined wavelength, are highly correlated with local tides, and propagate shoreward with strong surface expression. Solitons obey the Korteweg-de Vries(**KdV**) equation and have $sech^2$ shape. Little attention, however, in the acoustic community has been focused on their effect on sound propagation with the exception of the work of Baxter and Orr which was based on ray theory and calculated the influence of an oceanic internal wave packet on short-range (high-frequency) sound propagation. We were interested in determining what influence of such internal wave packets have on low-frequency sound propagation. **2.** Experiments, conducted by Zhou and his group over a four year period in August at the same area(with flat seabed), have shown that the frequency response of shallow water sound propagation in the Summer is a strong function of time and propagation direction, and sometime exhibits an abnormally large attenuation over some frequency range. These results can not be explained by using a conventional model of sound propagation(with bottom acoustic parameters and an average sound-speed profile of water column). For example, the curves in Fig.1 show averaged explosive signal power spectra as a function of frequency at 0.5km and 28 km from the source(water depth is about 37m). The difference between two curves is a measure of the sound transmission loss, i.e, the frequency response of sound propagation. Between 300 Hz and 1200 Hz, especially around 600 Hz, an abnormally large attenuation was found. Along

the same track and for similar average sound-speed profile in August, the frequency response including the abnormal attenuation frequency range are very different for different years. Fig.2 shows that the frequency response is a strong function of the propagation direction. Keeping the transmission distance constant (R=28km), the frequency response for seven different transmission direction(tracks) are so different that for some frequencies the sound intensity varied as much as more 25 dB!(But sometimes, almost identical frequency responses were obtained for different tracks.) Why does this strange phenomena happen only in the Summer when there is a strong thermocline? We hypothesize these results are caused by the influence of internal wave packets.

APPROACH : Review the characteristics of internal solitary waves in the coastal zone, and numerically calculate the effect of the internal wave packets with different parameters on long-range sound propagation using Parabolic Equation (**PE**) method (with **IFD** code).

RESULTS : For simplicity we follow Lee's model and assume the internal wave packets on the thermocline is expressed by a gated sine function as shown in Fig.3. We call λ_i the soliton wavelength, and $\mathbf{L}_p$ the packet length. We assume first there is only one internal wave packet, consisting of six solitons located at 15 km. Numerical results show that the transmission loss is very sensitive to the signal frequency and the internal wave packets parameters: **1.** For a given frequency and packet length, the transmission loss has a 'resonance-like' attenuation at some soliton wavelength (Fig.4). **2.** For a given frequency and soliton wavelength, the transmission loss is a 'resonance-like' function of the packet length(Fig.5). **3.** The frequency response of sound propagation and the abnormal attenuation frequency range are a sensitive function of the parameters of the solitons and wave packets. If three packets are put along the propagation track, each packet consisting of 6 solitons with a wavelength of 235 m, we obtain the frequency response as indicated by the circles in Fig.1 which fit the experimental data quit well. Due to the characteristics of internal solitons in the coastal zone(packets with well-defined wavelength, high tide correlation , shoreward-moving etc.), the projection of the solitons in the sound propagation direction at different times will be different. This explains, possibly, why the experimental frequency response is a strong function of the propagation direction and time, and why the abnormal attenuation frequency itself varies in time during the Summer. As an inverse problem, low-frequency acoustic measurements could be a potential tool for remote-sensing of internal wave packet activity in the coastal zone.

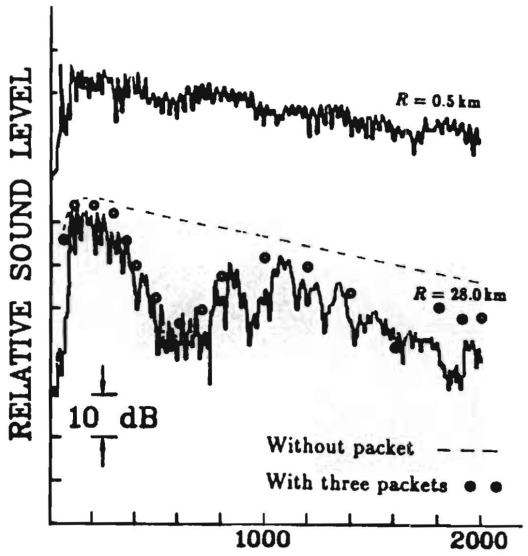

Fig. 1

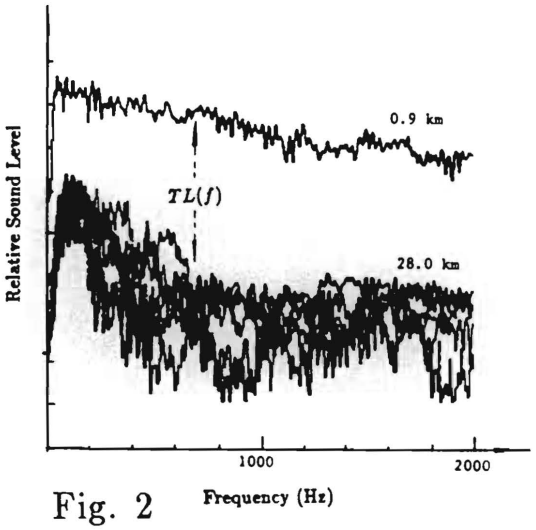

Fig. 2

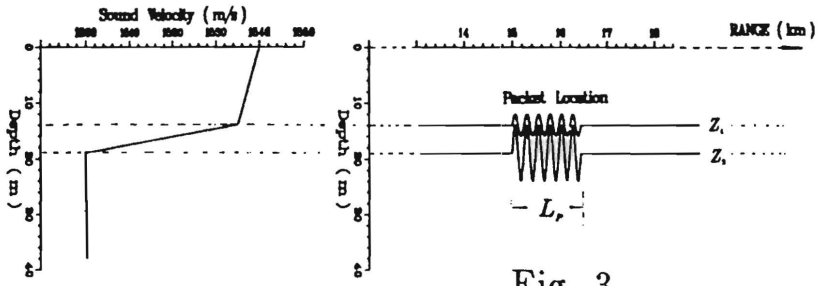

Fig. 3

For a packet: $15\,\text{km} + L_p \geq R \geq 15\text{km}$

$$Z_1 = 14.0 - 2.0 * \sin\left(\frac{2\pi R}{\lambda_i}\right)$$

$$Z_2 = 19.0 - 5.0 * \sin\left(\frac{2\pi R}{\lambda_i}\right)$$

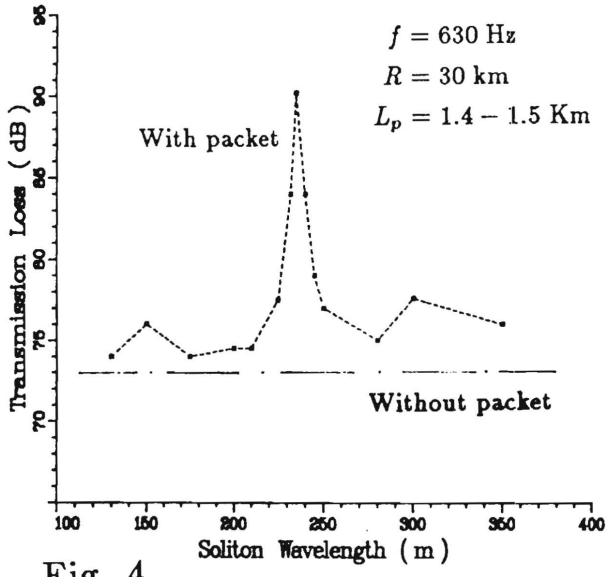

Fig. 4

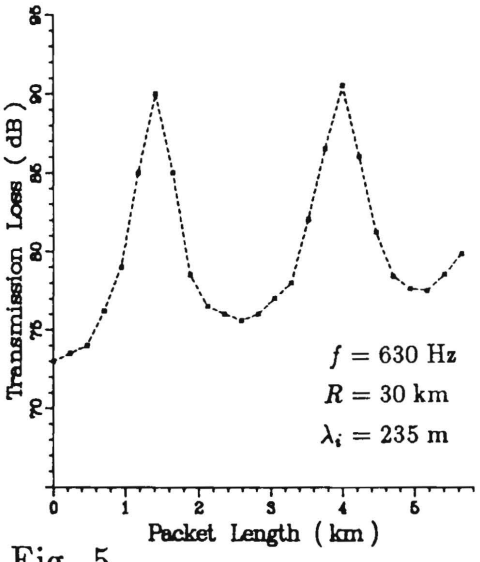

Fig. 5

E-25-M79

TITLE : Resonant Interaction of Sound Wave with Internal Solitons in the Coastal Zone

INVESTIGATORS : J. X. Zhou and P. H. Rogers
School of Mechanical Engineering
Georgia Institute of Technology
Atlanta, Georgia 30332–0405

OBJECTIVE : To investigate the interaction between internal wave solitons and low– frequency acoustic waves in the coastal zone.

BACKGROUND : Last year's research has shown that internal wave packets have a strong influence on low–frequency long–range sound propagation in the coastal zone, and the interaction between sound waves and internal solitons could offer an explanation for the measured frequency response of sound propagation in the Summer which is often a strong function of time and propagation direction, and sometimes exhibits an abnormally large attenuation over some frequency range. Specifics of the mechanism of interaction on **frequency resonance, soliton wavelength resonance and packet length resonance** still require explanation.

APPROACH : For a given model of oceanic internal solitons, we use normal–mode and PE computer programs to calculate the influence of internal solitons on shallow–water sound propagation. The acoustic field obtained from the PE code is decomposed into normal modes (a numerical spatial filtering technique), to analyze the characteristics of acoustic mode–coupling induced by the internal wave packets.

RESULTS : **1.** The numerical calculations have shown that the acoustic mode–coupling, caused by internal wave packets, are an important loss mechanism for shallow water sound transmission in the Summer. Due to the interaction of sound with the internal wave packets, in some cases a significant amount of energy is transferred from lower–order modes into higher–order modes that attenuate rapidly, and causes abnormally large transmission loss over some frequency range. **2.** The characteristic frequency, soliton wavelength and packet length resonances, exhibited in the interaction between sound waves and internal solitons, could also be explained by acoustic mode–coupling. For example, a single packet is located at a distance of 15 km. For a given frequency (630 Hz) and packet length (about 1.4–1.5 km), the transmission (of point source) at 30 km is a resonance–like function of soliton wavelength shown in Fig. a. Taking the first normal mode as the input field to the PE code, we obtained the depth distribution functions for 15, 20 and 30 km shown in Figs. b–d. After interaction with the packet, at the resonance soliton wavelength of 235 m, the shape is very different from the first mode and the amplitude becomes

much smaller, but for the wavelength of 200 m or 280 m, the shapes are still very close to that of mode 1. At a distance of 18 km we decompose the PE field into normal modes, and get the relative amplitudes of the exciting function for different modes shown in Figs. e–g. For the wavelength of 235 m, a significant amount of energy has been transferred from mode 1 into higher–modes, especially modes 3 and 4 (which have a much larger attenuation rate). For the wavelength of 200 m or 280 m, only a few percent of the *wave energy* is coupled into higher-order modes. For the case of frequency or packet length resonances similar results have been obtained.

3. The numerical results have shown that the principal transfer of energy caused by the interaction with internal wave packets occurs between modes whose eigenvalue difference equals the wavenumber of the spectrum peak of internal wave packets.

4. The results suggest that low–frequency acoustic measurements could be used for remote monitoring of internal wave activity and for extracting hydrological and meteorological characteristics of the water mass in the coastal zone. A joint at–sea experiment with oceanography community would be desirable.

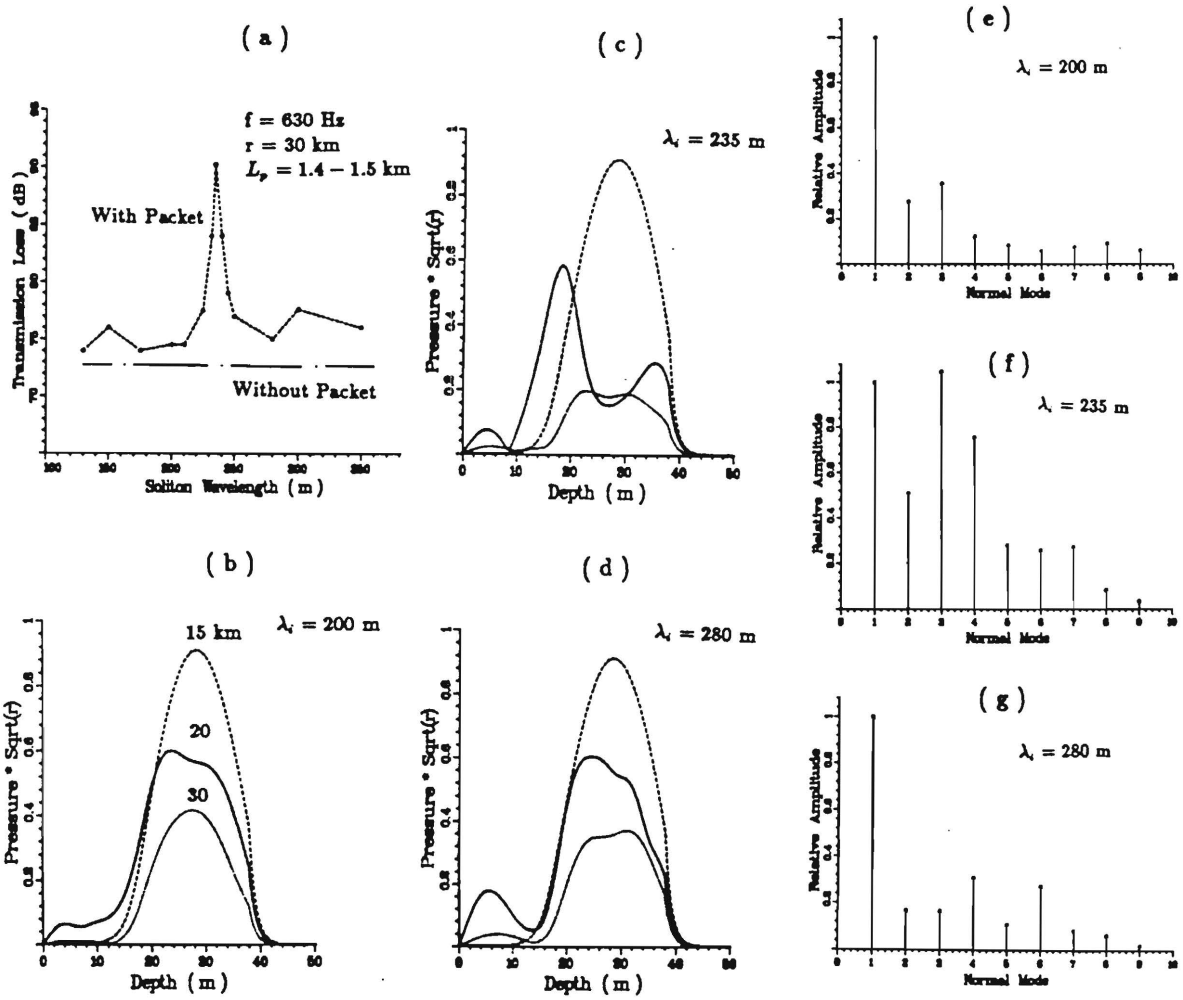

E-25-1111

Nonreciprocity of Long–range Reverberation in Wedged Continental Shelf

J. X. Zhou, X. Z. Zhang and P. H. Rogers

(School of Mechanical Engineering, Georgia Tech)

D. H. Guan

(Institute of Acoustics, Academia Sinica)

Today we would like to discuss some problems involving Long–range reverberation in shallow water.

Fig. 1

The title of the talk is "Nonreciprocity of Long–range Reverberation in Wedged Continental Shelf". The talk is divided into four parts. First we would like to talk a little bit about the background of current research on long–range reverberation in shallow water. The problem seems to fall into a "dilemma"(endless loop) with no way out. Second, we introduced an averaged angular power spectrum method for long–range reverberation in the Pekeris model to show how we could bypass such 'dilemma'. Based on a resulted transformation relation between arbitrary angle dependence of bottom scattering and the range dependence of reverberation in shallow water, some experimental data on bottom scattering at small grazing angles and low frequencies will be given in the third part. In the last part, using the WKB approximation to the adiabatic normal mode theory, we extend the problem into wedged homogeneous shallow water. The result shows that the monostatic reverberation intensities, obtained at two terminals with different depths, would not be reciprocal. Because of time limitations, the results are presented, rather than developed.

I. The status of current research on long–range reverberation in shallow water

Fig.2

Generally speaking, the 'long–range' means low–frequency, and the range is more than several hundred times of water depth. Here are two typical long–range reverberation decay curves for two frequencies(1000Hz, 1600Hz; 1/3 OCT), obtained from a shallow water with the depth of 29m using a explosive source. The ordinate is the relative reverberation level; The abscissa is the range–depth ratio. If a water depth is 100m, the ratio value of 400 corresponds that the reverberation signal comes from 40 km far away.. These reverberation curves(see Fig.1) were obtained in a Pekeris shallow water , i.e., the simplest shallow water model.

Fig.3

In the Pekeris model, the effect grazing angle of sound propagation can be expressed as Eq.(1), where Q is the bottom reflection-loss parameter at small grazing angle, defined as

$$-ln|V(\theta)| = Q\theta$$

Here are some Zhou's experimental results(from vertical coherence measurements of sound propagation), compared with Zhou and Smith theory. The results show that at long–range, the grazing angles of sound interacting with bottom are very small. For example, at a distance of 400 times of water, the main energy come from angles that are less 2.4° for 800Hz, less than 2° for 1600 Hz. Due to mode stripping, the farther the distance, the smaller the grazing angles of the effective sound propagation. What

about the bottom scattering at such small grazing angles and low frequencies?

Fig.4

The upper curves of Fig.4 is a copied from Urick's book. At small grazing angles , no data. The following is quoted from the proceedings of 1983 Shallow Water Acoustics Workshop:

"Grazing angles of primary importance to shallow water applications range from about 30° **to near** 0° **with the smaller angles being more important**..... To date, NOVOCEANO has not been able to report either bottom reflectivity or bottom backscattering values for any shallow water area."

Nine years have past, as we know, still no any progress in this area. The multipath in shallow water and the unclear mechanisms of bottom scattering at low frequency make the computation of long–range reverberation very complex. The theoretical acousticians have no adequate and reliable data base for bottom scattering to develop a practical theoretical model. Experimental acousticians say we have no suitable theoretical reverberation formula to use for measuring bottom scattering strength at small grazing angle. (Because the significant difficulty is that if the assumption used in extracting the scattering coefficients from the received reverberation has no enough data as a base, the resulting coefficients will not represent valid environmental parameters which should be independent of how the data were obtained and analyzed.) Thus the problem of long–range reverberation in shallow water seems to fall into an endless loop with no way out.

Some groups are working on developing theoretical model of bottom scattering at low frequency, and trying to get its angular and frequency dependence. A pressing problem is that how to judge the validity of their theoretical results at low frequency

and low grazing angle.(Currently available data are limited to high frequencies or larger grazing angles.)

Next we would like briefly to introduce a averaged angular power spectrum method for shallow water long–range reverberation, and to give some data on bottom scattering at small grazing angles and low frequencies.

II. An averaged angular power spectrum method for long–range reverberation

---

Fig. 5

For a point source in shallow water, applying the WKB approximation to the normal mode expression(Brekhovskih,Zhou), or using the ray method(Smith) or the flux method(Weston) the averaged sound field intensity can be expressed as Eq.(2)

where $\theta(z_0)$ and $\theta(z)$ are the equivalent ray angle of normal mode at the source depth or receiver depth, S is mode cycle distance. $ln|V(\theta)|$ is the bottom reflection–loss.

We call I_{aps} the angular power spectrum. Except the cylindrical spreading and the medium absorption, the sound velocity profile and the boundary condition together compose a angular filter of shallow water sound propagation. The angular expression of sound propagation can naturally be connected with the classical expression of bottom scattering in the angular domain. For a given signal duration, there are a lot of scattering signal simultaneously return to a receiver. The bottom scattering looks like a stochastic filter. The reverberation can be treated as a angle–weighted process. The net analog of shallow water reverberation can be expressed as Eq. (3). The forward transmission net, bottom scattering net plus backward transmission net.

Where the $M(\theta, \phi)$ is the bottom scattering coefficient for plane wave. θ is the

grazing angle of incident mode–ray, and ϕ is the scattering angle. A is a scattering area. The validity of a theoretical result from this expression will depend on the validity of scattering coefficient $M(\theta, \phi)$. Unfortunately as above–mentioned, at low frequencies and low grazing angles there is no data or general expression about the $M(\theta, \phi)$. It would be very complex function of bottom surface roughness, sediment type, sediment inhomogeneity, angle, frequency and so on. It still seems no way out.

Here we use a little trick to bypass the "endless loop".

Fig.6

Here is an arbitrary angle dependence of bottom scattering, ignoring the concrete analytical expression, i.e., no matter what is the main mechanism of bottom scattering, surface roughness, volume inhomogeneity or whatever. General speaking, The scattering coefficient $M(\theta, \phi)$ is a slowly changed function. The smaller the angle θ or ϕ, the smaller the scattering strength. If we consider backward scattering is reciprocal, i.e., $M(\theta, \phi) = M(\phi, \theta)$, then at small grazing angles **any scattering function** can always be expressed as Eqs.(4–5).

We introduce this phenomenological expression only as a **"bridge"** between long–range reverberation and bottom scattering, ignoring the concrete analytical expression. Next we will see that it is this little trick to help us to bypass the above–mentioned "endless loop".

Fig.7

In the Pekeris model the angular power spectrum is expressed by Eq.(6).

From Eqs.(3–6), we get an expression for long–range reverberation as Eqs.(7–8).

(The reverberation time $t_i = \frac{2r_i}{c}$, c–sound velocity.)

The result shows that the characteristics of long–range reverberation between distance r_{i-1} and r_i mainly depend on the bottom scattering indices μ_i, n_i in the region between θ_{i-1} and θ_i. The transformation between the range dependence of reverberation level RL and the angle dependence of bottom backscattering strength is shown in Fig.7.

From this transformation relation the scattering indices μ_i and n_i can be derived from two data on the experimental curve of reverberation level near r_i. Then we obtain the bottom backscattering strength at the angle θ_i (see Eq.(1)).

III. The reverberation–derived bottom scattering strength at small grazing angels.

Fig. 8

The bottom scattering strength for frequency band of $800Hz$–$4kHz$ and grazing angles of 2°–8° , shown here, is derived from at–sea experimental reverberation data.

For the reliability of results only those experimental long-range reverberation data were used for extracting bottom scattering that were about 9 dB higher than the environmental noise. (For comparison, the bottom scattering at larger angles obtained by other researchers from deep water measurements is included with dote or dashed lines.)

Fig. 9

Here(Fig. 9) is the bottom scattering strength derived from another reverberation

experiment.

Fig. 10

Russian acousticians Ivakin and Lysanov compared their theoretical bottom scattering model with our experimental data(Fig. 10), the discrepancy does not exceed 3 dB at any of the investigated angles and frequencies. Our results have two specific features which are different from high frequency results: **bottom scattering has more strong frequency dependence, and decrease much more rapidly as the grazing angle is decreased.** At very small angles, the bottom scattering index could be larger than Lambert's law scattering i.e., $n > 2$.

IV. Long–range reverberation in wedged homogeneous continental shelf

Fig. 11

Next we extend the results of long–range reverberation to shallow water of variable depth. (we consider the case of propagation directly up or down slop from the source)

If the water depth and sound velocity profile vary extremely slowly with horizontal distance, by neglecting any coupling between normal modes, Pierce obtained a adiabatic normal mode expression for sound propagation as Eq.(9) (a cylindrical coordinate has been assumed):

where .....

The adiabatic mode theory means that the local modes adapt to local environment. So the grazing angle of equivalent ray of normal modes satisfies Eqs.(10–11).

For a wedged homogeneous continental shelf the water depth can be expressed by

Eq.(12).

Applying WKB approximation to the Pierce's expression, the averaged sound intensity in homogeneous wedged shallow water can be expressed as Eq.(13).

The averaged angular power spectrum in wedged water is expressed by Eq.(14).

Fig. 12

Using above–mentioned angular power spectrum method, we get a averaged sound intensity in the most interested three–half law field area as Eq.(15). The averaged reverberation intensity is expressed by Eq.(16).

The sound propagation is reciprocal if we exchange the positions of the source and receiver. But the monostatic reverberation intensities, obtained at two terminations with a depth of H_1 or H_2, would not be reciprocal (see Eq.(17)).

Here N is the angular index of bottom scattering defined as Eq.(18). If there are two identical active sonars, but the water depth of their locations is different, the reverberation interference to the sonar at shallower area would be much smaller. For example, if $H_1 = 50m$, $H_2 = 200m$, $N = 2$ (so–call the Lambert's law scattering), then the reverberation interference at shallower area would be 12 dB less.

At last year's Shallow Water Acoustic Workshop held at Woods Hole, a report from NUSC, New London mentioned that the reverberation in continental shelf is not reciprocal. The authors of this talk hope their theoretical result could be, in some degree, helpful to explain the NUSC at–sea experiments.

Thanks !

Nonreciprocity of Long-range Reverberation in a Wedged Continental Shelf

J. Z. Zhou, X. Z. Zhang, P. H. Rogers and D. H. Guan

1. **Background (The shallow water reverberation problem seems to fall into "an endless loop" with no way out.)**
2. **Averaged angular power spectrum method for long-range reverberation in shallow water.**
3. **Transformation relation $\longrightarrow$ Bottom scattering at small grazing angles, derived from experimental reverberation data.**
4. **The WKB approximation $\longrightarrow$ adiabatic mode theory. Reverberation in a wedged shallow water is not reciprocal.**

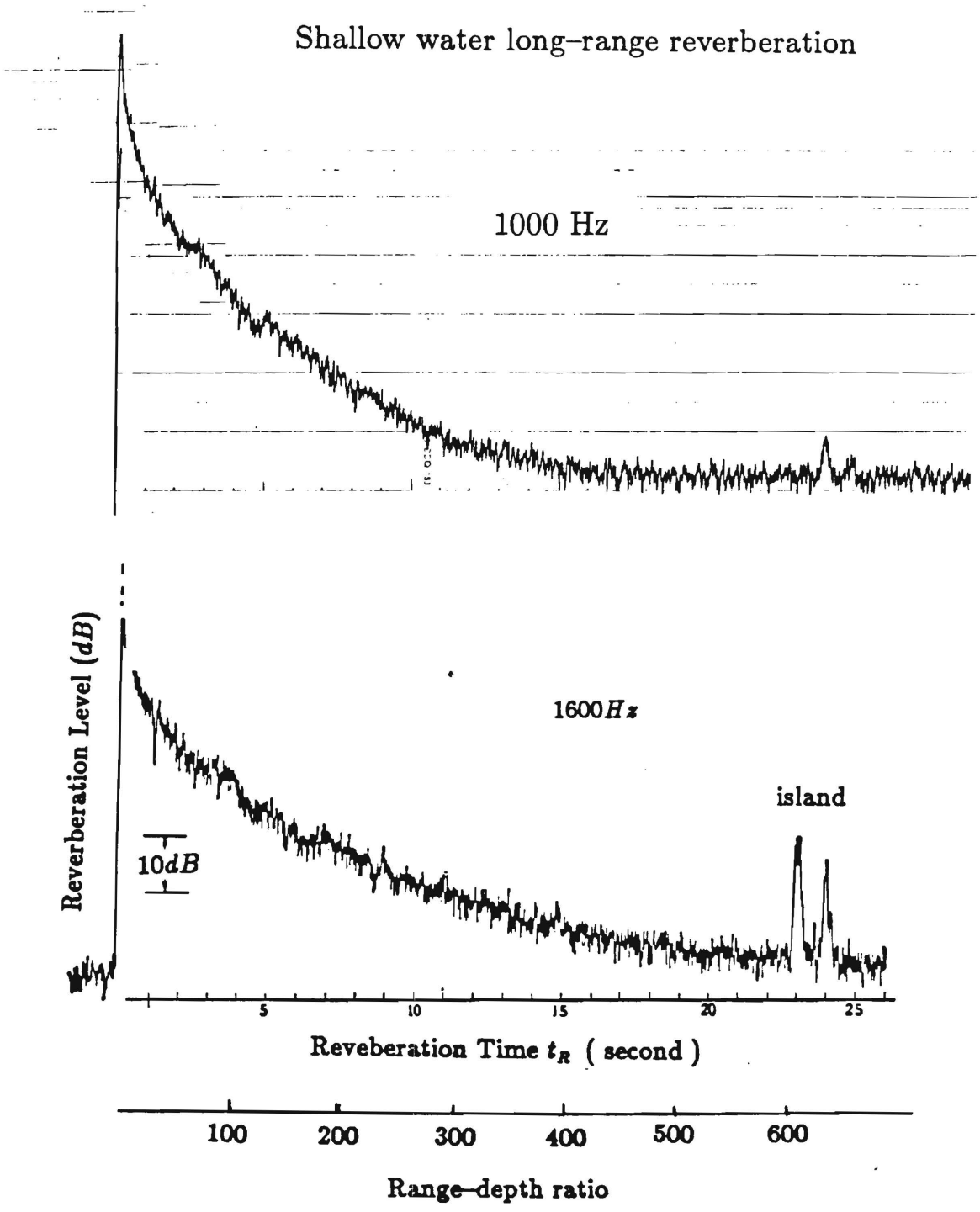
Shallow water long–range reverberation
1000 Hz
Reverberation Level (dB)
1600Hz
island
10dB
5
10
15
20
25
Reveberation Time t_R (second)
100
200
300
400
500
600
Range–depth ratio

$$\theta_{eff}(r) = \frac{1}{2}(\frac{\pi}{Q})^{1/2}(\frac{H}{r})^{1/2} \tag{1}$$

$$-ln|V(\theta)| = Q\theta$$

Q – the bottom reflection loss parameter at small grazing angle θ

The Vertical coherence of sound propagation in Pekeris model(**Smith, Zhou**)

$$\rho(r,d) = e^{-\frac{H}{4Qr}k^2d^2} = e^{-\frac{k^2d^2}{\pi}\theta^2_{\text{eff}}(r)}$$

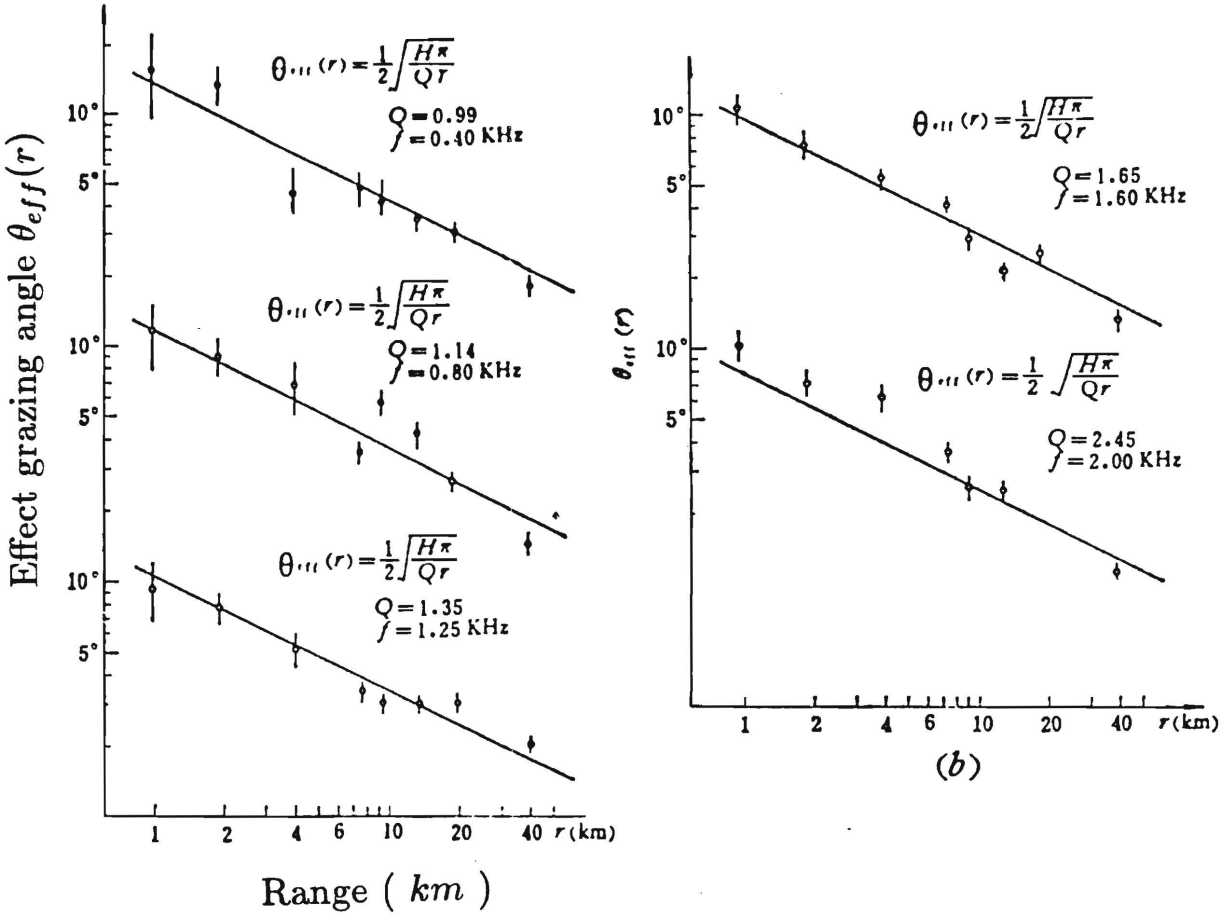

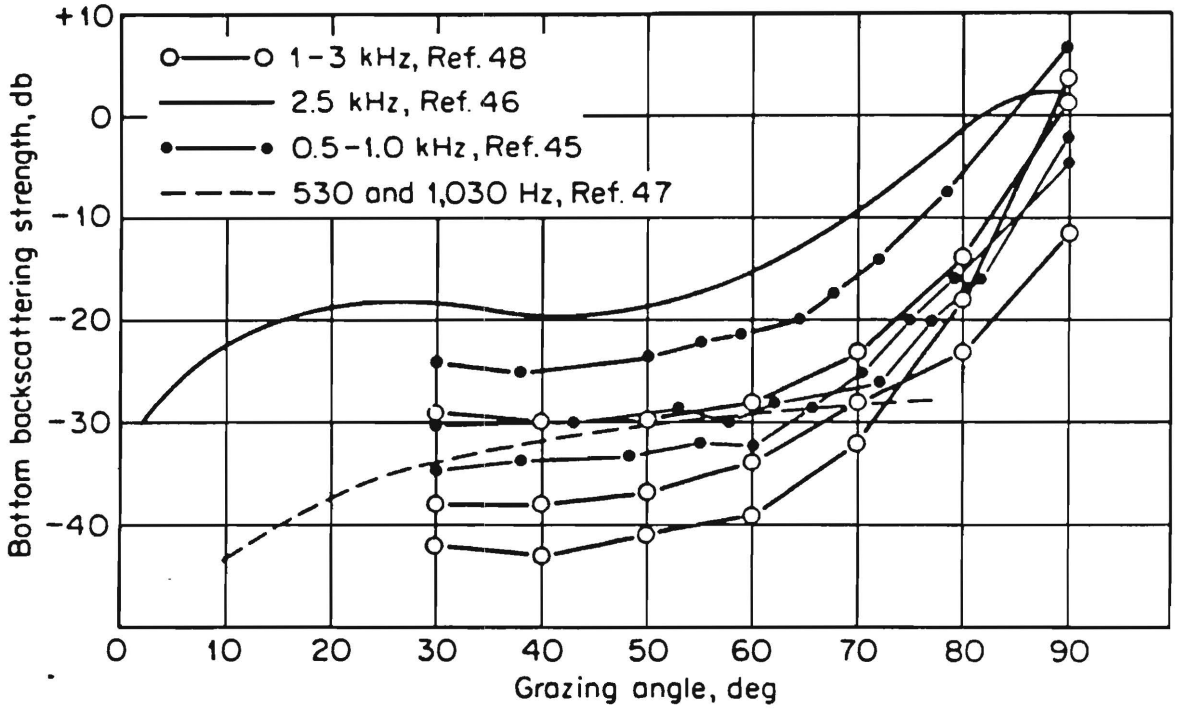

FIG. 8-22. Low-frequency deep-water bottom backscattering strength as reported in four sets of measurements.

Shallow Water Acoustics Workshops Proceedings (1983) :

"Grazing angles of primary importance to shallow water applications range from about 30° to near 0° with the smaller angles being more important..... To date, NOVOCEANO has not been able to report either bottom reflectivity or bottom backscattering values for any shallow water area. "

$$I(r,z;z_0) = \frac{2}{r}e^{-\alpha r}\int \frac{2e^{\frac{2\ln|V(\theta)|}{S}r}}{Stan\theta(z)}d\theta(z_0) = \frac{2e^{-\alpha r}}{Hr}\int I_{aps}(\theta,r,z;z_0)d\theta \quad (2)$$

$I_{aps}(\theta,r,z;z_0)$ – the angular power spectrum;

Boudary condition + sound velocity profile → a angular filter of sound propagation.

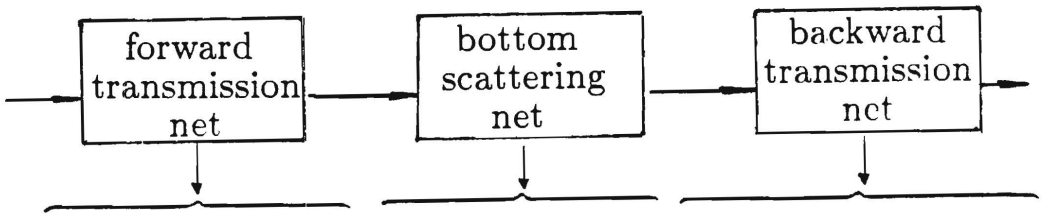

$$R(r.z;z_0) = \int\int \frac{e^{-\alpha r}}{Hr}I_{aps}(\theta.r,z') * A * M(\theta,\phi) * \frac{e^{-\alpha r}}{Hr}I_{aps}(\phi,r,z')d\theta d\phi \quad (3)$$

where the $M(\theta,\phi)$ is the scattering coefficient of plane wave from bottom.

$$M(\theta,\phi) = ?$$

It must be a very complex function of bottom surface roughness, sediment type, sediment inhomogeneity, angle, frequency and so on. Unknown ! No way out ?

Arbitrary angle dependence of equivalent bottom scattering:

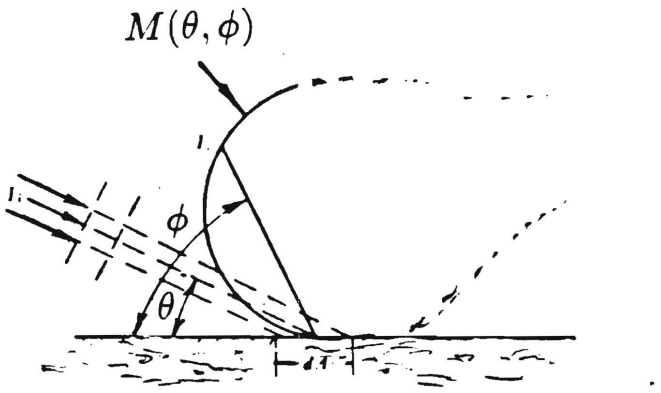

Reasonable assumptions at small grazing angles

1) Decreasing function of angle with decreasing grazing angle;

2) Reciprocal when incident angle and backward scattering angle exchange, i.e., $M(\theta,\phi) = M(\phi,\theta)$

$$M(\theta,\phi) = \left(\sum_i^N \sqrt{\mu_i}\Delta_i(\theta)\theta^{n_i}\right) * \left(\sum_i^N \sqrt{\mu_i}\Delta_i(\phi)\phi^{n_i}\right) \tag{4}$$

where

$$\Delta_i(x) = \begin{cases} 1, & \text{if } x \in [x_{i-1}, x_i]; \\ 0, & \text{otherwise.} \end{cases} \tag{5}$$

In the Pekeris model the angular power spectrum

$$I_{aps}(\theta, r) = e^{\frac{-Qr}{H}\theta^2} \tag{6}$$

From Eqs.(3–6), we get an expression for long–range reverberation as

$$R(r) = e^{-2\alpha r} \sum_{i}^{N} R_i * \Delta_i(r) \tag{7}$$

$$R_i(r) = \frac{\mu_i \pi c \tau}{(n_i + 1)^2} * \frac{1}{H^{(1-n_i)} Q^{(1+n_i)}} * \frac{1}{r^{(2+n_i)}} \tag{8}$$

Transformation relation between the range dependence of RL and the angular dependence of bottom scattering:

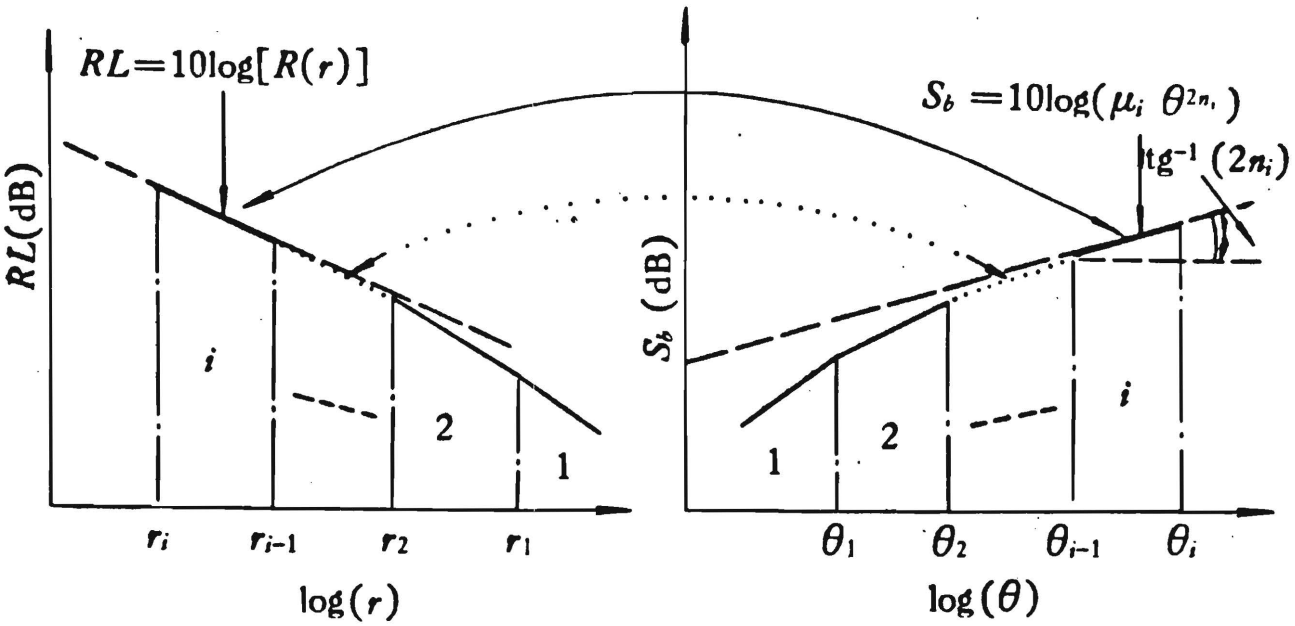

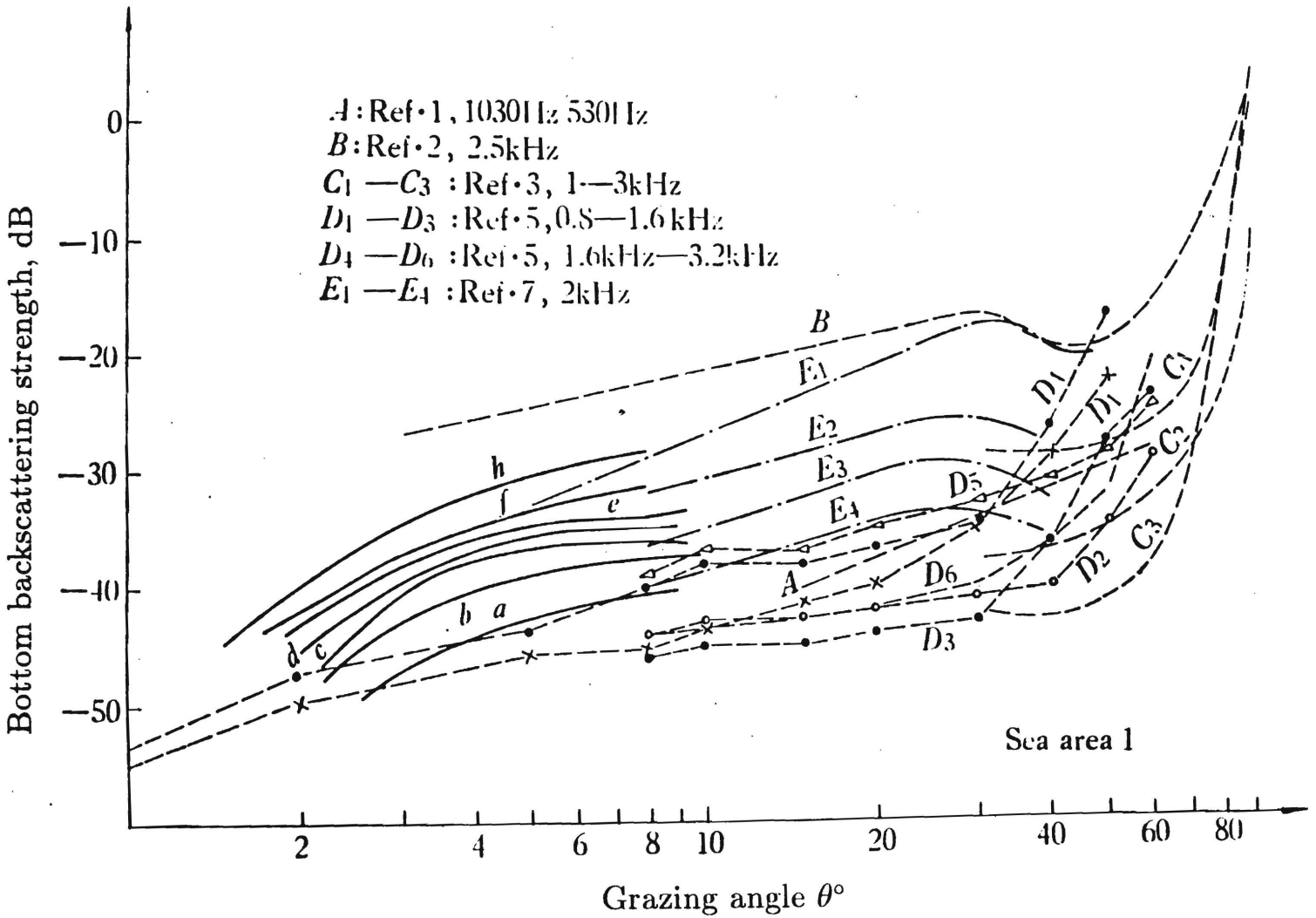
A: Ref·1, 1030Hz 530Hz
B: Ref·2, 2.5kHz
C1 —C3 : Ref·3, 1·—3kHz
D1 —D3 : Ref·5, 0.8—1.6kHz
D4 —D6 : Ref·5, 1.6kHz—3.2kHz
E1 —E4 : Ref·7, 2kHz
Bottom backscattering strength, dB
0
−10
−20
−30
−40
−50
2
4
6
8
10
20
40
60
80
Grazing angle θ°
Sea area 1

8

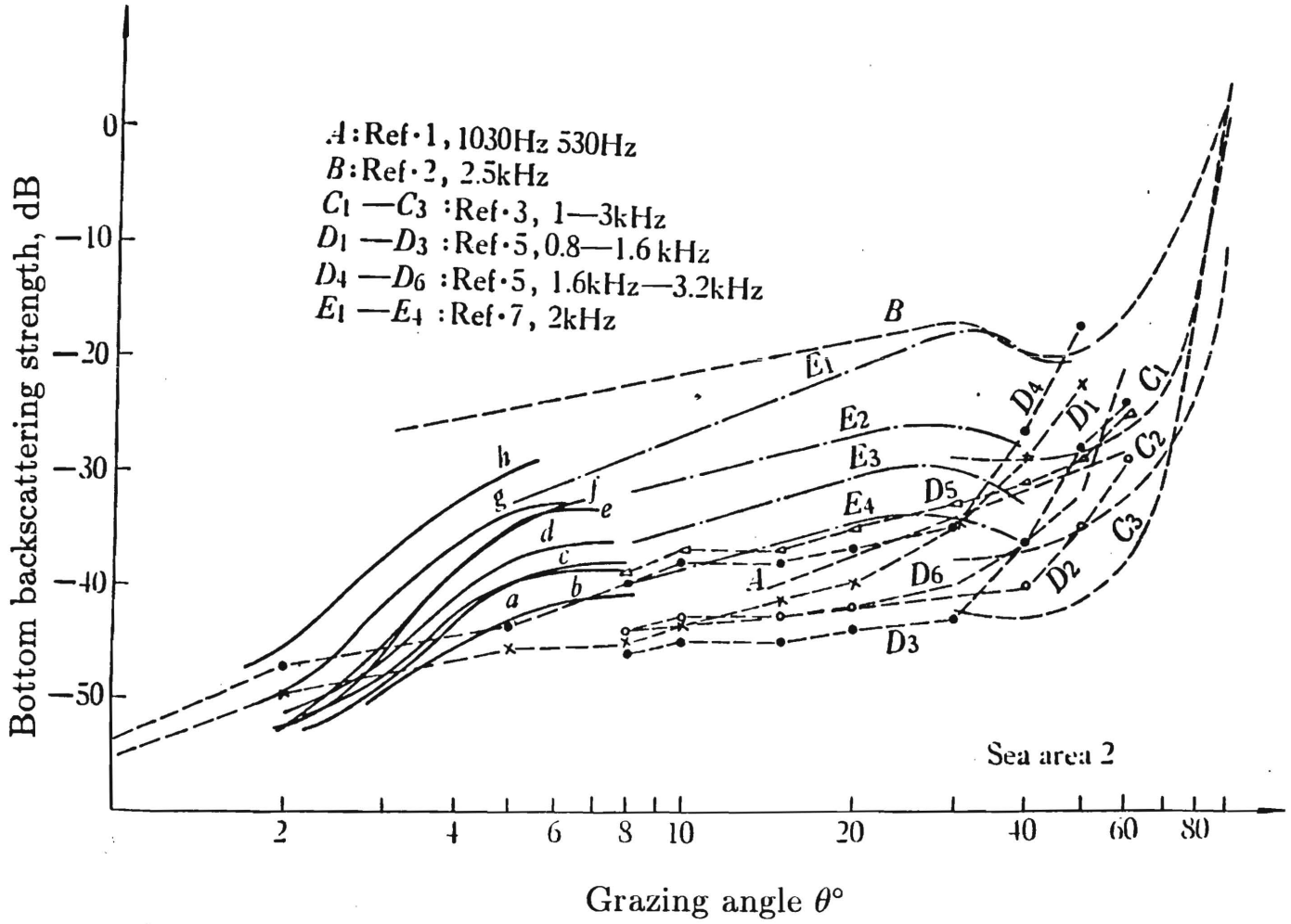
A:Ref·1, 1030Hz 530Hz
B:Ref·2, 2.5kHz
C1 —C3 :Ref·3, 1—3kHz
D1 —D3 :Ref·5, 0.8—1.6 kHz
D4 —D6 :Ref·5, 1.6kHz—3.2kHz
E1 —E4 :Ref·7, 2kHz
Bottom backscattering strength, dB
0
−10
−20
−30
−40
−50
2
4
6
8
10
20
40
60
80
Grazing angle θ°
Sea area 2
B
E1
E2
E3
E4
A
h
g
f
e
d
c
b
a
D4
D1
C1
C2
C3
D5
D6
D2
D3

9

Ivakin & Lysanov theory ——— Our data {.....
o o o o o

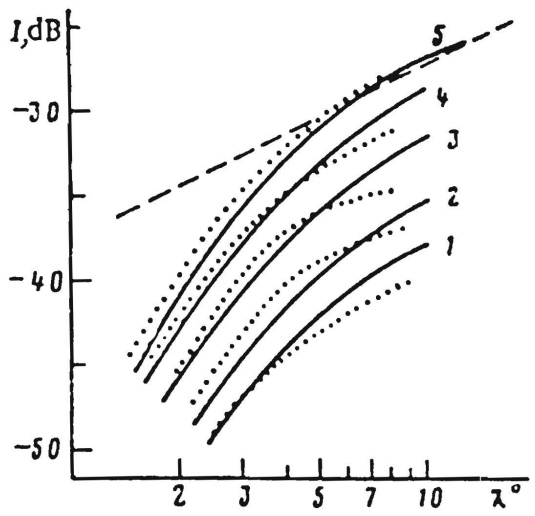

FIG. 1. Intensity of sound scattering by the bottom vs grazing angle at various frequencies: 1) 0.8 kHz; 2) 1.0; 3) 1.6; 4) 2.5; 5) 4 kHz.

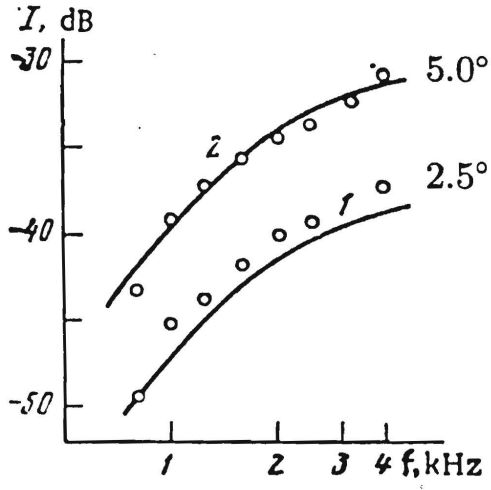

FIG. 2. Intensity of sound scattering by the bottom vs frequency at various grazing angles: 1) 2.5°; 2) 5°.

In shallow water of variable depth, the an adiabatic normal mode expression (**Pierce**) :

$$P(r,z;z_0) = \sqrt{\frac{2\pi}{r}}\, e^{-i\frac{\pi}{4}} \cdot \sum \frac{1}{\sqrt{k_m(r)}} \psi_m(0,z_0)\psi_m(r,z)\, exp\left[-i\int_0^r K_m(u)\, d\,u\right] \tag{9}$$

where

$$K_m^2(r) = k_m^2(r) + A_{mm}(r) \approx k_m(r) \tag{9a}$$

$$A_{mm} = \int \left(\psi_m \frac{\partial^2 \psi_m}{\partial r^2}\right) d\, z \tag{9b}$$

The adiabatic mode theory means that the local modes adapt to local environment. So the grazing angle of equivalent ray of normal modes satisfy

$$k_m(r) = k(r)\cos(\theta_m(r)) \tag{10}$$

$$H(r)\sin\theta_m(r) = H(0)\sin\theta_m(0) \tag{11}$$

For a wedged homogeneious continental shelf the water depth can be expressed by

$$H(r) = H(0)\,(1 + a\,r) \tag{12}$$

Appling WKB approximation we have the averaged sound intensity :

$$I(r) = \frac{2}{H(0)\,r}\int exp\left[\int_0^r \frac{L_n\,|\,V(\theta_m)\,|}{H(r)}\tan(\theta_m(r))\, d\,r\right] d\,\theta_m(r) \tag{13}$$

The averaged angular power spetrum

$$I_{ps}(\theta,r) = e^{\int_0^r \frac{L_n\,|\,V(\theta_m)|}{H(r)}\tan(\theta_m(r))\,dr} \tag{14}$$

The averaged intensity of sound propagation is:

$$I(r) = \sqrt{\frac{2\pi}{Q[H(0)+H(r)]}} * \frac{1}{r^{3/2}} \tag{15}$$

The averaged reverberation intensity is:

$$R(r) = \frac{\mu\pi^{(2-n/2)}c\tau}{4} \frac{H^n(0)}{[Q\frac{H(0)+H(r)}{2}]^{(1+n/2)}} \frac{1}{r^{(2+n/2)}} \tag{16}$$

Sound propagation is reciprocal if we exchange the positions of the source or receiver. But the monostatic reverberation intensities, obtained at two terminations with a depth of H_1 or H_2, would not be reciprocal.

$$\frac{R_{H_1}(r)}{R_{H_2}(r)} = (\frac{H_1}{H_2})^N \tag{17}$$

where N is the angular index of bottom backscattering defined as

$$BS(\theta) = 10\ log_{10}\ (\mu Sin^N\theta) \tag{18}$$

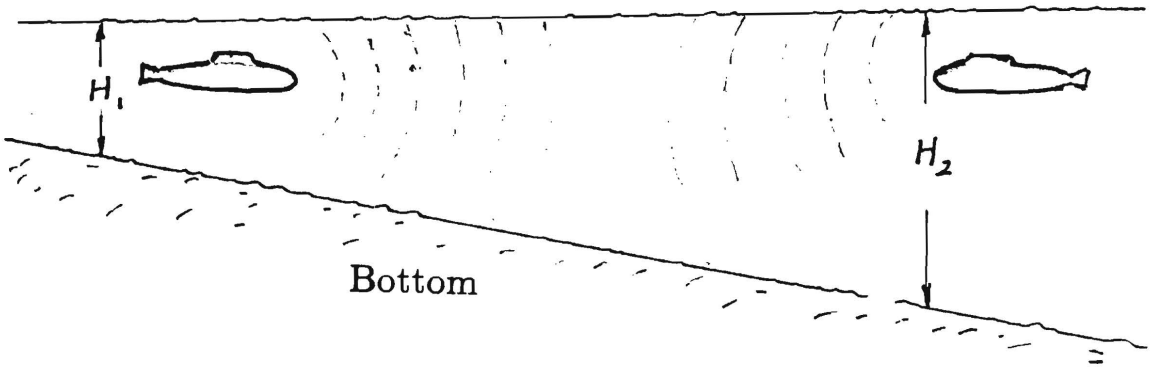

If $H_1 = 50m$, $H_2 = 200m$, $N = 2$, then the reverberation interference at shallower area would be $12dB$ less.

Resonant interaction of sound wave with internal solitons in the coastal zone

Ji-xun Zhou and Xue-zhen Zhang
Institute of Acoustics, Academia Sinica, Beijing 100080, People's Republic of China and School of Mechanical Engineering, Georgia Institute of Technology, Atlanta, Georgia 30332

Peter H. Rogers
School of Mechanical Engineering, Georgia Institute of Technology, Atlanta, Georgia 30332

(Received 20 February 1991; accepted for publication 30 May 1991)

Naturally occurring internal solitary wave trains (solitons) have often been observed in the coastal zone, but no reported measurements of such solitary waves include low-frequency long-range sound propagation data. In this paper, the possibility that internal waves are responsible for the anomalous frequency response of shallow-water sound propagation observed in the summer is investigated. The observed transmission loss is strongly time dependent, anisotropic and sometimes exhibits an abnormally large attenuation over some frequency range. The parabolic equation (PE) model is used to numerically simulate the effect of internal wave packets on low-frequency sound propagation in shallow water when there is a strong thermocline. It is found that acoustic transmission loss is sensitive to the signal frequency and is a "resonancelike" function of the soliton wavelength and packet length. The strong interaction between acoustic waves and internal waves, together with the known characteristics of internal waves in the coastal zone, provides a plausible explanation for the observed anomalous sound propagation in the summer. By decomposing the acoustic field obtained from the PE code into normal modes, it is shown that the abnormally large transmission attenuation is caused by "acoustic mode-coupling" loss due to the interaction with the internal waves. It is also shown that the "resonancelike" behavior of transmission loss predicted by the PE analysis is consistent with mode coupling theory. As an inverse problem, low-frequency acoustic measurements could be a potential tool for remote-sensing of internal wave activity in the coastal zone.

PACS numbers: 43.30.Bp, 43.30.Ft, 43.25.Cb

INTRODUCTION

Naturally occurring internal wave packets have often been observed in the coastal zone, especially in the summer. The mechanism for the generation of these nonlinear internal waves have been widely investigated in the geophysics and fluid mechanics community. Unfortunately, however, no reported measurements of such solitary waves include low-frequency long-range sound propagation data. The acoustic community has paid little attention to the effect of solitary waves on sound propagation with the exception of the work of Baxter and Orr that was based on ray theory and calculated the influence of an oceanic internal wave packet on short-range (high-frequency) sound propagation.[1] Experiments, conducted by Zhou and his group at Institute of Acoustics of the Chinese Academy of Sciences in Beijing over a four-year period at the same area of Yellow Sea, have shown that the frequency response of shallow water sound propagation in the summer is a strong function of time and propagation direction, and sometimes exhibits an abnormally large attenuation over some frequency range. A part of these results was reported before,[2,3] but it cannot be explained by a conventional range-independent model of sound propagation using reasonable bottom acoustic parameters and an average sound-speed profile.

In this paper, we investigate the possibility that the anomalous propagation results are due to the presence of internal waves. First, we briefly discuss the characteristics of internal wave packets in the coastal zone. We then review the aforementioned experimental results of Zhou *et al.* that exhibited the anomalous frequency response. In Sec. III, we hypothesize that this anomalous, anisotropic frequency response is caused by the influence of internal wave packets. We support the hypothesis with numerical simulation results obtained using the parabolic equation (PE) propagation model. In Sec. IV, we decompose the acoustic field obtained by using the PE model into the normal modes, and show that the abnormally large transmission loss which occurs over certain frequency ranges is due to "mode-coupling" loss induced by the internal wave packets. In Sec. V, we show that "resonancelike" behavior of the attenuation is consistent with mode coupling theory.

I. CHARACTERISTICS OF INTERNAL WAVE PACKETS IN THE COASTAL ZONE

Internal waves have been observed almost everywhere in the ocean.[4] In the open ocean they are best described as a stochastic phenomenon with a broadband frequency wave number spectrum.[5] However, analysis of extensive data on internal waves in the coastal zone,[6-22] has shown that these waves exhibit the properties of solitons. The experimental data includes: current and temperature measurements; vertical profiles from CTD, XBT, and acoustic echo sounding

devices; ship's radar and satellite (or space shuttle) images obtained at optical and radar frequencies. We are primarily interested in the effect of internal solitons on long-range sound propagation in the coastal zone, and not the mechanisms for the generation or propagation of internal wave packets (which has been widely investigated in the geophysics and fluid mechanics communities). We thus limit our discussion of internal waves to the following summary of the relevant characteristics of internal wave packets in the coastal zone.

(1) Internal waves in shallow water are frequently observed in deterministic groups (wave packets) with well-defined wavelengths that are describable as solitary waves (or solitons). These waves are usually observed in summer when they are trapped in a strong and shallow seasonal thermocline.

(2) Solitons in shallow water ($h/\lambda_i \ll 1$) are described to first order in wave amplitude by the Korteweg–de Vries (KdV) equation: $A_t + C_0 A_x + \mu A A_x + \delta A_{xxx} = 0$. The solitary waveforms often have a "sech^2" profile. When an initial solitary wave propagates, it often evolves more rank-ordered solitons and exhibits clear nonlinear and dispersive features such as higher-than-linear group velocity, and a decrease in wavelength and amplitude toward the rear of the packet.

(3) The number of wave packets are highly correlated with the strength of the local tides: The maximum number occurs during spring tides and the minimum number occurs during neap tides. Whether or not they occur is critically dependent on the structure of the background shear and stratification profiles.

(4) Solitary wave packets propagate shoreward, and are often generated by a tidally driven flow over sills, continental shelf edges, or other major variation in underwater topography.

(5) Because of the shallowness of the summer seasonal thermocline and the large amplitude of the coastal internal waves, strong surface expressions of solitons have been observed with a variety of remote sensors, including photographs and synthetic aperture radar (SAR) from satellites and space shuttles.

Naturally occurring large-amplitude internal solitons have been reported in many coastal zones of the world such as: the Massachusetts Bay,[6–8,11] the New York Bight,[20–22] Gulf of California,[10,13] Andaman Sea offshore Thailand,[9,18] the Australian North West Shelf,[19] the Sulu Sea between the Philippines and Borneo,[15,16] off the coast of Portugal,[12,18] off Hainan Island in the South China Sea and off the Strait of Gibraltar in Alboran Sea,[23] the Scotian Shelf off Nova Scotia,[14] the Celtic Sea,[17] and so on. They have also been observed in lakes.[24,25] As an example, an excellent record of an internal wave packet is shown in Fig. 1. It was obtained by Orr using high-frequency acoustic scattering in the Massachusetts Bay.[7,8] The period of the waves is Doppler shifted by the ship's speed of about 2.5 kn. The seasonal thermocline is displaced by 30 m (arrow 1) and the stratified point scatterers (zooplankton?) at 30 to 40 m are displaced more than 20 m (arrows 2 and 3). The heavy acoustic backscattering in the vicinity of arrow 4 and extending in an oscillatory pattern throughout the figure is possibly caused by turbulent mixing in the thermocline. The heavy scattering near 75 m is probably caused by euphausiid and mysid shrimp. Figure 2, taken from the work of Osborne and Burch,[9] shows how rough and smooth bands on the water surface can be caused by internal solitons. Such surface expressions have been detected by ship, satellite, and space shuttle in many areas. For example, Fig. 3, taken from the work of Liu,[21] is a line drawing of the internal wave packets in the New York Bight, observed from Seasat satellite, which clearly illustrates the anisotropic characteristics of internal waves in the coastal zone. There are numerous wave groups, all propagating shoreward. Each group consists of many solitons. The number of groups often depends on the local tide strength and the density profile of water column, i.e., it is a function of time.

The characteristics of internal wave packets in the coastal zone summarized here, will be helpful in explaining the anomalous experimental results, introduced in the next section.

II. FREQUENCY RESPONSE OF SHALLOW-WATER SOUND PROPAGATION IN THE SUMMER

Zhou and his group at Institute of Acoustics, Academia Sinica (IAAS) have measured the frequency response of shallow-water sound propagation under the condition of a

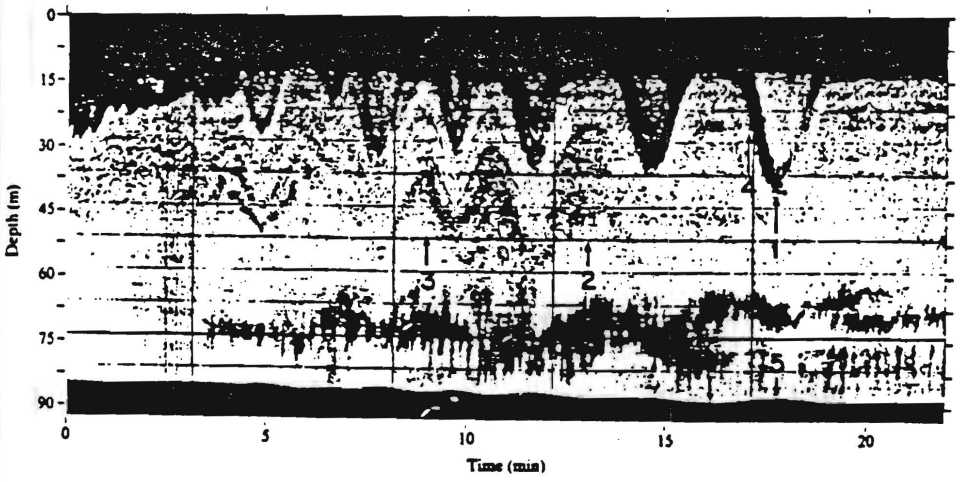

FIG. 1. A 200-kHz acoustic record of an internal wave packet observed in the Massachusetts Bay.

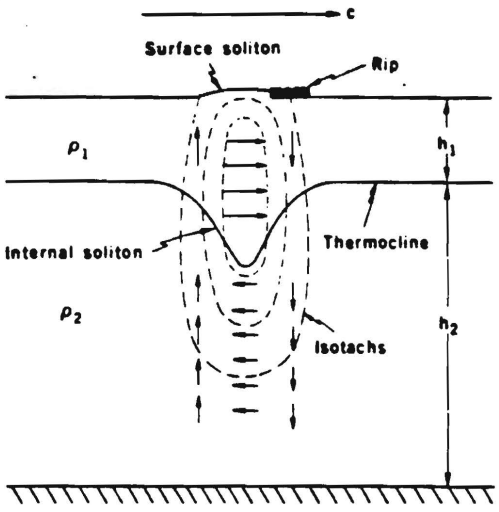

FIG. 2. A sketch of an internal soliton in a two-layer fluid model showing the fluid-particle velocities and the surface expression.

strong thermocline in the Yellow Sea off China. A great deal of data was collected over several years in the same area, (which had a characteristically flat seabottom with high-speed sediments). The data included measurements of sound propagation, long-range reverberation, sound field spatial coherence and utilized normal-mode spatial filtering techniques. The acoustic parameters of the bottom for this area were obtained by wideband acoustic measurements.[26,27] Generally speaking, the experimental data fits theoretical predictions very well. For example, transmission losses as a function of frequency for winter, late spring, and *sometimes* for summer were correctly predicted. However, it was found that, in the summer, even along the same experimental track, with similar averaged sound-speed profiles the frequency response of sound transmission could often be very different for different years.

Figure 4 shows power spectra that are obtained by averaging several explosive propagation signals. The upper curve is the power spectrum at a propagation range of 0.5 km, the lower one is at a range of 28 km. The difference between the two curves is a measure of the sound transmission loss between two receiving points, i.e., the frequency response of sound propagation. Between 300 and 1100 Hz, especially around 600 Hz, the transmission loss is abnormally large. The measured sound-speed profiles at the receiving ship are shown in Fig. 5. Both source and receiver were located below the thermocline. The anomalous transmission loss cannot be explained by conventional models of sound propagation (with a full complement of bottom acoustic parameters and an averaged sound-speed profile of water column). In order to explain this phenomenon, Zhou and his colleagues at IAAS made observations, every August for 4 years at same area. The abnormal attenuation frequency range varied with time. In Fig. 4, it occurs at around 600 Hz, but for different years or different propagation directions, it has been observed around 500, 1200, or 1600 Hz. Sometimes, there is no apparent abnormal attenuation frequency range.

In another experiment, the frequency response at a fixed range for six different radial directions was obtained. The results are shown in Fig. 6. The transmission distance was kept constant at 28 km, by moving the source ship along one quadrant of a circle centered at the receiving ship. Each curve represents an averaged value obtained from several explosive signals. Transmission loss is obviously a strong function of propagation direction. For different propagation directions, at some frequencies, the sound intensity varied as much as 25 dB! However, in another experiment, at the same

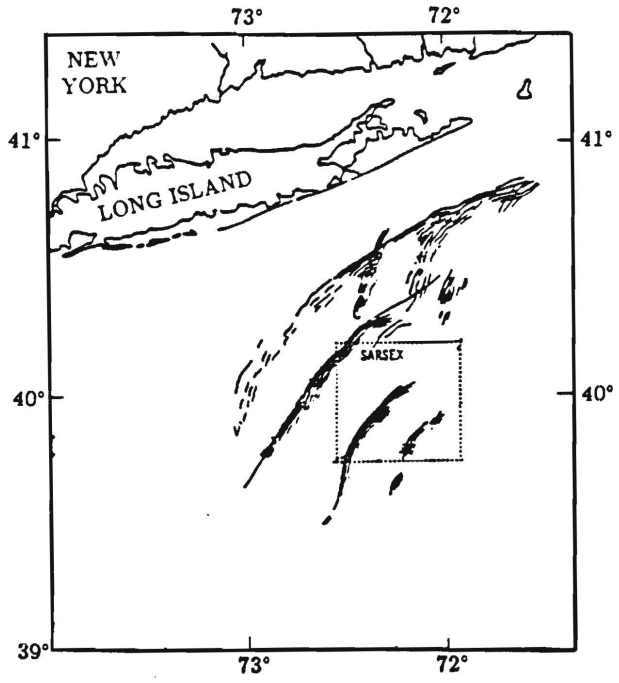

FIG. 3. Line drawing indicating internal wave packets in the New York Bight, observed from the Seasat satellite.

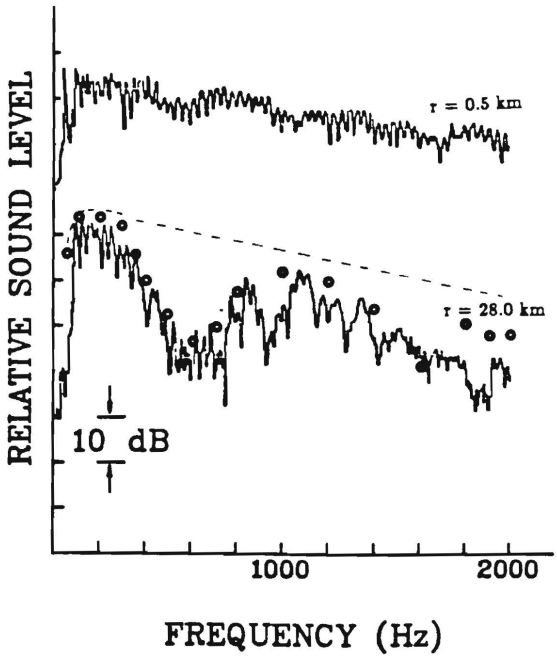

FIG. 4. Explosive signal power spectrum for shallow-water sound propagation in the summer which exhibits an abnormally large attenuation around 600 Hz (experimental data). Both source and receiver are located below the thermocline. Computational results (see Sec. III B): (1) without packet – – –. (2) with three packets O O O.

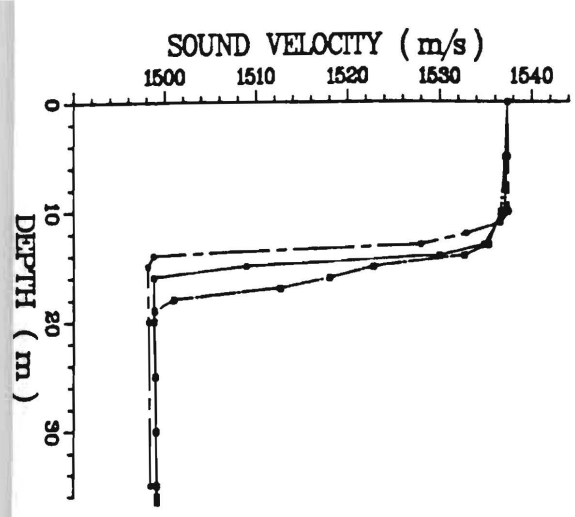

FIG. 5. Three sound-speed profiles measured at the receiving ship at different times.

place, in a different year, two orthogonal propagation directions were observed to have almost identical frequency responses. It was not at all clear why, when there is a strong thermocline, the frequency response of shallow-water sound propagation in the experimental area was often observed to be a strong function of both time and propagation direction, and sometimes exhibited abnormally large attenuation over some frequency range.

Using ray theory and experimental contours of sound speed versus range and depth, Baxter and Orr[1] calculated the influence of an internal wave packet on short range

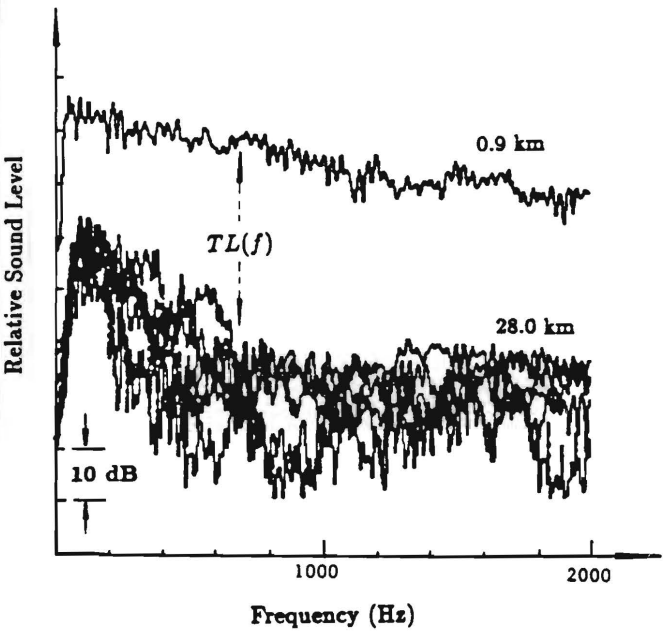

FIG. 6. Frequency response of sound transmission loss (TL) for the summer which shows different results for different propagation directions.

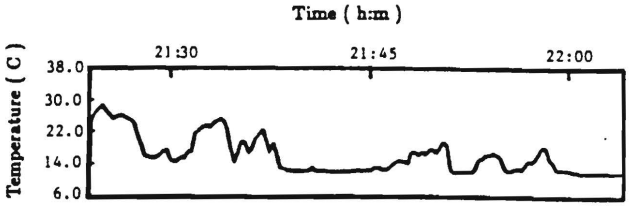

FIG. 7. A record of temperature versus time over a period of 42 min at a fixed depth (near the thermocline).

(high-frequency) sound propagation. The calculations showed that at a fixed position the intensity of sound field could vary by as much as 20 dB, relative to a case without the presence of the internal wave packet. We hypothesized that internal wave packets might have a strong influence on low-frequency long-range sound propagation in shallow water as well and could possibly explain Zhou's Yellow Sea propagation data. In the next section, we support this hypothesis with numerical simulation results obtained using the parabolic equation method.

III. NUMERICAL SIMULATION OF THE INFLUENCE OF INTERNAL WAVE PACKETS ON SOUND PROPAGATION

A. Oceanic model

The presence of internal waves makes the sound-speed profile of the water range dependent. Unfortunately, in Zhou's experiments there were no accompanying systematic measurements of the internal wave field; and only the sound-speed profile at the receiver was measured. During the time period over which the frequency response shown in Fig. 4 was obtained, it was found that the thermocline depth at receiving ship location did change with time. Figure 5 shows three sound-speed profiles that were obtained at different times.

During the experiment, Zhang[28] measured the temperature fluctuation as a function of time at the receiving ship. A record of temperature fluctuations over a period of 42 min at a fixed depth (around the thermocline) is shown in Fig. 7. The temperature fluctuated between about 13 °C and 27 °C. The possible presence of several individual solitary waves is indicated by temperature peaks due to the depression of the thermocline. Figures 5 and 7 give at least some evidence that there was solitary wave activity in the area of acoustic experiments.

Due to the fact that we have no data concerning specific characteristics of internal waves at the experimental site, for simplicity, following Lee's three-layer model of internal wave,[29] we assume that the internal wave packet can be expressed by a gated sine function as shown in Fig. 8(b). In this figure, if a packet begins at r_0, then, for $r_0 + L_p \geq r \geq r_0$,

$$Z_1 = 14.0 - 2.0 \sin(2\pi r/\lambda_i), \tag{1}$$

$$Z_2 = 19.0 - 5.0 \sin(2\pi r/\lambda_i). \tag{2}$$

The idealized sound-speed profile in the absence of internal waves for the numerical simulation is shown in Fig. 8(a). We call λ_i the soliton wavelength, and L_p the packet

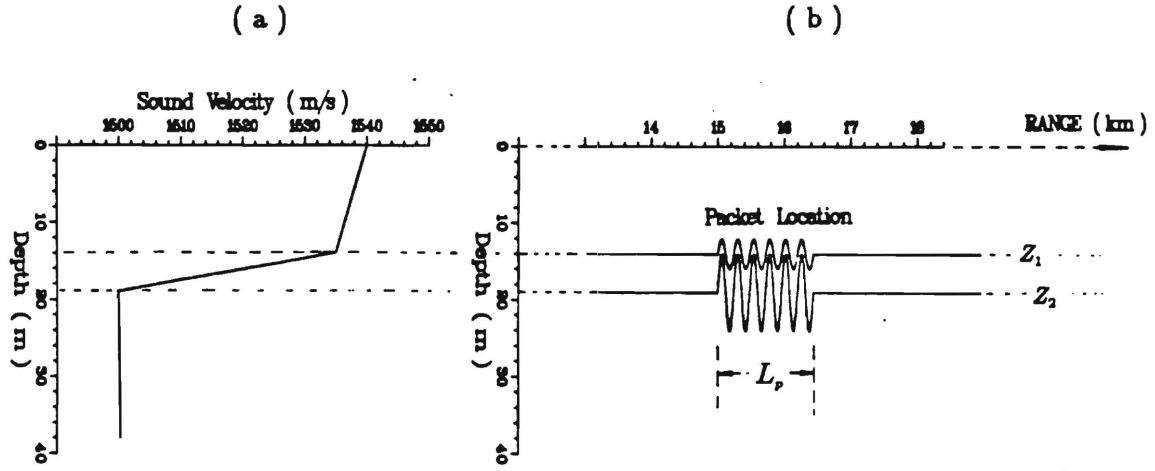

FIG. 8. Simplified oceanic model for an internal wave packet.

length. Referring back to Fig. 1, we see that an almost sinusoidal interface exists between the warmer surface layer and the underlying cooler water. The waveform of the soliton in Fig. 5 of Ref. 1 is also almost sinusoidal. The simplified, sinusoidal model, is thus seen to be not physically unreasonable. The main purpose of this work is to provide the first physical insight into the possible effects of internal wave packets on wideband low-frequency sound propagation in shallow water. It is not to predict the characteristics of internal waves for a specific area. Our simplification should not alter the qualitative results which follow.

The averaged values for bottom sound speed (c_b) and bottom acoustic attenuation (α_p) for the experimental area are given by[26,30]

$$c_b/c_w = 1.056, \tag{3}$$

$$\alpha_p = 0.34 f^{1.84} \text{ dB/m}, \tag{4}$$

where f is the frequency in kHz.

B. Comparison of numerical frequency response with experimental data

Numerical simulation results obtained using the parabolic equation (PE) method (IFD[31-33] code), show that internal wave packets can significantly change low-frequency transmission loss. The frequency response and, in particular, the abnormal attenuation frequency range are sensitive functions of the parameters of the soliton wave packets.

For example, using the simplified ocean model given in Fig. 8 and Eqs. (1)–(4), we put three internal wave packets located at 5, 15, and 25 km, along propagation track with each packet consisting of six solitons each with a wavelength λ_i of 235 m ($L_p = 6\lambda_i = 1410$ m). The transmission loss as a function of range for four frequencies (with a receiver depth of 32 m and a source depth of 25 m) is shown in Fig. 9. The difference between the results with and without the soliton packets present is small at 100 or 1000 Hz, but at 600 Hz the difference at 30 km is as much as 25 dB. The most interesting and encouraging result is that, in this case the numerical transmission loss as a function of frequency (shown in Fig. 4 by the circles) fits the experimental results quite well.

As a consequence of the characteristics of internal wave packets described in Sec. I (propagation in groups, well-defined wavelengths, high correlation with tides, shoreward propagation), the projection of the solitons in different acoustic propagation directions and for different times will be different. If we change the soliton wavelength in the three packets to 235, 300, 350, 400, and 500 m, we would get frequency responses as shown in Fig. 10, that are similar to the experimental results for different propagation directions shown in Fig. 6. Hence, interaction between acoustic waves and internal wave packets is consistent with Zhou's experimental results for shallow-water sound propagation in the summer.

Why does the abnormally large attenuation in Fig. 4 occur around 630 Hz for internal wave packets consisting of six solitons with a wavelength of 235 m? Why do internal wave packets with the same parameters have a much smaller effect on sound propagation at frequencies around 300 or 1000 Hz? In the next section, we will show that these are due to "resonances" in the acoustic mode-coupling induced by the internal wave packets.

IV. RESONANCE EFFECTS

A. Frequency resonance

For our numerical model of shallow water, with a water depth of 38 m, mode stripping caused by seabottom attenuation, results in only a few modes still being present at a distance of 15 km. If the source and receiver are located below the thermocline, for a realistic sea bottom, the first mode dominates the sound field at long-range over the frequency range of interest. In order to isolate the effect of internal wave packets on the mode coupling among acoustic normal modes, we put a single packet consisting of six solitons with a wavelength of 235 m at 15 km and use the first normal mode alone as the initial input field to the parabolic equation code. Thus, prior to interaction with the packet, we assume only one mode (the first) is present; higher-order modes are generated as the first mode propagates through the internal wave packet. The depth distribution function of

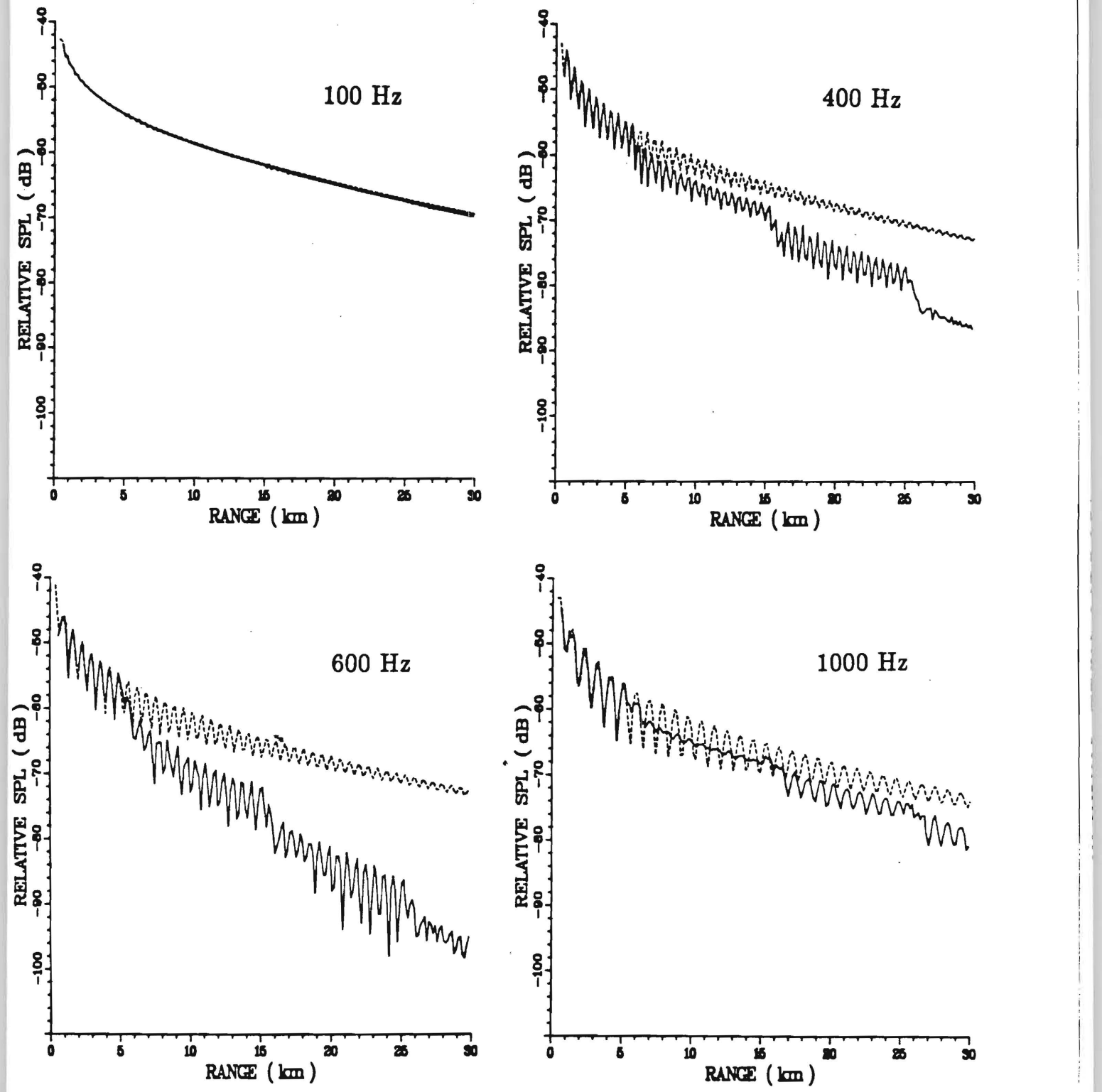

FIG. 9. Comparison between transmission loss without internal waves (- - -) and with three packets located at 5, 15, and 25 km (—). $L_p = 1410$ m. $\lambda_i = 235$ m.

sound pressure amplitude at 15, 20, and 30 km obtained by PE method are shown in Fig. 11. At a range of 15 km (before the wave has interacted with the internal wave packet), the shape of the first mode is maintained at all frequencies. After interaction with the internal wave packet, at 300 and 1000 Hz, the energy is still predominantly in the first mode. However, for 630 Hz, the depth distribution shape is quite different from the first mode, due to resonance scattering, and the amplitude is much smaller.

The mode coupling due to interaction with internal wave packets can be easily calculated. Neglecting the evanescent modes, which decay at large range, leaves only a

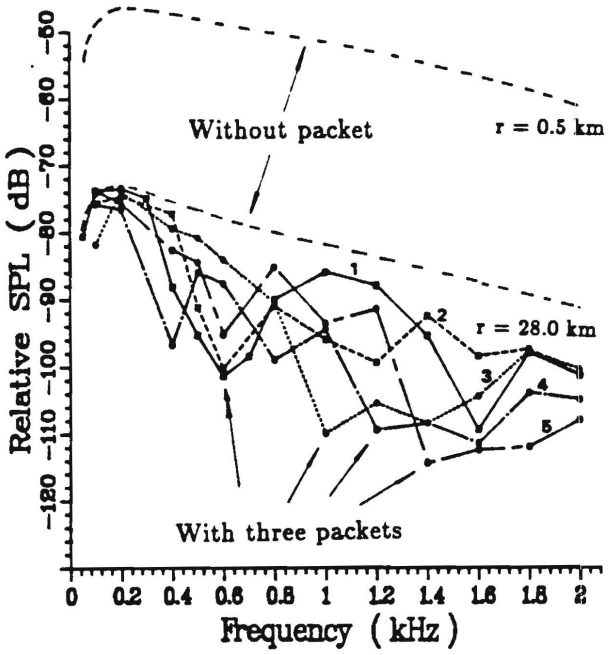

FIG. 10. The computational transmission loss at 28 km for three internal wave packets with different wavelengths λ_i = (1)235 m, (2)300 m, (3)350 m, (4)400 m, (5)500 m.

finite number of propagating modes at a given frequency. The propagated field $[\Phi_{PE}(r,z)]$ obtained by the PE method can be expanded in terms of a set of local modal eigenfunctions $[U_n(z)]$, corresponding to the sound velocity profile shown in Fig. 8(a), as follows:

$$\Phi_{PE}(r,z) = \sum_n A_{PEn}(r) U_n(z), \tag{5}$$

where the local modal eigenfunctions $U_n(z)$ satisfy the appropriate boundary conditions at the sea surface and bottom and the differential equation

$$\frac{d^2U_n}{dz^2} + [k^2(z) - k_n^2] U_n = 0, \tag{6}$$

where k_n is the eigenvalue (modal wave number). The modal eigenfunctions also satisfy the orthogonality relation

$$\int \rho(z) U_n(z) U_m(z) dz = \delta_{n,m}. \tag{7}$$

The Kronecker delta on the right side is unity if $n = m$ and is zero if $n \neq m$.

Multiplying both sides of Eq. (5) by $U_m(z)$ and integrating over depth with help of Eq. (7) (mode spatial filtering), we obtain

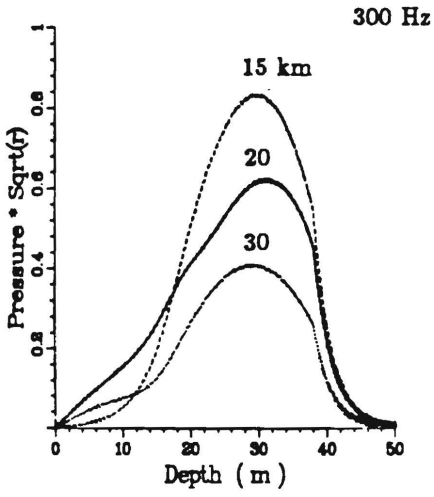

(a)

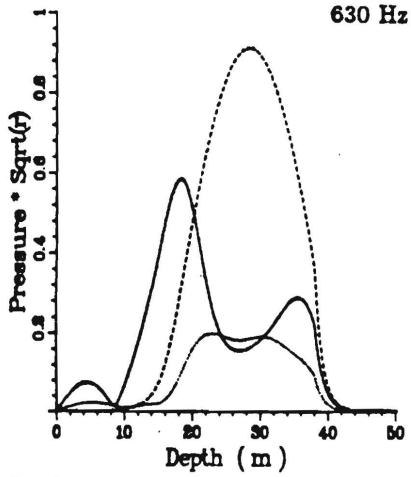

(b)

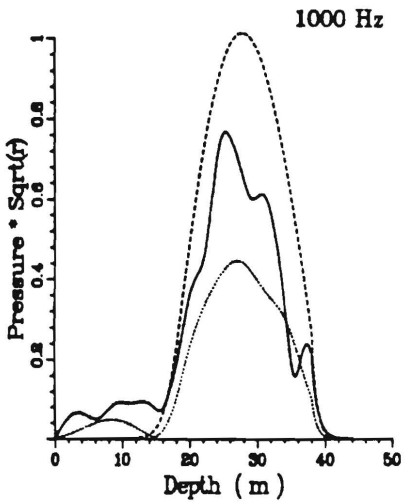

(c)

FIG. 11. The depth distribution function of sound-pressure amplitude for different frequencies at a range of 15 km (– – –), 20 km (—), and 30 km (–·–) obtained using the PE method. PE input field: mode 1. One internal wave packet at 15–16.41 km with λ_i = 235 m.

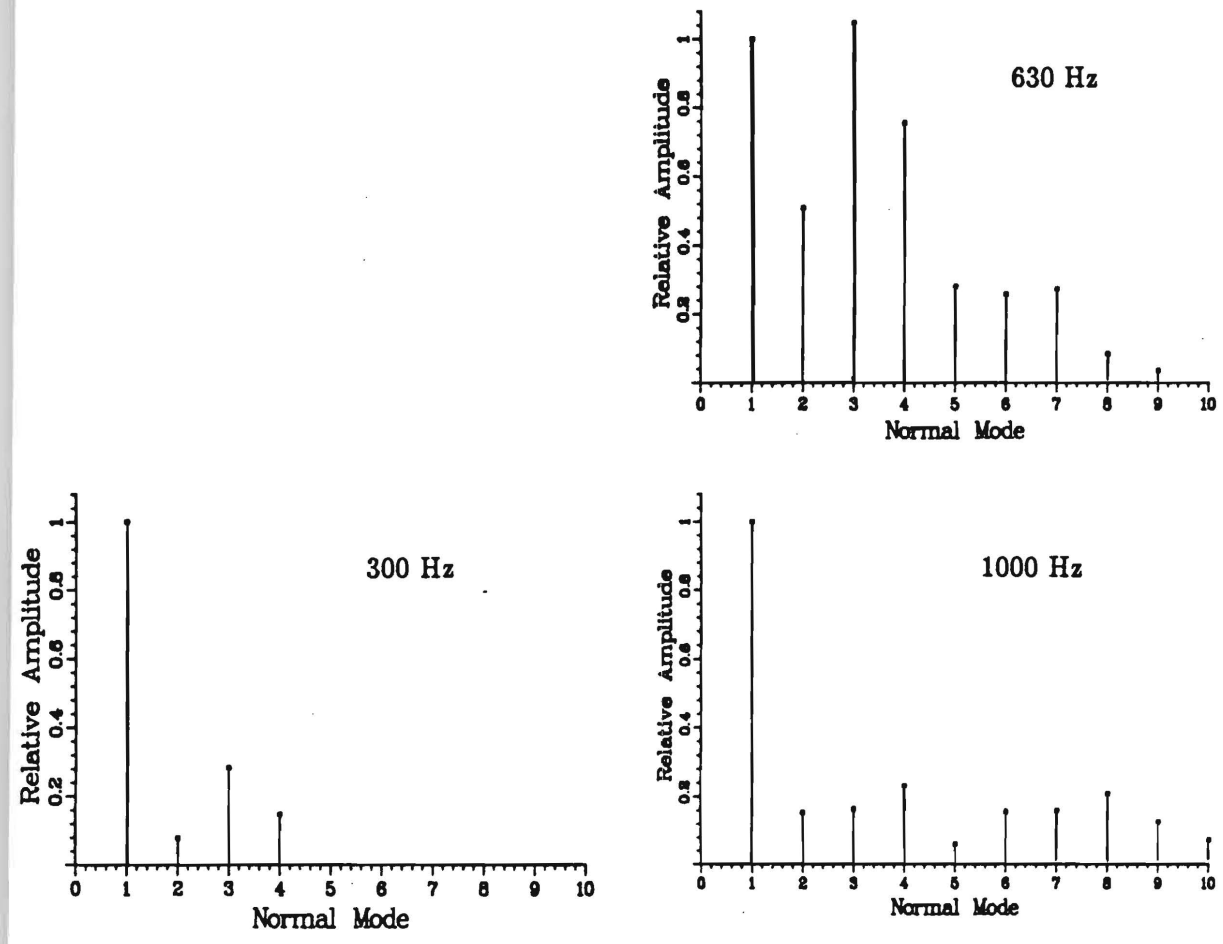

FIG. 12. The relative amplitudes of different modes at 18 km, showing frequency resonance of mode coupling. PE input field: mode 1. One packet at 15–16.41 km. $\lambda_i = 235$ m.

$$A_{\mathrm{PE}n}(r) = \int \rho(z)\Phi_{\mathrm{PE}}(r,z)\,U_n(z)dz. \tag{8}$$

After the interaction of the first mode with the internal wave packet, at selected ranges where no internal wave exists, the relative amplitude of higher-order mode to the first mode, A_{n1}, is given by

$$A_{n1} = \frac{|A_{\mathrm{PE}n}(r)|}{|A_{\mathrm{PE}1}(r)|} = \frac{|\int \rho(z)\Phi_{\mathrm{PE}}(r,z)\,U_n(z)dz|}{|\int \rho(z)\Phi_{\mathrm{PE}}(r,z)\,U_1(z)dz|} = \left(\frac{A_{nR}+A_{nI}}{A_{1R}+A_{1I}}\right)^{1/2}, \tag{9}$$

with

$$A_{nR} = \left(\sum_{j=1}^{m} \rho_1 \Phi_R(r,z_j)\,U_n(z_j) + \sum_{j=m+1}^{M} \rho_2 \Phi_R(r,z_j)\,U_n(z_j)\right)^2, \tag{10}$$

$$A_{nI} = \left(\sum_{j=1}^{m} \rho_1 \Phi_I(r,z_j)\,U_n(z_j) + \sum_{j=m+1}^{M} \rho_2 \Phi_I(r,z_j)\,U_n(z_j)\right)^2, \tag{11}$$

where $\Phi_R(r,z_j)$ and $\Phi_I(r,z_j)$ are the real part and the imaginary part of PE field in the jth depth increment, M is the number of layers and the water-bottom interface occurs between the layer m and layer $(m+1)$.[31] The quantity, A_{n1}, is a measure of the energy exchanged between the first mode and higher-order modes. In this manner using a normal-mode computer program, a PE computer program and the ocean model described in Sec. III, we were able to decompose the sound field obtained from PE into normal modes. The input field for the PE code is the first normal mode. In the absence of modal coupling only this mode would ever be present. Results for three different frequencies are shown in Fig. 12. The plots show the relative modal amplitudes at 18 km. For ranges less than 15 km, only the first mode is present. As indicated in Fig. 12, beyond 15 km there is interaction with the internal wave packet, and at 630 Hz a significant amount of energy has been transferred from mode 1 into higher-order modes that will attenuate rapidly thereafter. Relatively little modal coupling occurs at the other two frequencies. Table I shows the eigenvalue k_n and the attenuation rate β_n (corrected for cylindrical spreading) for the first seven normal modes, calculated by a normal mode program for the sound velocity profile shown in Fig. 8(a) and a frequency of 630 Hz.

TABLE I. The eigenvalue k_n, attenuation rate β_n and eigenvalue difference between modes 1 and n for the first seven normal modes, $f = 630$ Hz.

Mode n	k_n	β_n (dB/km)	$k_1 - k_n$
1	2.635 594 3	0.2454	0
2	2.626 325 6	0.9169	0.009 268 7
3	2.611 159 6	1.7661	0.024 434 7
4	2.591 298 6	2.4771	0.044 295 7
5	2.572 735 4	1.5938	0.062 858 9
6	2.563 417 2	1.7855	0.072 177 1
7	2.548 399 6	2.3948	0.087 194 7

From this analysis, it is evident that the modal coupling caused by internal waves can sometimes be an important loss mechanism for sound transmission in shallow water in the summer. At 300 and 1000 Hz, the mode-coupling effect is much weaker. Only a few percent of the *wave energy* is coupled into high-order modes. At 630 Hz, however, a significant amount of energy has been transferred from mode 1 into higher-order modes, especially mode 3 and mode 4, with much larger attenuation rate. The mode-coupling induced by internal wave packets exhibits a *frequency resonance* effect, and can cause abnormally large transmission loss around the resonance frequency. The abnormally high attenuation observed by Zhou *et al.* over certain frequency ranges is consistent with interaction with internal waves. In Sec. V, we will discuss what determines the "resonance frequency."

B. Soliton wavelength resonance

We continue to consider a single packet located at a distance of 15 km. We now fix the acoustic frequency at 630 Hz and the packet length (L_p) at 1.4–1.5 km and calculate the effect of soliton wavelength (λ_i) on transmission loss. Figure 13(a) shows the transmission loss as a function of soliton wavelength at a range of 30 km (with a receiver depth

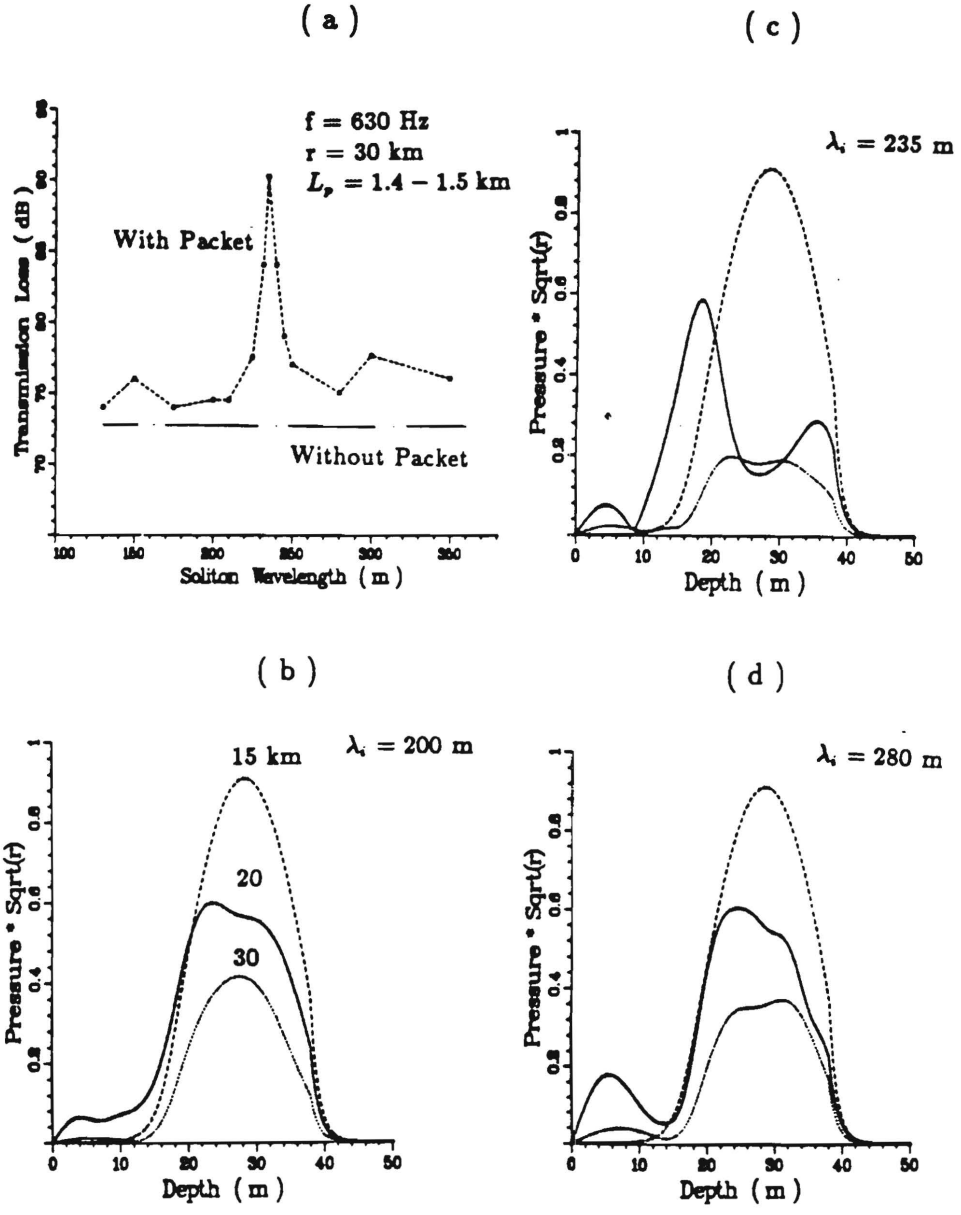

FIG. 13. (a) Soliton wavelength resonance. (b)–(d) The depth distribution function of sound-pressure amplitude for different soliton wavelengths at 15 km (– – –), 20 km (—), and 30 km (••) obtained by PE method. PE input field: mode 1. One packet at 15–16.41 km. $f = 630$ Hz.

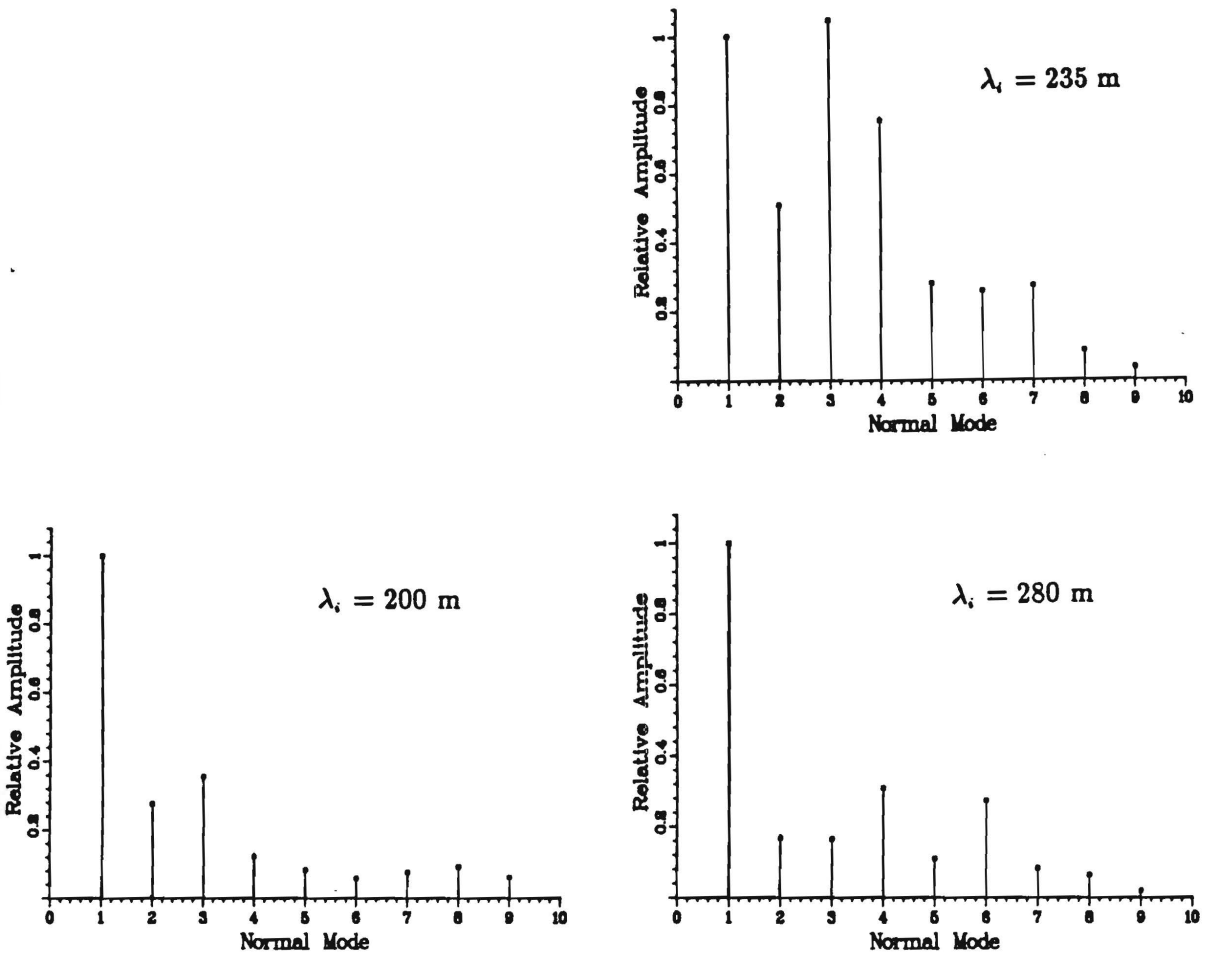

FIG. 14. The relative amplitudes of different modes at 18 km, showing soliton wavelength resonance of mode coupling. PE input field: mode 1. One packet at 15–16.41 km. $f = 630$ Hz.

of 32 m and a source depth of 25 m). Transmission loss exhibits a resonancelike maximum at a soliton wavelength of 235 m. For other soliton wavelengths between 120 and 350 m, the difference between transmission loss with and without the presence of an internal wave packet is not significant. Taking first normal mode as the input field to the PE code, we obtained the depth distribution functions shown in Fig. 13(b)–(d). After interaction with the packet, for a soliton wavelength of 235 m, the shape is very different than that of the first mode, but for 200 and 280 m, the shapes are very close to that of mode 1.

At a distance of 18 km, we again decompose the PE calculated sound field into normal modes and get the results for three different soliton wavelengths shown in Fig. 14. For a soliton wavelength of 235 m, a significant amount of energy has been transferred from mode 1 into higher-order, higher-loss modes. However, for soliton wavelengths of 200 and 280 m, the mode-coupling effect is rather weak. That is, the mode coupling and, hence, the loss induced by internal wave packets exhibits a *soliton wavelength resonance* effect.

C. Packet length resonance

Once again, considering a single packet located at a range of 15 km, we now hold acoustic frequency (630 Hz) and soliton wavelength (235 m) constant, and calculate the effect of internal wave packet length (or, equivalently, the number of solitons) on transmission loss. Figure 15(a) shows the transmission loss as a function of packet length at 30 km (with a receiver depth of 32 m and a source depth of 25 m). The transmission loss is a periodic, "resonancelike" function of the packet length (L_P). Taking first normal mode as the input field to the PE code, we obtain the depth distribution functions for the sound field for three packet lengths shown in Fig. 15(b)–(d). At 18 km, after interaction with the packet, the shape of the depth distribution function for a six-soliton packet is very different from that of the first mode. However, for a longer packet consisting of 11 solitons it is close to the shape of the first mode and close even in amplitude to the results without a packet.

At a distance of 18 km, we again decompose the PE sound field into normal modes, and get the results for two different packet lengths shown in Fig. 16. For a 1410-m packet (six 235-m solitons), a significant amount of energy has been transferred from mode 1 into higher-order modes. For a longer packet (2585 m, i.e., for 11 solitons), the mode-coupling effect is much weaker. That is, the mode-coupling and hence the loss induced by internal wave packets exhibits a *packet length resonance* effect.

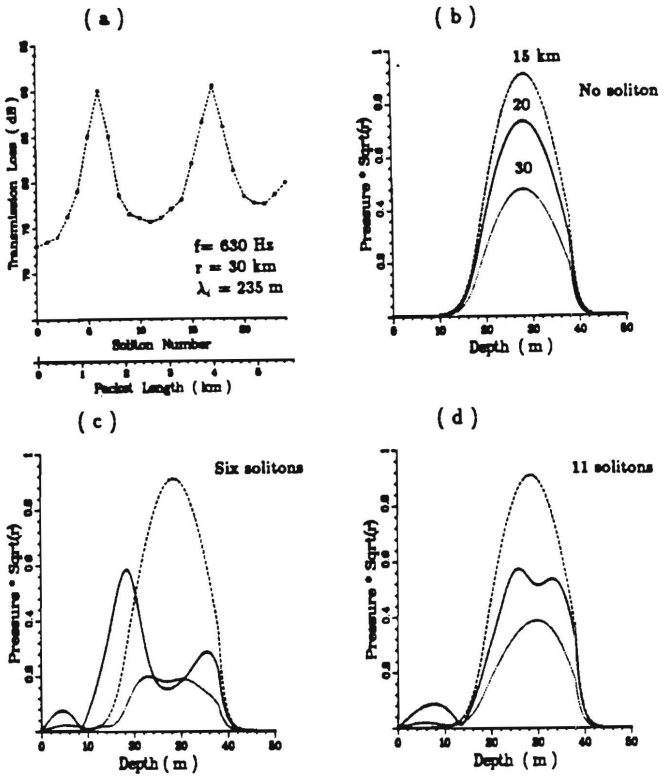

FIG. 15. (a) Packet length resonance. (b)–(d) The depth distribution function of sound-pressure amplitude for different packet lengths at 15 km (– – –), 20 km (—), and 30 km (···) obtained by PE method. PE input field: mode 1. One packet beginning from 15 km. $f = 630$ Hz.

V. MODAL COUPLING ANALYSIS

Dozier and Tappert,[34] and McDaniel and McCammon[35] have shown that the exchange of energy between acoustic modes n and m induced by random internal waves in the deep sea or lateral seabed inhomogeneities in shallow water exhibits a wave number resonance effect. The principal transfer of energy will occur between modes whose eigenvalue difference equals the wave number of the spectrum peak of the internal waves or sub-bottom roughness. This result is also applicable to our numerical results shown in Figures 11–14. Significant energy transfer will occur between modes m and n if

$$k_{\text{int}} \approx k_n - k_m, \tag{12}$$

where $k_{\text{int}} = 2\pi/\lambda_i$ is the wave number of the internal wave. [If the mode couping is considered to be a quantum mechanical phonon–soliton interaction, Eq. (12) is a statement of conservation of momentum. The corresponding statement of conservation of energy $\omega_{\text{int}} = \omega_n - \omega_m$ can be shown to correspond, macroscopically, to the Doppler shift which results from scattering from the moving internal wave.] For our numerical model of internal wave packets with a wavelength of 235 m, the wavenumber of the spectrum peak of the internal wave $k_{\text{int}} \approx 2\pi/235 = 0.026\,737\,0$. Comparing this value of k_{int} with the eigenvalue differences between mode 1 and mode n shown in Table I, it is found that k_{int} is almost equal to the eigenvalue difference between acoustic normal

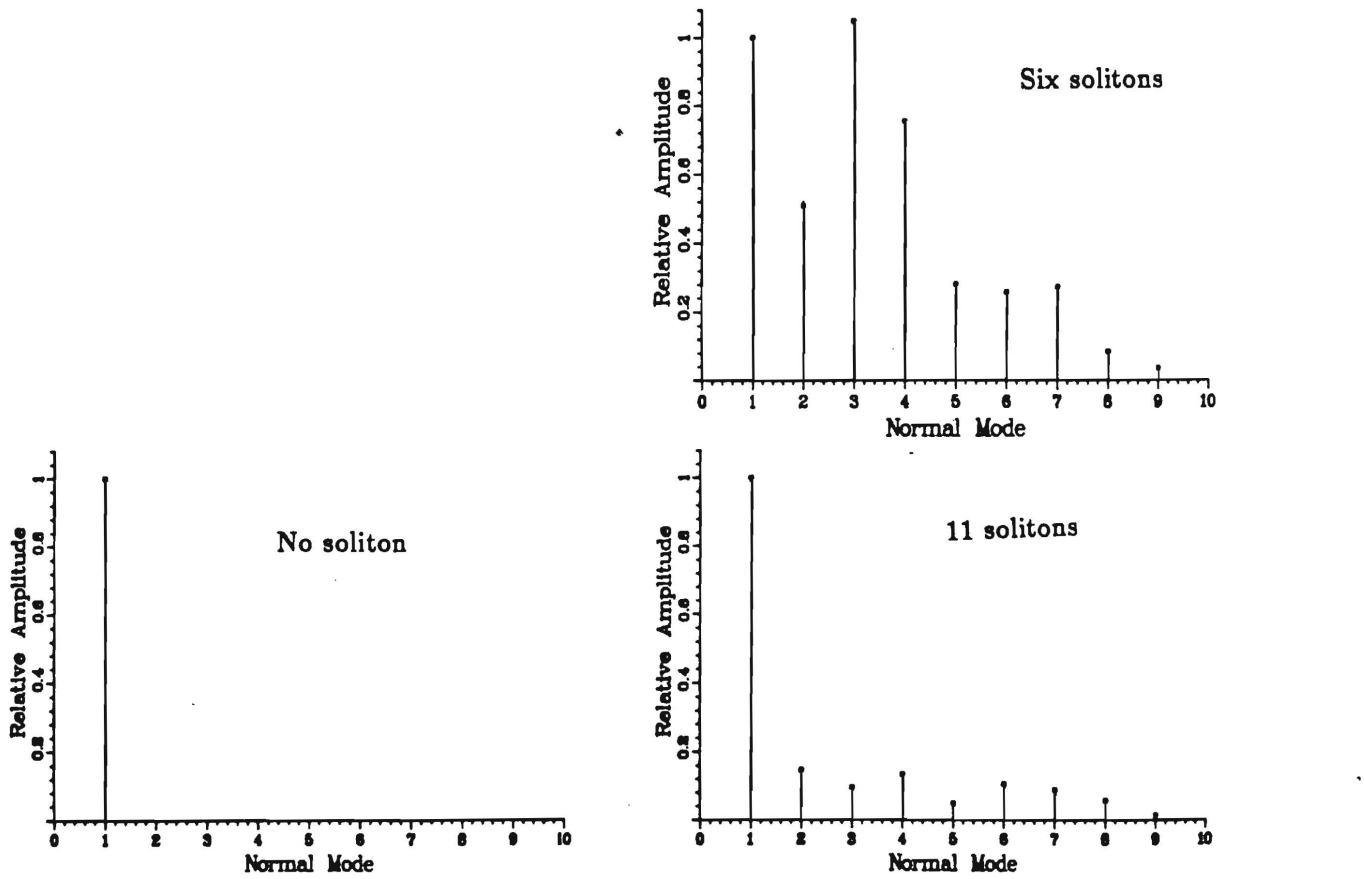

FIG. 16. The relative amplitudes of different modes at 18 km, showing packet length resonance of mode coupling. PE input field: mode 1. One packet beginning from 15 km. $f = 630$ Hz. $\lambda_i = 235$ m.

modes 1 and 3. Thus one would expect a significant amount of energy to be transfered from mode 1 to mode 3 (but not, say, to mode 2). Moreover, k_{int} is also reasonably close to the differences between the eigenvalues of modes 3 and 4 and between modes 4 and 6, etc. Hence, one would expect some transfer of energy from mode 1 to mode 4 via mode 3, or from mode 1 to mode 6 via modes 3 and 4, and so on. These simple arguments explain why a significant amount of energy is transferred from mode 1 into higher-order modes, especially modes 3 and 4, and why and where the acoustic wave frequency and soliton wavelength resonances occur.

The packet length resonance effect mentioned in Sec. IV is not so easily explained, and it is still not clear how to predict where it will occur. We present here a preliminary explanation for the phenomenon given by S. T. McDaniel.[36] If the backscattered field is neglected, the equation governing mode coupling between mth and nth modes due to range dependence of the ocean environment, can be expressed as [see Eq. (14) in Ref. 37 for notation]

$$\frac{du_n}{dr} = \frac{1}{2}\sum M_{nm} u_m \exp[i(\bar{k}_m - \bar{k}_n)r]. \tag{13}$$

Let a resonant coupling condition be

$$M_{nm} = -2K_L \exp[-i(\bar{k}_m - \bar{k}_n)r] \tag{14}$$

and $M_{mn} = -M_{nm}$. We consider only two modes, modes 1 and m, which are assumed to satisfy the resonant coupling condition. From Eqs. (13) and (14), we obtain

$$\frac{du_1}{dr} = -K_L u_m, \tag{15}$$

$$\frac{du_m}{dr} = K_L u_1, \tag{16}$$

or

$$\frac{d^2 u_{1,m}}{dr^2} + K_L^2 u_{1,m} = 0. \tag{17}$$

If all of the energy is assumed to be initially in the first mode ($u_1 = 1$ and $u_m = 0$) the solution to Eq. (17) is

$$u_1 = \cos(K_L r), \tag{18}$$

$$u_m = \sin(K_L r). \tag{19}$$

Equation (19) predicts that the magnitude of the excited higher-order modes will be periodic with range. The resonant coupling parameter K_L determines for what packet lengths u_m has a maximum value (or u_1 has a minimum value). From Eq. (19), the packet length "resonance" will occur when $K_L L_P = (n + 1/2)\pi$. From the first packet length resonance in Fig. 15(a), we have $K_L L_P = K_L \times 235 \times 6 = \pi/2$ and $K_L = 1.11$/km; from the second resonance length, we have $K_L L_p = K_L \times 235 \times 17 = 3\pi/2$ and $K_L = 1.18$/km. The two values obtained for K_L are almost the same. The agreement is quite satisfactory considering that the mode coupling occurred between more than just two modes (modes 1 and 3) and K_L would be changed with the coupling strength. The mode coupling is a periodic (resonance) function of the internal wave packet length, and, hence, acoustic transmission loss at long-range must vary with the packet length. It is shown that the "resonancelike" behavior of transmission loss predicted by the PE analysis in this paper is consistent with mode coupling theory.

VI. CONCLUSION

In summary, (1) we have briefly reviewed the characteristics of naturally occurring internal wave packets in the coastal zone which differ in many respects from open sea internal waves. We demonstrate that such internal wave packets can have a strong influence on low-frequency long-range sound propagation in shallow water. (2) The measured frequency response of sound propagation during the summer is often a strong function of both time and propagation direction, sometimes the sound propagation has an abnormally large attenuation over some frequency range. (3) Numerical calculations have shown that the interaction between the acoustic waves and internal wave packets and particularly resonance effects in the acoustic mode-coupling induced by internal wave packets could be an important loss mechanism for shallow-water sound propagation in the summer. Modal coupling induced by internal waves could explain the anomalous acoustic experimental results. (4) The fact that the acoustic mode-coupling induced by internal wave packets exhibits *frequency, soliton wavelength, and packet length resonances* [and perhaps existence of the Doppler shift alluded to in Sec. V, as well] suggest that low-frequency acoustic measurements could be used for remote monitoring of internal wave activity and extracting of hydrological and meteorological characteristics of the water mass in the coastal zone.

The analysis and numerical calculations presented here are based on a simplified oceanic model. Although the simplification should not alter the qualitative results presented, a more refined model would be desirable for a more detailed comparison with observations. It is, of course, also possible that some seabottom structure (for example, a surficial layer of low speed), mode-coupling due to the seabed roughness or sediment inhomogeneities and fish shoals could also produce an extra acoustic attenuation over some frequency range. It would thus be desirable for the acoustic, marine geology and geophysics communities including remote-sensing groups to work together to conduct joint at-sea experiments at a specific sea area. If data on internal wave activity (solitary or random), seabottom parameters, and sound propagation were obtained simultaneously and systematically, our understanding of the interaction between internal waves and sound waves in the coastal zone and low frequency acoustic propagation loss in shallow water would be greatly enhanced.

ACKNOWLEDGMENTS

This research was supported by ONR (Grant No. 00014-89-J-1839) and the IAAS. The authors wish to thank Dr. M. H. Orr for his support and valuable suggestions during the course of this research and Dr. S. T. McDaniel for her help in the explaining the packet length resonance. The at-sea experiment and data analysis on sound propagation were conducted under the support of the Chinese Academy of

Sciences, while Zhou and Zhang were at the IAAS. J. X. Zhou and X. Z. Zhang would like to express their appreciation to Professor D. Z. Wang and Professor D. H. Guan for their support and helpful comments, to their colleagues at the Institute of Acoustics, especially to E. S. Luo, B. C. Li and Y. Zhang for at-sea experimental assistance and for sharing experimental data.

[1] L. Baxter and M. H. Orr, "Fluctuations in sound transmission through internal waves associated with the thermocline: A computer model for acoustic transmission through sound velocity fields calculated from thermistor, CDT, XBT, and acoustic backscattering," J. Acoust. Soc. Am. **71**, 61–66 (1982).

[2] E. C. Shang, "Some new challenges in shallow water acoustics," in *Proceedings of 12th ICA Associated Symposium on Underwater Acoustics* (Tech. Univ. of Nova Scotia, Halifax, NS, 1986), pp. 149–152.

[3] D. H. Guan, "Invited lectures: Some recent progress in shallow water acoustics," Proc. 13th ICA **5**, 109–117 (1989).

[4] C. Garrett and W. Munk, "Internal waves in the ocean," Ann. Rev. Fluid Mech. **11**, 339–369 (1979).

[5] C. Garrett and W. Munk, "Space-time scales of internal waves," Geophys. Fluid Dyn. **2**, 225–264 (1972).

[6] D. Halpern, "Observation on short-period internal waves in Massachusetts Bay," J. Mar. Res. **29**, 116–132 (1972).

[7] L. R. Haury, M. G. Melboune, and M. H. Orr, "Tidally generated internal wave packets in Massachusetts Bay," Nature **278**, 312–317 (1979).

[8] M. H. Orr, "Remote acoustic sensing of the oceanic fluid and biological processes," Woods Hole Oceanogr. Inst. Tech. Rep. WHOI-80-2 (1980).

[9] A. R. Osborne and T. L. Burch, "Internal solitons in the Andaman Sea," Science **208**, 451–460 (1980).

[10] J. R. Apel and F. I. Gonzalez, "Nonlinear features of internal waves off Baja California as observed from the SEASAT imaging radar," J. Geophys. Res. **88**, 4459–4466 (1983).

[11] R. P. Trask and M. G. Briscoe, "Detection of Massachusetts Bay internal waves by the synthetic aperture radar (SAR) on SEASAT," J. Geophys. Res. **88**, 1789–1799 (1983).

[12] T. D. Allan, *Satellite Microwave Remote Sensing* (Horword, New York, 1983).

[13] L. L. Fu and B. Holt, "Internal waves in the Gulf of California: observation from a spaceborne radar," J. Geophys. Res. **89**, 2053–2060 (1984).

[14] H. Sandstrom and J. A. Elliott, "Internal tide and solitons on the Scotian Shelf: a nutrient pump at work," J. Geophys. Res. **89**, 6415–6426 (1984).

[15] A. K. Liu, J. R. Holbrook, and J. R. Apel, "Nonlinear internal wave evolution in the Sulu Sea," J. Phys. Oceanogr. **15**, 1613–1624 (1985).

[16] J. R. Apel, J. R. Holbrook, A. K. Liu, and J. J. Tsai, "The Sulu Sea internal soliton experiment," J. Phys. Oceanogr. **15**, 1625–1651 (1985).

[17] R. D. Pingree and G. T. Mardell, "Solitary internal waves in the Celtic Sea," Prog. Oceanogr. **14**, 431–441 (1985).

[18] I. S. Robinson, *Satellite Oceanography* (Wiley, New York, 1985).

[19] P. E. Holloway, "Internal hydraulic jumps and solitons at a shelf break region on the Australian North West Shelf," J. Geophys. Res. **92**, 5405–5416 (1987).

[20] R. F. Gasparovic, J. R. Apel, and E. S. Kasischke, "An overview of the SAR internal wave signature experiments," J. Geophys. Res. **93**, 12304–12316 (1988).

[21] A. K. Liu, "Analysis of Nonlinear internal waves in the New York Bight," J. Geophys. Res. **93**, 12317–12329 (1988).

[22] B. L. Gotwols and R. E. Sterner II, "Measurements of surface wave modulations from internal waves during the SAR internal wave signature experiment," J. Geophys. Res. **93**, 12330–12338 (1988).

[23] D. C. Honhart, *Oceanography from the Space Shuttle* (UCAR and ONR, Washington DC, 1989).

[24] K. H. Hunkins and M. Fliegel, "Internal Undular Surges in Seneca Lake: A Natural Occurrence of Solitons," J. Geophys. Res. **78**, 539–548 (1973).

[25] D. M. Farmer, "Observations of long nonlinear internal waves in a lake," J. Phys. Oceanogr. **8**, 63–73 (1978).

[26] J. X. Zhou, "Normal mode measurements and remote sensing of sea-bottom sound velocity and attenuation in shallow water," J. Acoust. Soc. Am. **78**, 1033–1008 (1985).

[27] J. X. Zhou, X. Z. Zhang, P. H. Rogers, and J. Jarzynski, "Geoacoustic parameters in a stratified sea bottom from shallow-water acoustic propagation," J. Acoust. Soc. Am. **78**, 2068–2074 (1987).

[28] Y. P. Zhang (private communication, 1983).

[29] O. S. Lee, "Effect of an internal wave on sound in the ocean," J. Acoust. Soc. Am. **33**, 677–681 (1961).

[30] J. X. Zhou, X. Z. Zhang, and P. H. Rogers, "Effect frequency dependence of sea-bottom attenuation on the optimum frequency for acoustic propagation in shallow water," J. Acoust. Soc. Am. **82**, 287–292 (1987).

[31] D. Lee and G. Botseas, "IFD: An implicit finite difference computer model for solving the parabolic equation," Naval Underwater Systems Center, New London, CT (1982), TR No. 6659.

[32] G. Botseas, D. Lee, and K. E. Gilbert, "IFD: Wide angle capability," Naval Underwater Systems Center, New London, CT (1983), TR No. 6905.

[33] D. Lee, "The State-of-the-art Parabolic Equation approximation as applied to underwater acoustic propagation with discussion on intensive computations," an invited paper at 108th ASA meeting, and NUSC Tech. Rep. 7247 (1984).

[34] L. B. Dozier and F. D. Tappert, "Statistics of normal mode amplitudes in a random ocean. 1. Theory," J. Acoust. Soc. Am. **63**, 353–365 (1978).

[35] S. T. McDaniel and D. F. McCammon, "Mode coupling and the environmental sensitivity of shallow-water propagation loss predictions," J. Acoust. Soc. Am. **82**, 217–223 (1987).

[36] This was pointed to us by Dr. S. T. McDaniel (private communication).

[37] S. T. McDaniel, "Mode coupling due to interaction with the seabed," J. Acoust. Soc. Am. **72**, 916–923 (1982).

ICA BEIJING 1992

THE EFFECTS OF INTERNAL SOLITONS OR BOTTOM RELIEF ON SOUND PROPAGATION IN SHALLOW WATER

Xue-zhen ZHANG and Ji-xun ZHOU

Institute of Acoustics, Academia Sinica, P.O.Box 2712, Beijing 100080, People's Republic of China and School of Mechanical Engineering, Georgia Institute of Technology, Atlanta, GA 30332, USA

Peter H. ROGERS

School of Mechanical Engineering, Georgia Institute of Technology, Atlanta, GA 30332, USA

Introduction

Strong bottom interaction, variable media and multipath propagation make shallow water acoustics very challenging. One of unexplained phenomenon for shallow water sound propagation, in the contrast with the so–called the optimum propagation frequency, is that high acoustic propagation loss over some frequency range is frequently reported[1–3]. Weston attributes such a phenomenon to fish activities[1]. In some case it is associated with sediment shear-wave resonances within the layer of sediment[2]. Fig. 1 shows a frequency response for shallow–water sound propagation in the summer (with a strong thermocline shown in Fig. 2) in the Yellow Sea off China, obtained by Zhou and his group at the IAAS[3]. Around 600 Hz and above 1100 Hz the transmission loss is abnormally large. Several years of observations, all made in August at the same area with a similar strong thermocline, have shown that the frequency responses of sound propagation is often a strong function of both time and propagation direction. The variability of the high loss frequency range and the apparent anisotropic characteristics of sound propagation occur with no obvious explanation in terms of fish swim bladder resonance. For the strong thermocline shown in Fig. 2, if both sound source and receiver are located beneath the thermocline, the sea surface influence on the long–range sound field(or lower modes) is negligible. While it might be possible that one could use the Weston fish model(or some other model) to quantitatively match the experimental data, we consider the possibility that the acoustic normal–mode conversion caused by internal soliton or bottom relief packets may also explain the data.

Ocean models

1. Internal soliton packets. Our numerical results have shown[3] that the acoustic mode–coupling induced by internal wave packets with a gated sine waveform (model I) exhibits frequency, soliton wavelength and packet length resonances. The interaction between the acoustic waves and internal wave packets could provide a plausible explanation for

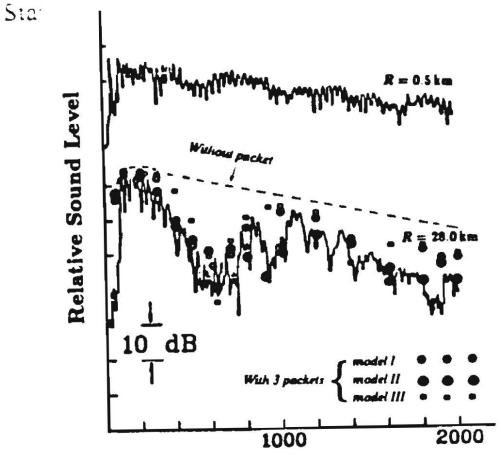

FIG. 1.

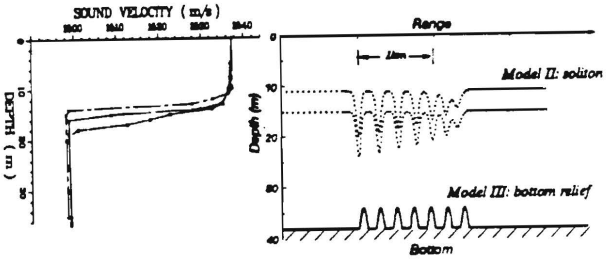

FIG. 2.

the observed anomalous propagation in the summer. Now we extend the model to consider the influence of the characteristic properties of more realistic oceanic soliton packets.

Solitons in shallow water ($h/\lambda_i << 1$) are described to first order in wave amplitude by the Korteweg-de Vries (KdV) equation: $A_t + C_0 A_x + \mu A A_x + \delta A_{xxx} = 0$. A solution to this equation is $A(x - ct) = a * sech^2(\frac{x-a}{L})$. The density (temperature) profiles corresponded to Fig. 2 is very reasonably described by a two–layer fluid model. The soliton phase speed c and wavelength λ_i(and scale parameter L) are then easy to obtain. When the initial solitary wave propagates, it often evolves more rank–ordered solitons and exhibits clear nonlinear features. Instead of the previous simple gated sine function, three packets with typical characteristics of internal solitons are used: the classical $sech^2$ soliton shape which decreases in wavelength and amplitude toward the rear of the packet(Model II, shown in Fig. 2).

2. Bottom relief group. For simplicity, we assume that an undulating seabed can be expressed by a half sine function, shown in Fig. 2(Model III).

Approach

The presence of internal soliton or bottom relief packets makes the environmental parameters range dependent. The parabolic equation (PE) model is used to numerically simulate the effect of internal soliton packets or bottom relief

groups on sound propagation in shallow water. We arbitrarily put three packets of solitons or bottom relief located at 5 km, 15 km and 25 km along propagation track. The PE method[4–5] is used to calculate the frequency response of acoustic transmission loss. When analyzing the characteristics of acoustic mode–coupling, we put just a single group of solitons or bottom relief at 15 km and use the first normal mode alone as the initial input field to the PE code (IFD). The acoustic field obtained using PE model is decomposed into the normal modes. The results are compared with mode–coupling theory[6–8] in order to improve our understanding of how mode conversion acts to become an important mechanism of acoustic attenuation in shallow water.

Results and discussion

1. Similar to model I and model III, internal wave packets with the classic characteristic properties of soliton could also cause abnormally large attenuation for acoustic propagation in shallow water. The differences between the results with and without the soliton packets is shown in Fig. 1 by • • • .

2. The interaction of sound waves with soliton or bottom relief group exhibits (signal) frequency, (radial inhomogeneity) wavelength and packet length resonances. As an example, the bottom relief wavelength and group length resonances are shown in Fig. 3 ($f = 630Hz, r = 30km$).

3. For a shallow water with a strong thermocline the apparent resonance interaction of sound waves with three ocean models could only occur under a specific circumstance: when the acoustic mode coupling caused by environmental parameter variation transfers a significant amount energy from lower mode into higher–order modes with much larger attenuation rate. For example, the PE field at $18km$ is decomposed to normal modes with the results shown in Fig. 4($f = 630Hz, r = 18km$). Apparently, after the interaction of the first mode with a packet at 15 km a significant amount energy has been coupled into higher–order modes.

4. The "resonacelike" behavior of transmission loss predicted by the PE analysis is consistent with mode coupling theory. Significant energy transfer will occur between mode m and n if $k_{inh} \approx k_m - k_n$, here k_{inh} is the wave number of the spectrum peak of the radial inhomogeneity. The mode coupling is a periodic (resonance) function of the soliton (or relief) group length.

5. The main intention of this work is to show what would happen to sound propagation if soliton or bottom relief packets are present, not to solve an inversion problem for internal waves or to determine sound propagation for a specific area. It is expected that any abnormal attenuation for sound propagation in a real shallow water environment might be caused by any combination of several different mechanisms, internal wave(or bottom relief) interaction must be considered as one such mechanism.

ACKNOWLEDGMENTS: Work Supported by the IAAS and ONR, USA.

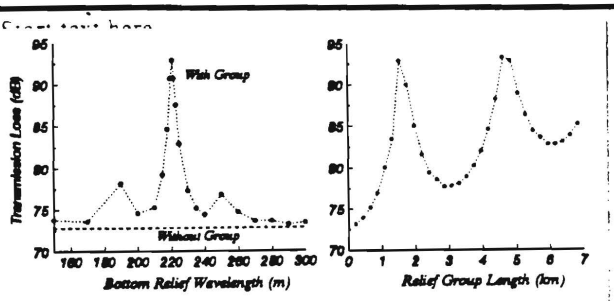

FIG. 3.

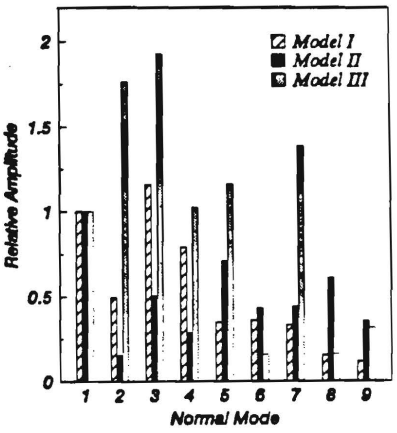

FIG. 4.

REFERENCES

1. W. E. Weston, *J. Sound Vib.* **18**, 499–510(1971).
2. S. J. Hughes, D. D. Elis, D. M. F. Chapman and P. R. Staal, *J. Acoust. Soc. Am.* **88**, 283–297(1990).
3. J. X. Zhou, X. Z. Zhang and P. H. Rogers, *J. Acoust. Soc. Am.* **90**, 2042-2054(1991).
4. D. Lee and G. Botseas, Naval Underwater Systems Center, New London, CT (1982), TR No.6659.
5. G. Botseas, D. Lee and K. E. Gilbert, Naval Underwater Systems Center, New London, CT (1983), TR No.6905.
6. L. B. Dozier and F. D. Tappert, *J. Acoust. Soc. Am.* **63** , 353–365(1978).
7. S. T. McDaniel and D. F. McCammon, *J. Acoust. Soc. Am.* **82**, 217–223(1987).
8. S. T. McDaniel, *J. Acoust. Soc. Am.* **72**, 916–923(1982).

IEEE Proc. OCEANS '93, 1, 87-92 (1993).

Anomalous Sound Propagation in Shallow Water due to Internal Wave Solitons *

Ji-Xun Zhou, Xue-Zhen Zhang and Peter H. Rogers
(School of Mechanical Engineering, Georgia Institute of Technology, Atlanta, GA 30332, USA)
Dezhao Wang and Ensheng Luo
(Institute of Acoustics, Academia Sinica, Beijing 100080, People's Republic of China)

Abstract - **At-sea experimental data and numerical simulation results will be given to show that, acoustic normal-mode coupling induced by internal solitons could be an important loss mechanism for shallow water sound propagation.**

I. INTRODUCTION

Strong boundary interactions, multipath propagation and an amazingly complex waveguide environment make shallow water acoustics very challenging. In the summer, with warming of the surface water, the strong and well defined thermoclines associated with internal waves occur very often for many coastal zones of the world. Under such circumstances the variability of the water column (due to the internal waves) and the strong bottom interaction (due to the negative gradient velocity profile) cause some sound propagation phenomena that have not been well understood. In this paper, one "Summer Effect", the acoustic mode–coupling attenuation caused by solitary internal waves, is discussed.

The geophysics, fluid mechanics and remote sensing communities have investigated the mechanisms for the generation and propagation of internal waves in the coastal zone. Analysis of extensive data has shown that these naturally occurring waves exhibit the properties of solitons. They are very different from deep sea internal waves. Unfortunately, no reported measurements of such solitary waves include simultaneous measurement of long-range sound propagation. Moreover, the acoustic community has paid little attention to possible effects of tidally generated internal *soliton features* on sound propagation in shallow water.

Acoustic experiments have shown that the frequency response of sound propagation in the summer is often a strong function of time and propagation direction, and sometimes exhibits an abnormally large attenuation over some frequency range. This anomalous, anisotropic frequency response can not be explained by conventional sound propagation models. Zhou, Zhang and Rogers have hypothesized a new possible attenuation mechanism to explain these results; acoustic normal mode coupling caused by internal waves[1]. In this paper, the numerical simulation of this mechanism is extended to more realistic solitons with classic characteristic properties. Additional experimental data are offered to support the hypothesis of a soliton scattering loss mechanism.

II. AT-SEA ACOUSTIC EXPERIMENTS

At-sea acoustic experiments were conducted by the IAAS Shallow Water Acoustics Group over a four-year period at the Yellow Sea. The sea bottom in the whole area is flat without apparent layer structure. The mean grain diameter of the surficial sediment (M_d) is approximately 0.0492 mm; 38.9% is sand, 40.3% is silt and 20.8% is clay. The averaged ratio of the sediment and water sound speeds $C_{bottom}/C_{water} \approx 1.06$. The bottom attenuation $\alpha \approx 0.34\ f^{1.84}$ dB/m/kHz.

1) Strong Thermocline At the test area strong thermoclines with more than $10°C$ temperature difference are often present during the summer. Average sound velocity profiles obtained at the receiving ship location

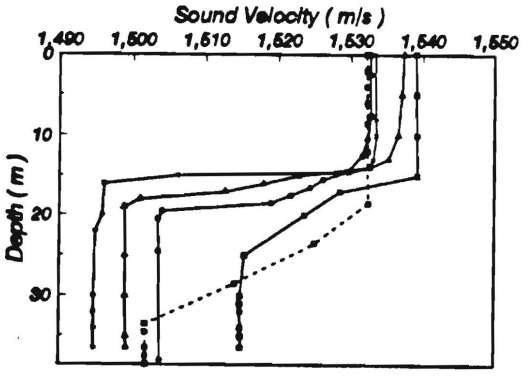

Fig. 1 Sound speed profiles.

for 4 years are shown by solid lines in Fig. 1. For a fixed location, the thermocline depth changed with time and for a given depth close to the thermocline, the temperature varied with time. This indicated the possible presence of solitary waves in the area[1].

2) Apparent Sound Signal fluctuation Internal waves can result in acoustic signal fluctuation. Fig. 2

* This work was supported by ONR, USA and the IAAS.

0-7803-1385-2/93/$3.00

Encl (A)

shows a set of experimental data. The source was an electrodynamic transducer fixed at 1 m above the sea bottom, transmitting a 442 Hz CW signal. A receiving

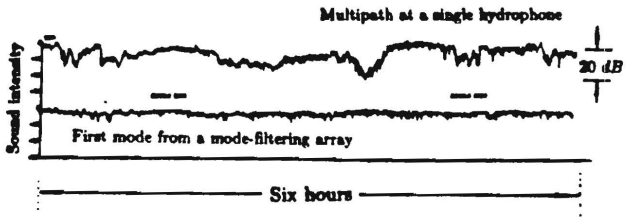

Fig. 2 442 Hz CW signal fluctuation.

hydrophone array was located at 3 km away. The upper curve in Fig. 2 is sound pressure level in dB, obtained during a six hour period by a single hydrophone which was below the thermocline. The lower curve was obtained by using the array as a normal mode filter for the first mode. For the single hydrophone, slow oscillations of up to 29 dB in level have been observed. For the first mode (which propagates principally below the thermocline) there are no apparent slow fluctuations. The time scales of the slow fluctuations received by a single hydrophone possess the characteristics of internal waves. The fluctuations might be explained as the interference between different acoustic normal modes, some of which pass through internal waves.

3) Transmission Loss with Strong Depth Dependence Strong thermoclines such as those shown in Fig. 1 separate the water column into two clear propagation

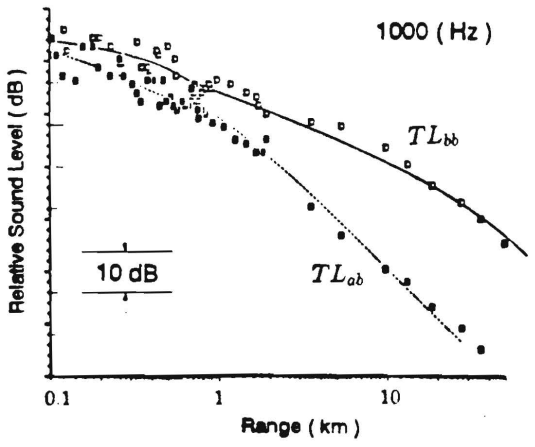

Fig. 3 Strong source/receiver depth dependence for sound propagation.

channels. The main propagation channel is the lower part of the water column below the thermocline, where the sound speed is much lower. If both source and receiver are located below the thermocline, the acoustic transmission loss (TL_{bb}) is similar to that in a Pekeris shallow water waveguide. If a sound source and a receiver are separately located above and below the thermocline, the transmission loss TL_{ab} would be much larger than TL_{bb}. Fig. 3 shows experimental data obtained in the summer. The strong thermocline in the area results in a very strong source/receiver depth dependence for sound propagation.

4) Unexplained Phenomenon : A great deal of acoustic data was collected over several years in the same area. The data included measurements of sound propagation, long-range reverberation, sound field spatial coherence and mode spatial filtering. Generally speaking, the experimental data fit theoretical prediction very well[2-4]. However, one unexplained phenomenon is that an unusually high propagation loss is often observed over some frequency range. An example is shown in Fig.4. Both sound source and receiver

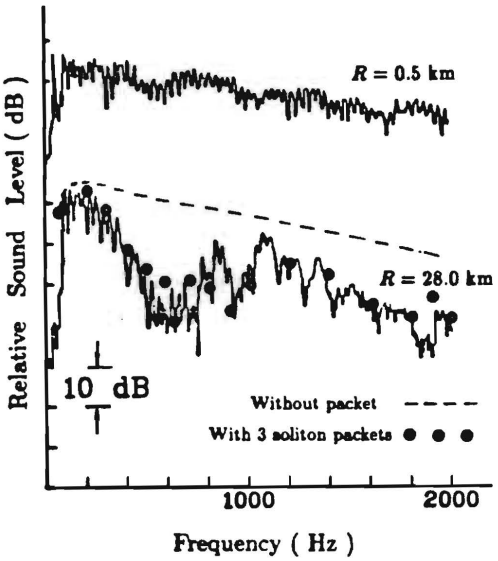

Fig. 4 Explosive signal power spectrum for shallow water sound propagation in the summer which exhibits an abnormal high loss. Hypothesized soliton interaction model (● ● ●) can explain the experimental data (see Sec. IV).

were below the thermocline. The difference between two power spectra is a measure of the sound transmission loss (both sound source and receiver were below the thermocline). Between 300 Hz and 1100 Hz (especially around 600 Hz), and above 1100 Hz, we observed abnormal attenuation. Four years' observation has shown that even along the same experimental track, with similar average sound-speed profiles the frequency response of sound transmission, and the abnormal attenuation frequency range would often be very different in different years. In one experiment, during a spring tide period , the sound speed profile obtained at the receiving ship was similar to other years, but at a location 28 km away from the receiver, a sound speed profile shown by the dashed curve

in Fig. 1 was obtained. This implies that there was a strong horizontal gradient of the sound-speed profile in the area. We fixed the receiver ship, and kept transmission distance at 28 km, by moving the source ship along *a quarter of circle*. For six propagation directions (at 18° intervals) in two hours we observed six different frequency responses as shown in Fig. 5. (Both sound source and receiver were below the thermocline). At some

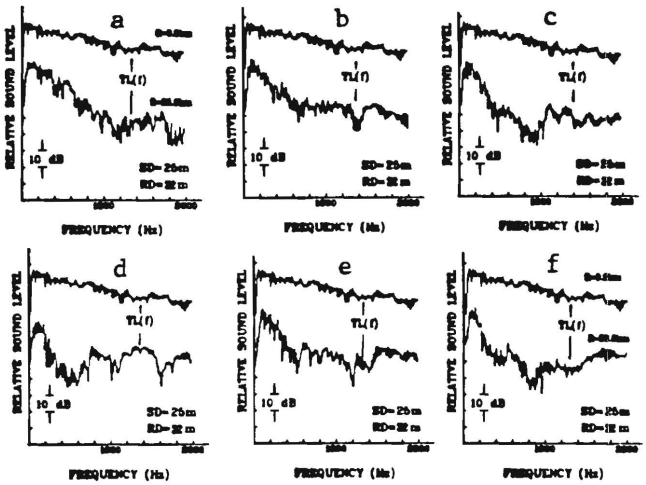

Fig. 5 Acoustic transmission loss (TL) *vs.* propagation direction.

frequencies, for different directions, the sound intensity varied as much as 25 dB ! However at the same place, in a different year, two orthogonal propagation directions were observed to have almost identical frequency responses.

In summary, sound propagation in shallow water with a strong summer thermocline is often a strong function of time and propagation direction, and sometimes exhibits an abnormally large attenuation over some frequency range. Abnormally high propagation loss in shallow water over a certain frequency range may be caused by the shear-wave resonance in the sediment layer[5] or by the interface waves of the Stoneley type at the sediment-substrate interface[6]. Our observations, however, must be attributed to an intermittent phenomenon which specially occurs in the summer. We hypothesize that an attenuation mechanism based on the interaction of sound wave with internal solitons can explain these observations.

III. CLASSIC CHARACTERISTICS OF INTERNAL SOLITONS

Some notable papers on soliton observation have been given in Ref. 1. The characteristic properties of internal solitons can be summarized as follows:

1. Internal waves in the coastal zone are frequently observed in deterministic groups with well–defined wavelengths which can be described as internal solitary waves. These waves are usually observed in Summer when they are trapped in a strong and shallow seasonal thermocline.

2. Solitons in shallow water are described to first order in wave amplitude by the Korteweg-de Vries (KdV) equation. When the initial solitary wave propagates, it often evolves more rank–ordered solitons and exhibits clear nonlinear features: higher–than–linear group velocity, and decreases in wavelength, crest length and amplitude toward the rear of the packet.

3. The number of wave packets is highly correlated with the strength of the local tides: the maximum number occurs during spring tides. Whether or not they occur is critically dependent on the structure of the background shear and stratification profiles.

4. Solitary wave packets propagate shoreward.

5. Because of the shallowness of the thermocline and the large amplitude of the coastal internal waves, strong surface expressions of solitons have been observed with photographs and synthetic aperture radar(SAR) on satellites and space shuttles.

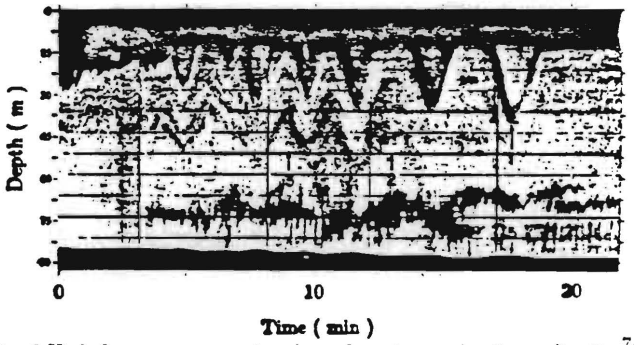

Fig. 6 High frequency acoustic echoes from internal solitons (by Orr[7])

Fig. 6 is an excellent acoustic record of internal solitons. It was obtained by Orr using high-frequency down–looking sonar in the Massachusetts Bay[7].

IV. NUMERICAL SIMULATION OF SOUND PROPAGATION

Using the parabolic equation propagation model[8], Zhou, Zhang and Rogers numerically simulated the interaction of sound waves with internal solitons[1]. Due to the lack of data needed to construct a definite internal soliton model for the Yellow Sea, for simplification and to give a clear physical picture of the problem, it was assumed that the internal wave packets had a gated sine waveform. The numerical results showed that the interaction exhibits frequency resonance, soliton wavelength resonance and packet length resonance. Under resonance conditions, the acoustic mode-coupling induced by the

internal waves can transfer a significant amount of energy from lower modes to higher, lossier modes, and become an important loss mechanism. Decomposing the PE sound field into normal modes, it has been shown that the resonance behavior is consistent with mode coupling theory[9-11]. In this paper, the numerical simulation is extended to include the classic characteristic properties of more realistic ocean soliton packets: large amplitude, $sech^2$ waveforms which decrease in wavelength and amplitude toward the rear of the packet.

Internal solitons obey the KdV equation:

$$A_t + C_0 A_r + \mu A A_r + \delta A_{rrr} = 0 \tag{1}$$

An important solution to Eq. 1 is

$$A(r,t) = -a * sech^2(\frac{r - Ct}{L}) \tag{2}$$

The density profiles in the experimental area are well described by a two-layer fluid model. The upper, warm layer is assumed to have depth h_1 and density ρ_1; for the lower layer (below the thermocline) the respective quantities are h_2 and ρ_2. $A(r,t)$ is the interface (soliton) displacement between the two fluids. When $\rho_1 \approx \rho_2 \approx \rho$, the constant coefficients of Eq. 1 can be expressed as[12]

$$C_0 = [g\frac{\Delta\rho}{\rho}\frac{h_1 h_2}{h_1 + h_2}]^{1/2} \tag{3}$$

$$\mu \approx -\frac{3}{2}[\frac{h_2 - h_1}{h_1 h_2}]C_0 \tag{4}$$

$$\delta \approx C_0 h_1 h_2 / 6 \tag{5}$$

The soliton phase speed C and the scale length L are

$$C = C_0[1 + \frac{a}{2}(\frac{h_2 - h_1}{h_1 h_2})] \tag{6}$$

$$L^2 = \frac{4}{3}\frac{h_1^2 h_2^2}{(h_2 - h_1)\, a} \tag{7}$$

From density profiles in the experimental area, $\Delta\rho = (\rho_1 - \rho_2) \approx 3.7$, $\rho \approx 1024.7\ kg/m^3$. If $h_1 = 13$ m and $h_2 = 25$m, then the linear wave speed $C_0 \approx 0.55$ m/s. Because we do not have enough data to construct a definite soliton model for the Yellow Sea, we assume that each internal wave packet consists of seven solitons, and can be expressed as:

$$Z = Z_0 + F(r)$$

$$F(r) = -\sum_{i=1}^{7} a_i \Delta_i sech^2\left(\frac{r - r_i}{L_i}\right) \tag{8}$$

$$\Delta_i = \begin{cases} 1 & \text{for } |r - r_i| \le 4L_i \\ 0 & \text{for } other \end{cases}$$

The amplitude and scale length of each soliton in a group are related to its speed by (6-7). The a_i are selected to match numerical results with experimental data. The a_i are between 9 m and 1.3 m. The a resultant soliton packet waveform is shown in Fig. 7. It corresponds to a decrease in amplitude (from 9 m to 3 m) and wavelength (from 270 m to 145 m) toward the rear of the packet.

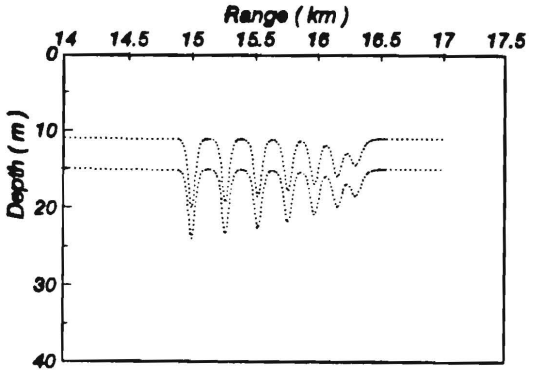

Fig. 7 Internal soliton model.

The PE method is used to calculate the frequency response of acoustic transmission loss. Using the internal wave model of Fig. 7, we put three such soliton packets at 5, 15, and 25 km along sound propagation track. In this case , if both sound source and receiver are located below the thermocline, the numerical transmission loss at 28 km as a function of frequency shown (in Fig.4 by the circles) fits the experimental data very well. In order to investigate the acoustic normal mode-coupling

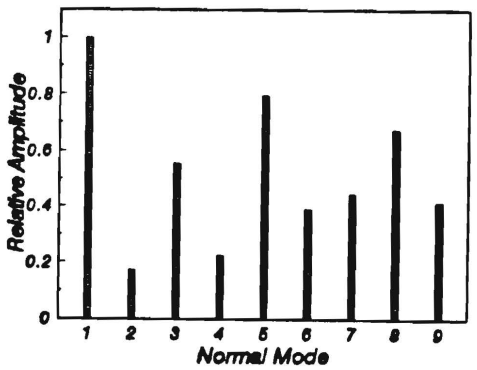

Fig. 8 Mode coupling from mode 1 into higher-order modes.

induced by internal solitons, we put a single packet like that of Fig. 7 at 15 km, and use the first normal mode alone as the initial input field to the PE code. Prior to interaction with the packet (or without the packet), only the first mode is present. After the interaction of the fist mode with the soliton packet, we decompose the PE

calculated sound field into normal modes. Fig. 8 shows the relative modal amplitudes at 17 km for 630 Hz.

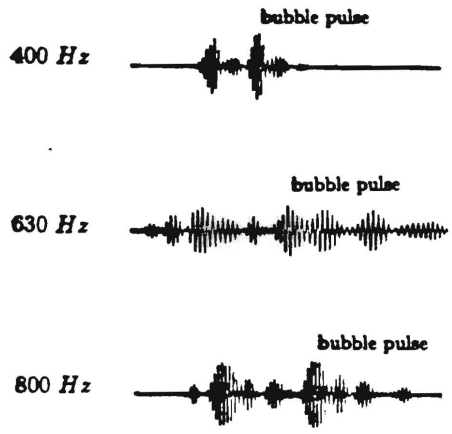

Fig. 9 Explosive propagation signal waveforms (1/3 Oct.)

A significant amount of energy has been transferred from mode 1 into higher-order modes that will attenuate rapidly thereafter. Thus modal coupling due to internal waves can become important attenuation mechanism for summer sound propagation in the Yellow Sea. Fig. 9 is a set of 1/3 Oct. waveforms for explosive propagation signal received at 37 km. For 400 Hz or 800 Hz, one can distinguish a few different modes, such as mode 1, mode 2 etc. But at 630 Hz, the signal suffers significant spreading in the time domain. It seems that many modes are involved, and it is hard to distinguish individual modes. The observed waveforms are in good agreement with our numerical prediction, and support the soliton scattering hypothesis.

V. DISCUSSION AND CONCLUSION

The numerical results have shown that internal wave packets with the classic characteristic properties of soliton can significantly change the acoustic transmission loss. All of our earlier conclusions obtained for internal wave packets with a gated sine waveform[1] are qualitatively validated here. The acoustic mode-coupling induced by internal solitons could be an important attenuation mechanism in shallow water with a strong summer thermocline.

The required presence of a *strong thermocline* is key to understanding this new hypothesized mechanism for the Yellow Sea. As an example, for a summer sound speed profile , we have normal mode eigenfunctions for the first 8 modes shown in Fig. 10 (at 630 Hz). If both source and receiver are located below the thermocline, for higher frequencies and at long range, because of mode stripping the lower modes will dominate the sound field. The thermocline looks like upper boundary of the main channel. The acoustic transmission loss (TL_{bb}) is similar to that in a Pekeris shallow water waveguide. If a sound source is located above thermocline, and a receiver located below the thermocline, mainly high-order modes with higher attenuation rates can be excited or received, transmission loss (TL_{ab}) would be much larger than (TL_{bb}). The experimental data for sound propagation in Fig. 3 clearly exhibit such characteristics. Resonant interaction of sound waves with internal solitons[1] causes acoustic mode-coupling which can transfer a significant amount energy from lower modes to higher modes, i.e., change the transmission loss from TL_{bb} to TL_{ab}.

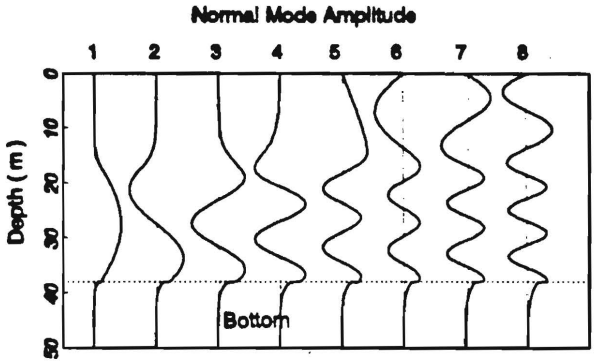

Fig. 10 Normal mode function for strong thermocline (630 Hz).

Based on his early observations in the Bristol Channel, Weston[13] has claimed that internal wave scattering "results in fluctuation rather than attenuation", and hypothesized that the abnormal sound attenuation in the Yellow Sea discussed in Section II is caused by fish absorption and scattering. It is well accepted that the internal wave scattering results in fluctuation (see our results shown in Fig. 2.) Although fish absorption and scattering are acceptable, in general, as an acoustic loss mechanism, it is not necessarily correct here. The main problem is that Weston overlooks the *big difference in the sound speed profiles* between the Yellow Sea and the Bristol Channel. In the Bristol Channel the thermocline is very weak, the temperature difference between the surface and bottom never exceeds half centigrade degree at any time of year. Unlike the Yellow Sea in the summer where there are two propagation channels, the Bristol Channel is basically similar to a Pekeris shallow water waveguide. For the frequency range we are interested, lower modes would propagate over the whole water column. This is very different from the situation in the Yellow Sea. In the Yellow Sea the lower modes basically propagate below the thermocline (see Fig. 10), and the sea surface effects are negligible. The difference of attenuation rates between lower modes and higher modes in the Bristol Channel would not be as large as in the Yellow Sea (see [1]). The transmission loss in the Bristol Channel would not have as strong source/receiver depth dependence as the Yellow Sea shown in Fig. 3. Thus, if there

were the acoustic mode-coupling induced by internal solitons in the Bristol Channel, it would have very different characteristics from that for the Yellow Sea. Moreover, the observed frequency responses of sound propagation in the Yellow sea (such as in Fig.4 & Fig. 5) do not exhibit the classic characteristics, associated with swim-bladder resonance. For example, in Fig.4 the abnormal attenuation not only occurs between 300 Hz and 1100 Hz, but also above 1100 Hz. The frequency responses in Fig. 5 were obtained from a very small area in two hours, which are very different along six different propagation direction. The experimental area is not a fishing ground. It is very hard to believe that there were so many fish producing such different effects on sound propagation. Fig. 11 shows average power spectra obtained from several explosive signals. These data contradict the fish attenuation hypothesis for the Yellow Sea case. The hydrophone was located below the thermocline. Explosive sources were detonated separately at 6 m and 25 m. At a distance of 28 km, we obtained two curves which correspond TL_{bb} (the same as Fig. 5f) and TL_{ab}. If fish absorption and

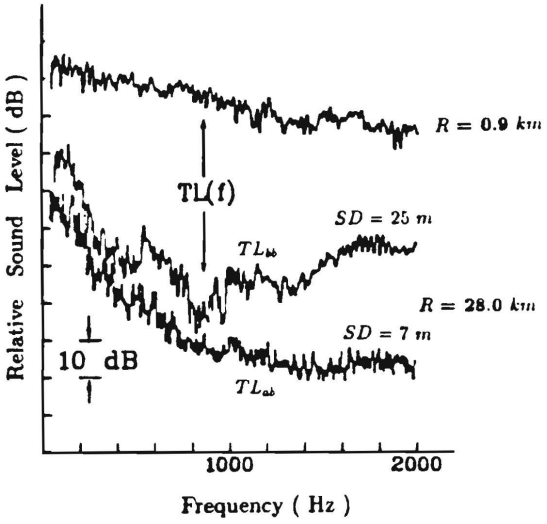

Fig. 11 TL *vs.* detonation depth of the explosive source.

scattering caused the large attenuation for TL_{bb} (i.e., for lower modes) between 300 Hz and 1600 Hz (especially around 800 Hz), it should have similar effect on TL_{ab} (for higher-order modes) in same frequency range. But this did not happen; the experimental data do not support the fish hypothesis. The case is much stronger for solitons in the present application.

Internal solitons can significantly influence oceanic current measurements, undersea navigation and antisubmarine warfare operation. Knowledge of internal wave behavior is necessary for the design of offshore production facilities. The resonant acoustic mode-coupling induced by internal soliton packets suggests that the low frequency acoustic measurements could be used for remote monitoring internal wave activity and for extracting hydrological characteristics of the water column in the coastal zone. In order to fully prove soliton loss mechanism, and to enhance our understanding of interaction of sound waves with internal solitons, it would be desirable for the acoustic, geophysics and marine biologic communities including remote-sensing groups to conduct joint at-sea experiments.

REFERENCES

[1] J. X. Zhou, X. Z. Zhang and P. H. Rogers, "Resonant interaction of sound wave with internal solitons in the coastal zone," J. Acoust. Soc. Am. **90**, 2042-2054 (1991).

[2] J.X. Zhou, " Normal mode measurements and remote sensing of sea-bottom sound velocity and attenuation in shallow water," J. Acoust. Soc. Am. **78**, 1033-1008 (1985).

[3] J.X. Zhou, X.Z. Zhang and P. H. Rogers, " Effect of frequency dependence of sea-bottom attenuation on the optimum frequency for acoustic propagation in shallow water, " J. Acoust. Soc. Am. **82**, 287-292 (1987).

[4] J.X. Zhou, X.Z. Zhang, P. H. Rogers and J. Jarzynski, "Geoacoustic parameters in a stratified sea bottom from shallow water acoustic propagation, " J. Acoust. Soc. Am. **8**, 2068-2074 (1987).

[5] S. J. Hughes, D. D. Elis, D. M. F. Chapman and P. R. Staal, "Low-frequency acoustic propagation loss in shallow water over hard-rock seabeds covered by a thin layer of elastic-solid sediment," J. Acoust. Soc. Am. **88**, 283–297(1990).

[6] J.M. Hovem and A. Kristensen, "Reflection loss at a bottom with a fluid sediment layer over a hard solid half-space", J. Acoust. Soc. Am. **92**, 335-340(1992).

[7] M.H. Orr "Remote acoustic sensing of the oceanic fluid and biological process," Woods Hole Oceanogr. Inst. Tech. Rep. WHOI-80-2 (1980).

[8] G.Botseas, D.Lee, and K.E. Gilbert, "IFD: Wide angle capability," Naval Underwater System Center, New London, CT (1983), TR No.6905.

[9] L.B. Dozier and F.D. Tappert, "Statistics of normal mode amplitudes in a random ocean. 1. Theory," J. Acoust. Soc. Am. **63**, 353-365 (1978).

[10] S. T. McDaniel, "Mode coupling due to interaction with the seabed," J. Acoust. Soc. Am. **72**, 916-923 (1982).

[11] S.T. McDaniel and D.F. McCammon, "Mode coupling and the environmental sensitivity of shallow-water propagation loss predictions," J. Acoust. Soc. Am. **82**, 217-223 (1987).

[12] A. R. Osborne and T.L. Burch, "Internal solitons in the Andaman Sea," Science **208**, 451-460 (1980).

[13] D.E. Weston, "Mechanisms of ocean acoustic attenuation: Scattering by internal solitons, by sea surface waves, and by fish," J. Acoust. Soc. Am. **92**, 3435-3437 (1992).

IEEE Proc. OCEANS '96, 1, 1-8 (1996).

Modal Characteristics of Acoustic Signal Fluctuations Induced by Shallow Water Internal Waves *

Ji-Xun Zhou and Xue-Zhen Zhang
(School of Mechanical Engineering, Georgia Institute of Technology, Atlanta, GA 30332, USA
and Institute of Acoustics, Academia Sinica, Beijing 100080, People's Republic of China)

Peter H. Rogers
(School of Mechanical Engineering, Georgia Institute of Technology, Atlanta, GA 30332, USA)

Abstract - **Measured internal waves from the Yellow Sea and the Massachusetts Bay are used as inputs into numerical simulation on acoustic fluctuations. It is shown that the fluctuations induced by large amplitude shallow-water internal waves strongly depend on receiver depth and distance, and exhibit anisotropy. Different acoustic modes have different sensitivities to internal waves. Both acoustic intensity and phase fluctuation spectra are different from the shallow-water IW spectrum, and become much broader. Individual acoustic mode fluctuations directly and clearly correspond to the characteristics of IWs. For shallow water with a strong thermocline, there is a group of acoustic modes, arrival time variation of which is more sensitive to IWs than others. Arrival time of the first mode is most stable.**

I. INTRODUCTION

The shallow water acoustic environment is characterized by extreme variability. One of the causes in water column variability is the existence of internal waves. In general, IWs have often been observed with a very different character in shallow water versus deep water. The broadband Garrett-Munk spectrum of IWs describes only the background fraction of the IW spectral density, which decreases monotonically as the frequency increases. The spectral density of shallow water IWs, measured within the season thermocline, exceeds the GM spectrum level over the whole frequency range and, almost always, exhibits peaks and plateaus at high frequencies. In these particular frequency ranges, IWs show a significant intermittence, high amplitudes, quasi-sinusoidal behavior in both time and space domains, and a narrow bandwidth, characterized by large-amplitude soliton packets. [1-4]

In recent years, acoustic interactions with IWs in shallow water have attracted increasing interest in shallow water acoustics[3-18]. It has been shown that the resonant mode-coupling between the lower-order acoustic modes and the very lossy, higher-order modes, induced by shallow-water internal waves (no matter whether they are linear or nonlinear), could be a potentially important loss mechanism for summer sound propagation in some shallow water areas. It was hypothesized that an IW caused anomalous, anisotropic transmission loss observed in acoustic data taken in the Yellow Sea[3,6]. The mode-coupling hypothesis has been analytically tested and supported by King *et al.*[7,8], Chin-Bing *et al.*[9], and Broadhead and Ali[10]. Using a horizontal hydrophone array, Rubenstein and Brill [11] and Shmelerv *et al.*[12] examined internal wave induced phase front curvature in shallow water. Bondar' *et al.*[13-14] and Borisov *et al.*[1,18] measured intensity and phase fluctuation of low-frequency acoustic signals along stationary tracks in shallow water. Lynch *et al.* and Traykovski used modal and ray based techniques to study acoustic travel-time fluctuations due to shallow water internal waves [5,16]. Tielbuerger *et al.* analyzed sound field intensity fluctuations (the scintillation index) in a stochastic shallow water, caused by broadband IWs plus large-amplitude solitary waves[17] .

In this paper, we will discuss acoustic signal fluctuation caused by shallow water IWs. Special attention will be given to the analysis of the modal characteristics of acoustic interactions with internal waves, i.e., acoustic modal sensitivity to internal waves. Analyses of individual acoustic mode interactions with internal waves should permit both a qualitative and quantitative understanding of the effects of internal waves on multimode signal fluctuations. In Sec. I, a set of Yellow Sea experimental data is introduced . Then, measured IWs in the Yellow Sea are used as input parameters to simulate IW- caused acoustic fluctuations, and to explain the observed signal fluctuation characteristics. In Sec. II, a typical internal soliton packet, measured by Orr in the Massachusetts Bay [19], will be used to analyze the effects of large amplitude IWs on acoustic fluctuations in shallow water. Intensity and phase fluctuations of both multipath signal and individual modes, as well as their spectra, will be analyzed.

II. ACOUSTIC SIGNAL FLUCTUATIONS DUE TO SHALLOW WATER INTERNAL WAVES

* This work was supported by ONR, USA and the IAAS.

0-7803-3519-8/96 $5.00 © 1996 IEEE

Encl. (B)

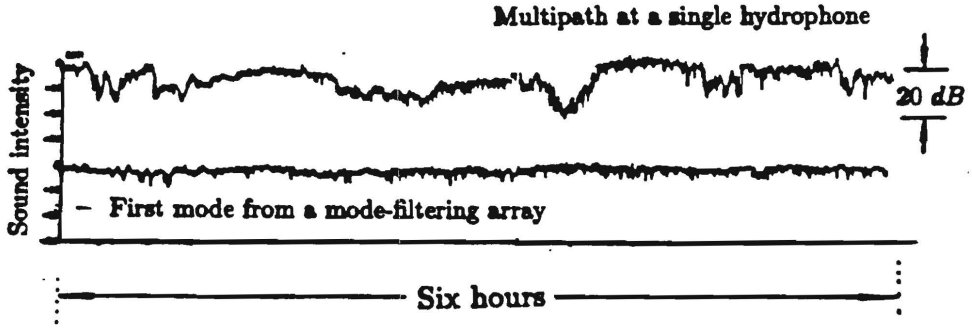

Fig. 1 442 Hz CW signal fluctuations in the Yellow Sea.

It is well known that internal waves can result in acoustic signal fluctuations. Due to the nonlinear large amplitude characteristics of shallow water internal waves, low-frequency acoustic intensity variations, caused by internal waves in shallow water, often reach 20 dB [11,13].

Figure 1 shows a set of signal fluctuation data obtained in August 1981 in the Yellow Sea with a water depth of 36.5 m. The upper curve is a multimode signal obtained at a single hydrophone which was located below the thermocline (RD=25.5m). The lower curve was obtained by using an array in a whole water column as a normal mode filter for the first mode. Both were obtained from a fixed 442 Hz CW source which was located 3 km away (SD=35.5m). For the single hydrophone, slow oscillations of up to 28 dB in level are observed, which are similar to other observations [11,13]. For the first mode, however, there are no comparable slow fluctuations. In the next section, we will show that these characteristics can be explained by internal wave interactions.

B. Numerical Simulation

In July 1993, a research group at the Institute of Acoustic, the Chinese Academy of Sciences measured internal wave field in the Yellow Sea [20] . Fig. 2 shows a set of IWs recorded at a site which is close to where the acoustic fluctuation data shown in Fig. 1 were obtained. Unfortunately, due to low-pass filtering and time averaging, important high frequency characteristics of the internal waves are not present, and directional information is unavailable.

We use Fig. 2 to calculate the internal wave induced signal fluctuations. Locally, we assume the internal waves to be plane wave. A sound wave of 442 Hz propagates perpendicularly to the IW propagation direction. For comparing with the measurement shown in Fig. 1, we assume that over a range of 3 km, all SVPs between the source and the receiver vary simultaneously as the internal wave time series shown in Fig. 2. Using these SVP time series in a two-dimensional (2-D) adiabatic normal mode model, we get the intensity fluctuations for a multimode signal and the first mode shown in Fig. 3. (This 2-D treatment that horizontal refraction and azimuthal scattering of sound are negligible.)

The numerical results show that the multimode signal has slow, strong fluctuations (maximum variation up to 28 dB), but the intensity of the first mode (dash line) remains almost constant. The numerical results of the

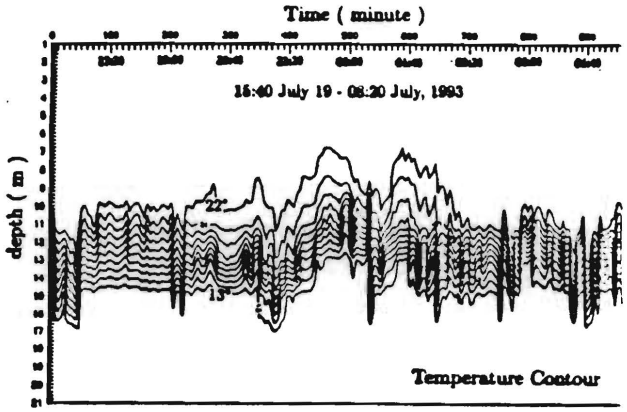

Fig. 2. Internal wave field in the Yellow Sea

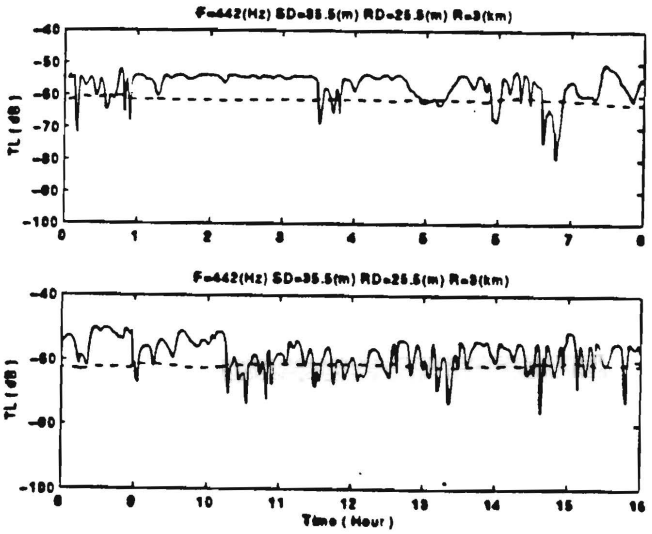

Fig. 3 Numerical results on sound fluctuations due to IWs; sound wave propagates parallel to IW fronts.

first six hours are very similar to the experimental data shown in Fig. 1. This is just a coincidence.

In Fig. 4, we repeat the above computations but the sound waves propagate parallel to the IW propagation direction. Assuming that the internal wave speed is 0.55 m/s and using a PE code, we calculate sound intensity fluctuations. The results indicate that the intensity fluctuations are smaller than in the case when sound propagates parallel to IW fronts. That is, acoustic signal fluctuations, induced by shallow water IWs, should exhibit strong horizontal anisotropies. Acoustic signal intensity fluctuations, simultaneously measured in different directions, might offer some information about the internal wave propagation direction in shallow water.

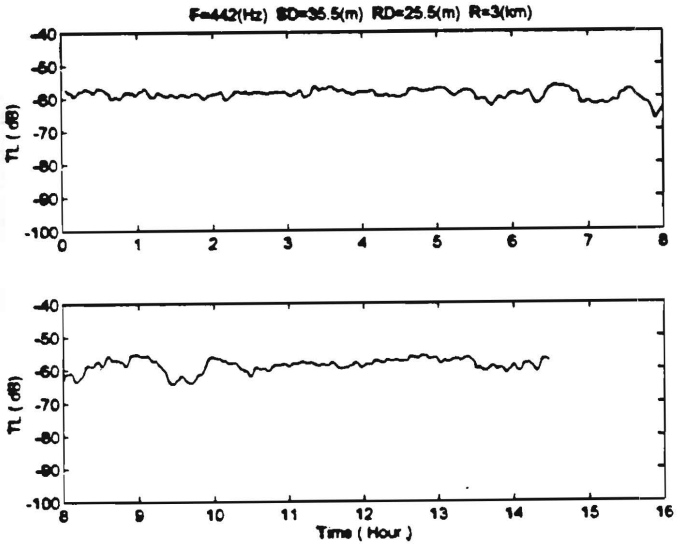

Fig. 4 Numerical results on sound fluctuations due to IWs; sound wave propagates perpendicularly to IW fronts.

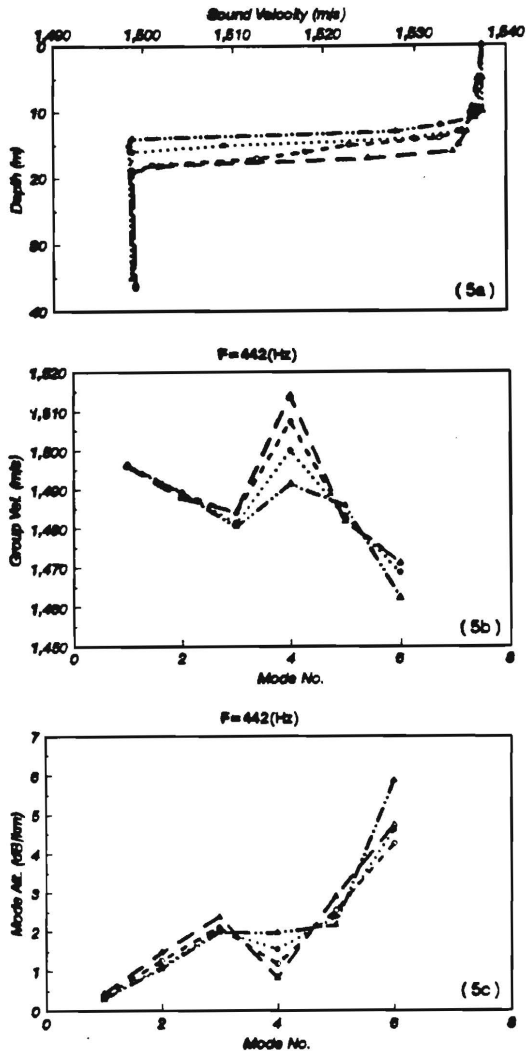

Fig. 5 Modal sensitivity to the change in thermocline depth due to internal waves.

C. A group of acoustic modes sensitive to internal waves

Both observed data and numerical results show that during the Summer in the Yellow Sea, the intensity of the first acoustic mode (below the thermocline) was rather stable. The following numerical simulation will further explain this result.

At different times during the 1981 experimental period , four sound velocity profiles were obtained at the receiver location (shown in Fig. 5a). The change in thermocline depth due to internal waves is readily apparent. Using these SVPs and a normal mode code, we calculate group velocity and attenuation rate for different normal modes. The results are shown in Fig. 5b and 5c. It is found that different normal modes can have very different sensitivities to internal waves. The fourth mode is much more sensitive to the internal wave induced variations in SVP than mode 1. The first mode was so insensitive to the internal waves that sound intensity remained nearly constant. The multimode signal is composed of different modes, some of which have strong interaction with internal waves. If several modes have comparable contributions to the total field, the multimode interference would cause large fluctuations.

Fig. 5 shows an interesting phenomenon. For a given frequency, in shallow water with a strong thermocline such as in the Yellow Sea, acoustic normal modes can be separated into three different categories: (1) lower-order modes (group A) that mainly propagate in the lower part of the water column below the thermocline; (2) higher-order modes (group C) that propagate in a whole water column; (3) between group A and group C, there is a special group of modes (group B) that propagates in a whole water column, but its propagation path of the equivalent mode-ray in the warm part of the water column (above the thermocline) is much longer than in the cool part of

the water column. They also arrive at the receiver from a distant sound source first. So as far as arrival time is concerned, the first mode is most insensitive to internal waves. With the increase of mode order, acoustic normal mode becomes more sensitive. The group B is most sensitive. Thereafter, modes of group C become less sensitive.

III. A CASE ANALYSIS - THE EFFECTS OF LARGE-AMPLITUDE IWs ON ACOUSTIC FLUCTUATIONS

A. Internal soliton model

Large-amplitude solitary IWs are often observed in shallow water. Fig. 1 of [3] shows a very large amplitude internal soliton packet with a well defined wavelength. It

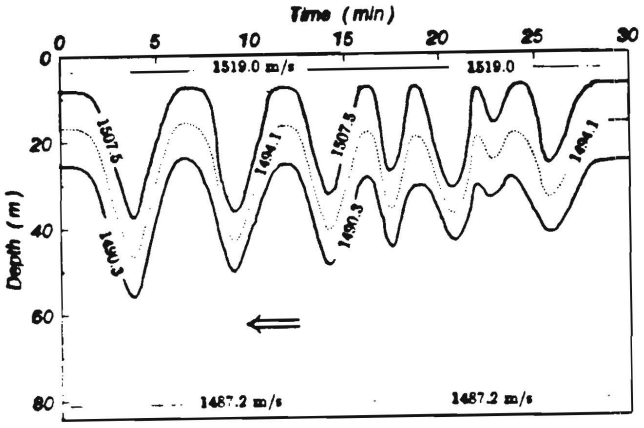

Fig. 6 Large amplitude solitary IWs in the Massachusetts Bay

was obtained by Orr in the Massachusetts Bay [19]. Based on the measured density-depth profile data and the experimental ship velocity [21], we obtained the approximate internal wave time series shown in Fig. 6. The internal wave period is about 6 to 7 minutes.

Assuming that the sound wave of 200 Hz propagates perpendicularly to the IW packet propagation direction, we use a 2-D IW model to calculate fluctuations for multipath signals and individual modes (as we did in Sec. 2.2, using a 2-D model of the adiabatic normal mode).

B. Multimode sound fluctuations

Numerical simulations show that multimode sound intensity/phase fluctuations strongly depend on propagation distance and receiver depth. Fig. 7 and Fig. 8 show multimode sound intensity and phase fluctuations at 5 km for three different receiver depths (RD=6, 30, 60m). Sound intensity and phase fluctuation spectra at 5 km for three different depths are shown in Fig. 9 and Fig. 10. (For both intensity and phase spectra, DC or quasi-DC components have been deleted before FFT processing.)

Fig. 9 and Fig. 10 show that both acoustic intensity and phase fluctuation spectra are very different from Orr's large-amplitude IW narrow band spectrum, and become much wider. At some receiver distance/depth, acoustic fluctuation spectra have a peak wave number which corresponds to the internal soliton spectrum. However, in general, the numerical results obtained from this special case show that acoustic fluctuation spectra in shallow water are different from internal wave spectra.

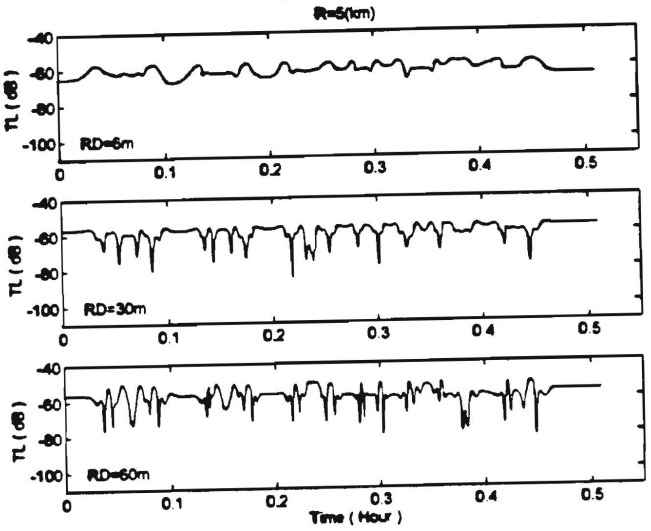

Fig. 7 Multimode acoustic intensity fluctuations.

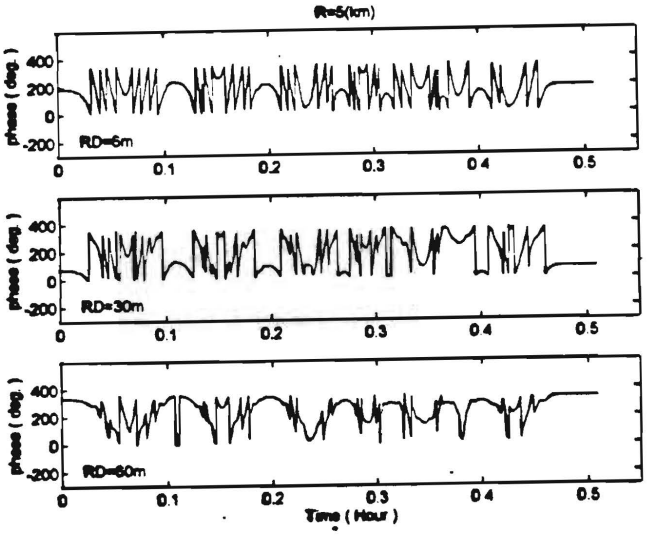

Fig. 8 Multimode acoustic phase fluctuations.

C. *Individual mode signal fluctuations*

Fig. 11 and Fig. 12 show separately the intensity and phase fluctuations of individual acoustic modes (caused by Orr's soliton packet) at three different receiver depths (6, 30, 60m). Apparently, individual mode signal fluctuations directly and clearly correspond to the characteristics of the internal wave packet. Intensity and phase fluctuation spectra of an individual mode are shown in Fig. 13-14. Both are almost the same as the IW spectrum.

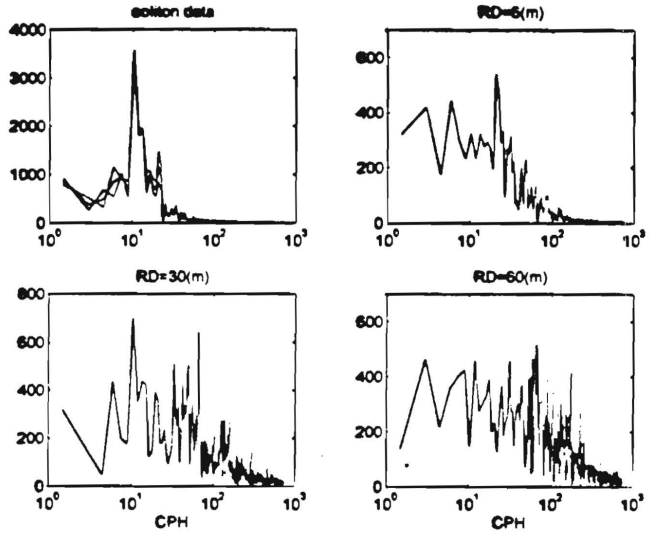

Fig. 9 Multimode signal intensity fluctuation spectra.

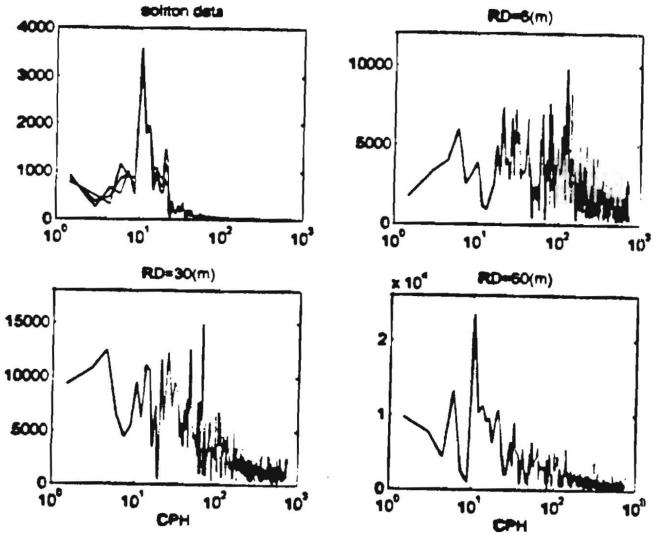

Fig. 10 Multimode signal phase fluctuation spectra.

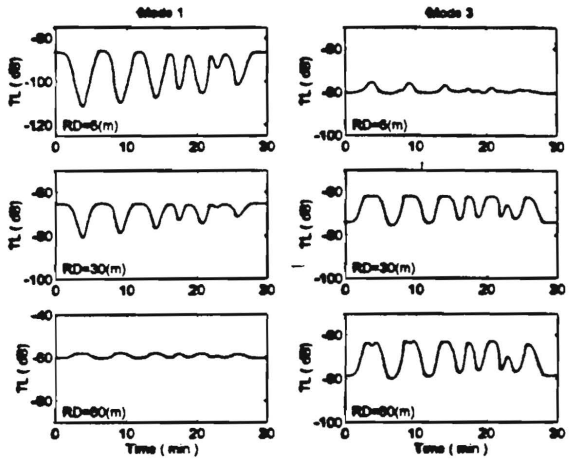

Fig. 11 Individual mode intensity fluctuations.

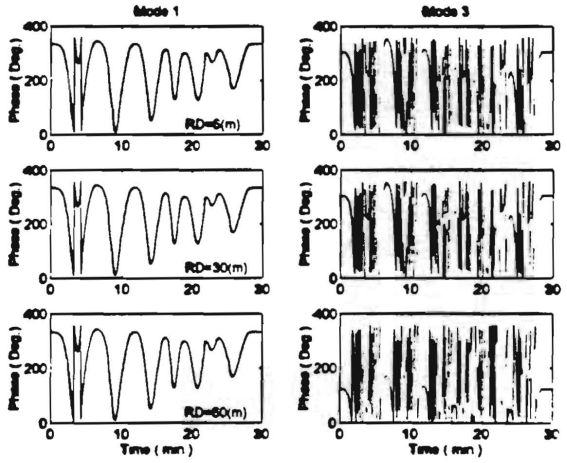

Fig. 12 Individual mode phase fluctuations.

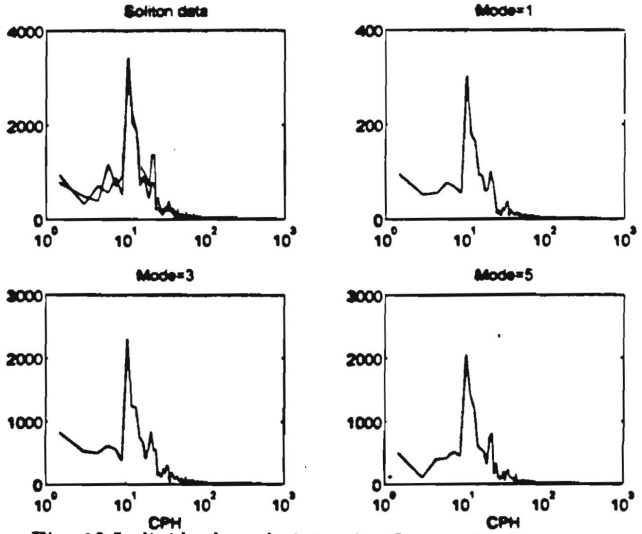

Fig. 13 Individual mode intensity fluctuation spectra.

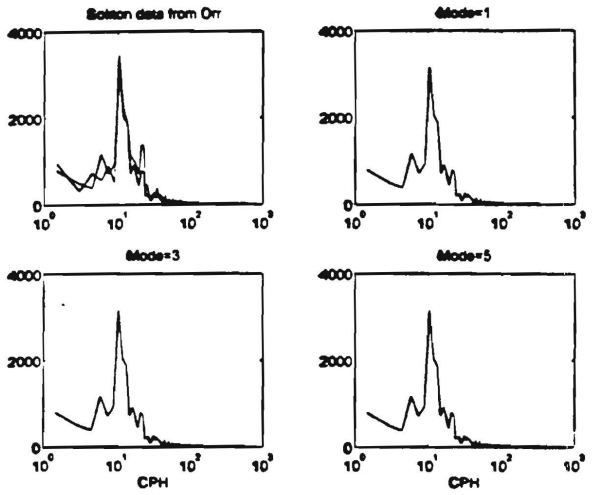

Fig. 14 Individual mode phase fluctuation spectra.

D. Arrival time fluctuations

Figure 15 shows arrival time fluctuations at 4 km for the first six normal modes, caused by the large-amplitude IWs shown in Fig. 6. It is shown that the lower modes are insensitive to the presence of the internal wave packet, but higher modes are very sensitive. Even with such large amplitude solitons (with an amplitude more than 1/3 of the water depth) , the first mode arrival time is rather stable.

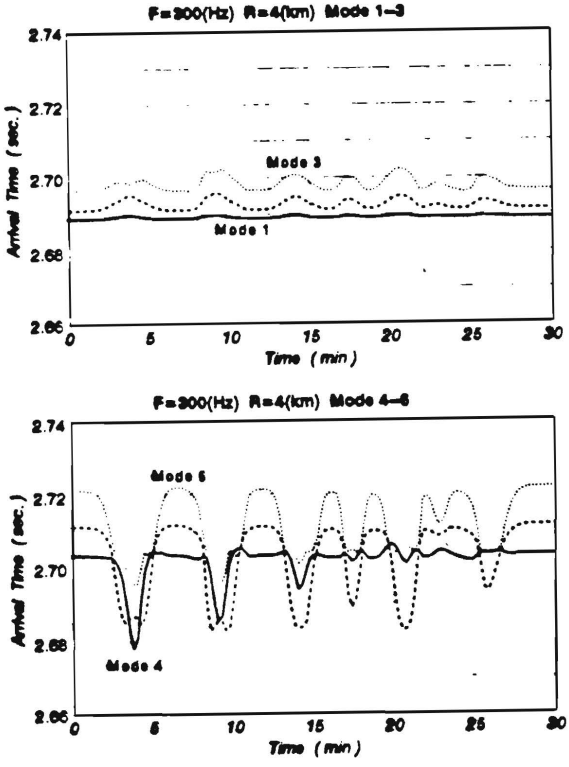

Fig. 15 Arrival time fluctuations for the first 6 normal modes.

E. Horizontal anisotropies of acoustic fluctuations

In order to show horizontal anisotropies of acoustic fluctuations, induced by large amplitude solitons, we assume that a receiver/source pair is separated 5km. Let the nonlinear soliton packet shown in Fig. 6 (whole packet length is about 1.3km) pass between them with an average speed of 0.70 m/s. That is, the internal wave packet propagates parallel to the sound propagation direction. Acoustic intensity fluctuations at 5km, obtained from the PE code, are shown in Fig. 16. The numerical results are

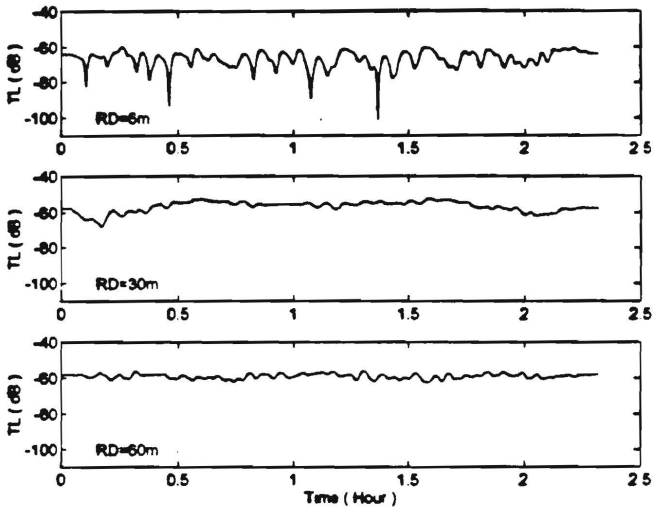

Fig. 16 Sound intensity fluctuations due to a moving soliton packet between a source and a receiver.

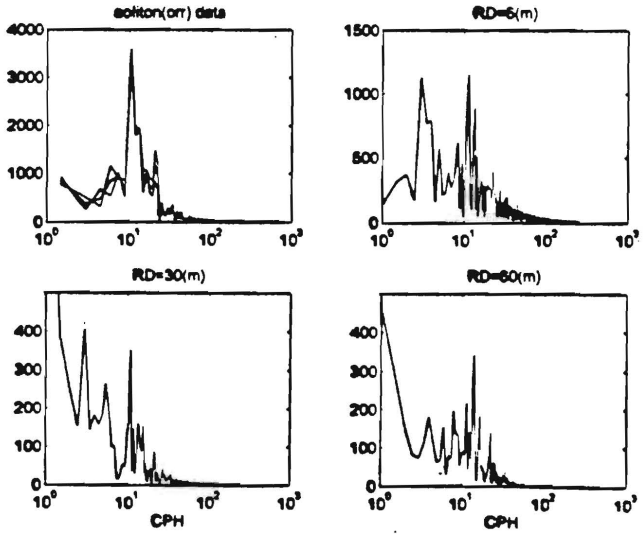

Fig. 17 Sound intensity spectra obtained from Fig. 16.

very different from that shown in Fig. 7 for a case where the IW packet propagates perpendicularly to the sound

propagation direction. Sound intensity fluctuations at depths of 30m and 60m are much smaller than those at 6m. The intensity fluctuation spectra obtained from Fig. 16 are shown in Fig. 17. Although fluctuation spectra at three depths are different from the internal soliton spectrum (become much broader), all of them exhibit a peak at a place which corresponds to the peak of Orr's soliton spectrum.

IV. SUMMARY AND DISCUSSION

Acoustic signal fluctuations due to shallow water IWs have been discussed. Measured internal wave profiles from the Yellow Sea and the Massachusetts Bay are used as inputs to numerical modeling. It is shown that internal wave induced low-frequency signal fluctuations in shallow water often reach 20 dB, and are strongly dependent on source/receiver depths, transmission distance and sound propagation direction. Generally speaking, multimode acoustic signal fluctuation spectra, caused by large-amplitude IWs, and are different from the internal wave spectra, and are much broader. Individual mode fluctuations directly correspond to the characteristics of the internal waves, and hence acoustic fluctuation spectra are very similar to the IW spectra. Certain acoustic modes are more sensitive to IW effects than others. Arrival time fluctuations, for example, are strongly mode dependent. In shallow water with a strong thermocline, the first mode has been found to be the most stable. These results might be useful for monitoring IW activities in shallow water.

For the sake of simplicity, our numerical simulations are based on very simple two dimensional, deterministic IW models. It assumes that the characteristic length of the IW field is always larger than the first Fresnel zone. This restricts the results to relatively short ranges and higher frequencies. The 2-D treatment also assumes that horizontal refraction and azimuthal scattering of sound are negligible. A 3-D acoustic/internal wave model would be desirable.

ACKNOWLEDGMENTS

The authors wish sincerely to thank Dr. Jeff Simmen for his support and helpful comments. Special acknowledgment is given to Dr. Marshall Orr who helped us to quantitatively use Massachusetts Bay's soliton data in our modeling. The Yellow Sea measurements were conducted under the support of the Institute of Acoustics, Academia Sinica. Professor Renhe Zhang is appreciated for sharing the experimental data shown in Fig. 2.

REFERENCES

[1] N.G. Borisov, A.V. Gritsenko, S.B. Kozitskii, O.I. Nikora, A. N. Rutenko, M. Yu. Trofimov, and A.E. Filonov,"Underwater sound signal fluctuations caused by internal waves," Acoust. Phys. 40, 664-670 (1994).

[2] J.R. Apel, L.A. Ostrovsky and Yu. A. Stepanyants, "Internal solitons in the Ocean" (Report MERCJRA0695, APL, The Johns Hopkins University (1995), to be submitted)

[3] J. X. Zhou, X. Z. Zhang and P. H. Rogers, "Resonant interaction of sound wave with internal solitons in the coastal zone," J. Acoust. Soc. Am. 90, 2042-2054 (1991).

[4] M.H. Orr and J.F. Lynch, " The New Jersey Shelf shallow water random media propagation experiment," J. Acoust. Soc. Am. 98, 2864 (1996).

[5] J.F. Lynch, G.L. Jin, R. Pawlowicz, D. Ray, A. J. Plueddemann, C-S. Chiu, J. H. Miller, R. H. Bourke, A. R. Parsons, R. Muench, "Acoustic travel-time perturbations due to shallow-water internal waves and internal tides in the Barents Sea Polar Front: Theory and experiment," J. Acoust. Soc. Am. 99, 803-821 (1996).

[6] J.X. Zhou, X.Z. Zhang, P.H. Rogers, D. Z. Wang and E.S. Luo, "Anomalous sound propagation in shallow water due to internal wave solitons," IEEE Proc. Oceans' 93, 1, 87-92 (1993).

[7] D.B. King,S.A. Chin-Bing, and R.W.McGirr, "Effects of shallow water internal waves on broadband acoustic wave propagation," in Theoretical and Computational Acoustics Vol. 2, D.Lee and M.H. Schultz, ed. pp793-807. (World Scientific, Singapore, 1994)

[8] D.B. King and S.A. Chin-Bing, "Scattering effects of internal waves in the shallow water ocean environment," Proc. of the SPIE int'l Symposium on OE/Aerospace Sensing (Olando, 1994).

[9] S.A. Chin-Bing, D.B. King, and R.W. McGirr, "Computer modeling of time-domain and frequency-domain acoustic signal in a shallow water ocean environment with internal waves," Mathematical Modeling and Scientific Computing 3, (1994).

[10] M.K. Broadhead and H.A. Ali, "Dissipative shallow water internal waves and their acoustical properties," IEEE Proc. Oceans 95, 1,673-684 (1995)

[11] D. Rubenstein and M.H. Brill, "Acoustic variability due to internal waves and surface waves in shallow water, " in Ocean Variability and Acoustic propagation, ed. by J.Potter and A. Warn-Varnas (Kluever Academic, Dordrecht,1991), 215-228.

[12] A. Yu. Shmelerv, A.A. Migulin, and VG. Petnikov, "Horizontal refraction of low- frequency acoustic waves in the Barents Sea stationary track experiment," J. Acoust. Soc. Am. 92, 1003-1007 (1992).

[13] L.F. Bondar, S.V. Borisov, A.V. Gritsenko, V. A. Zakharov, V.I. Il'ichev, D.G. Kovzel', Yu. N. Morgunov, and A.N. Rutenko, "Intensity and phase fluctuation of low-frequency acoustic signals along stationary tracks in shelf regions of the Sea of Japan," Acoust. Phys. 40, 497-504 (1994).

[14] L.F. Bondar', S.V. Borisov, V.N. Zhirko, N.F. Kabanov, S.V. Kalinin, Y.N. Morgunov, A.N. Rutenko A.I. Chudakov, and A.N. Shvyrev, "Short-period intensity and phase fluctuations of acoustic signal along shallow stationary tracks," Acoust. Phys. 42, 18-24 (1996)

[15] Special session on "Acoustic interaction with internal waves in shallow water," at the 130th ASA meeting (Chaired by J.F. Lynch and K:B. Smith), J. Acoust. Soc. Am. 98, 2863-2864 /2868-2870 (1996).

[16] P. Traykovski, "Travel-time perturbation due to internal waves: Equivalence of modal and ray solution," J. Acoust. Soc. Am. 99, 822-830 (1996).

[17] D. Tielbuerger, S. Finette and S. Wolf, "Acoustic propagation through an internal wave field bounded by a shallow water waveguide," submitted to J. Acoust. Soc. Am. (1996).

[18] S.V. Borisov, N.F. Kabanov and A.N. Rutenko, "Experimental study of sound field fluctuations on fixed paths," Acoust. Phys. 42, 301-311 (1996).

[19] M.H. Orr, "Remote acoustic sensing of the oceanic fluid and biological processes," WHOI Tech Rep. WHOI-80-2(1980)

[20] R.H. Zhang, private communication

[21] M.H. Orr, private communication

SHALLOW-WATER ACOUSTIC REVERBERATION AND ITS INVERSE PROBLEM

J. X. Zhou and X. Z. Zhang

(School of Mechanical Engineering, Georgia Institute of Technology)

In this paper, we will discuss some problems involving long-range reverberation in shallow water. The title of the paper is " Shallow-water acoustic reverberation and its inverse problem ".

Fig. 1

First, we discuss motivations of the research. Then, we would like to introduce an angular power spectrum method for calculating sound propagation, reverberation and their spatial coherence in shallow water. In part III, simple solutions for sound propagation, reverberation and echo to reverberation ratio will be given for four typical cases such as a Pekeris model, a wedged shallow water, a linear negative gradient layer and a strong thermocline shallow water. Part IV shows some at-sea reverberation data, including average reverberation intensity and vertical cross-correlation. In the last part, as an inverse problem of shallow water reverberation, we will give some preliminary results on the bottom reflectivity and bottom scattering at small grazing angels and low frequencies, obtained from reverberation measurements.

I. INTRODUCTION

Now computational ocean acoustics is significantly affecting the way we do research. Only the numerical approach allows us to include the full complexity of the acoustic problem. However, the seabed dominates shallow water acoustics problems. Sea bottom properties and bottom scattering mechanisms are usually poorly known. The detailed interference

Encl. (c)

pattern, the find structure of sound field, is not always physical meaningful to engineering applications. A simple analytical expression averaged over frequency or space, sometimes, could give better insight to some physical problems.

Let me show three Figures to ask some questions:

Fig. 2

Fig. 2 is a typical 1/3 Oct. reverberation decay curve received by a single hydrophone from a single explosive signal in a Pekeris model with a water depth of 29 meters. It carries definite information about bottom forward reflection (two-way propagation) and bottom scattering (reverberation). An echo shows that a small island is far away from a receiver about 600 times of water depth. Due to normal mode stripping, even at a shorter distance A shown on the reverberation curve, the effective grazing angle for sound propagation interacting with bottom is about 2 or 3 degree. Can we extract bottom scattering strength and bottom reflectivity at such small angels from this reverberation data?

Fig. 3

Fig. 3 shows two situation involving sonar detection of submarines in two typical continental area. If two submarines have identical sonar system, the target strength of two submarines is same, which one is at the favorable position and will get the large echo-reverberation ratio? How much larger will it be? What depth of source dropped from a helicopter will yield the best echo-reverberation ratio for the negative gradient condition ?

Fig. 4

Fig. 4 is copied from Urick's book, showing Echo, noise and reverberation as functions of range. Echo to reverberation ratio is a decreasing function with increasing range. But, in another paper, he reported "a peculiarity sometimes observed with echo-ranging sonars in shallow water: an echo-to-reverberation ratio remains nearly constant, or even increases somewhat, with increasing range or time."(JASA 48, 1970). According to this observation, the reverberation interference would not be a problem for sonar detection in shallow water. How to explain these phenomena ?

In this talk, we would like to give some answers to above-mentioned questions. First, we would like to introduce an "angular power spectrum method" for calculating shallow water reverberation.

II. ANGULAR POWER SPECTRUM METHOD

Fig. 5

In shallow water, the velocity potential due to a point source can be expressed as a sum of normal modes (see Eq.1 in Fig. 5), the sound field intensity can be expressed by Eq.4. If we are interested in average field characters only, do not care the fine structure, i.e., the sound field characters are averaged over a given frequency or space, then the second interference term of Eq.(4) can be neglected. We have Eq. 5 for average sound intensity.

Fig. 6

According to the W.K.B approximation solution of the wave equation, the depth distribution of normal mode has the form expressed by Eq.6 in Fig. 6. The angle of equivalent mode-rays and the eigenvalue of the lth mode has a relationships as Eq.7. The

attenuation coefficient of the lth mode can be expressed by Eq. 8. The cycle distance of the equivalent mode-ray, S_l can be expressed as Eq. 9. Where $|V_{b,s}(\theta)|$ is the reflection coefficient of a plan wave with grazing angle θ at the boundary. For higher frequencies ($kH \gg 1$), the beam displacement on bottom reflection is negligible because of $\delta_l \ll S_l$. ξ_l, η_l are the upper and lower reflection (or turning) depth of equivalent mode-rays. ϵ_{ξ_l} and ϵ_{η_l} are the phase shift due to the reflection or turning at ξ_l and η_l.

Fig. 7

Using a smooth envelope $E(z)$ of WKB solution to present the energy depth distribution of normal modes (see Fig. 7), neglecting the energy in the exponential decay area, then using a differential relation for a definite integral shown Eq. 11 and changing the summation of eq.(10) into a integral with respect to θ, we get a general expression for average field intensity in shallow water expressed by Eq. 12.

Fig. 8

We call I_{aps} as "the angular power spectrum of average sound field". This expression is exactly same as the result obtained by Brekhovskikh (normal mode method), Smith (statistic ray method) or Weston (energy flux method). It is a very interesting expression. The average sound intensity in shallow water only depends on two simple parameters which have very clear and intuitive physical meaning: the bottom reflection coefficient $V(\theta_b)$ and the (sound velocity controlled) cycle distance of mode-ray. For some typical sound velocity profiles in shallow water, computations are very simple. Here the "mode-rays" are different from the conventional geometric rays that have definite propagation paths in the space. According to Guthrie and Tindle, a mode-ray, i.e., eigenray of a normal mode, obey same

Snell law: $k(z)cos\theta_(z) = k(z_0)cos\theta_l(z_0) = k_l$. **They are fuzzy everywhere in the space**. The interference of adjacent many modes forms a physical ray with limited width, and converges to a geometric ray at high frequency.

Except the geometric cylindrical spreading loss ($\frac{1}{H\tau}$) and water medium absorption, the action of sound velocity and sea bottom to shallow water sound propagation looks like a angle filter.

(2) Average shallow water reverberation

Fig. 9

For the angular power spectrum method, the average field intensity is calculated by summing up the power spectrum of plane waves for all normal modes propagating in different directions.

The classic bottom scattering coefficient is expressed as a function of the incident and scattering angles. Therefore, this method link the transmission process naturally with the boundary scattering in the angle domain. Up-going and down-going local plan waves, decomposed from a mode, have equal grazing angle and (almost) equal energy at any depth in the water column. For bottom reverberation computation only down-going one should be treated as the incident wave.

For a given signal duration τ, there are a lot of bottom scattering signals that simultaneously return to a receiver. The bottom scattering looks like a stochastic filter. The scattering field can be treated as a angle-weighted process. The calculation for average shallow water reverberation, and a network analogy are given in Fig. 9.

Where $I_{aps}(\theta, r, \tilde{H}; z_0)$ is the angular power spectrum incident nearby bottom ($\tilde{H}$) at a distance of r when a source is at a depth of z_0; $I_{aps}(\phi, r, z;\ \tilde{H})$ is the angular power

spectrum returned to a receiver at a depth of z, scattering from a bottom area at a distance of r. We call $R_{aps}(\phi, r, z; \tilde{H})$ as the angular spectrum of average reverberation.

(3) Spatial coherence in shallow water

If we know a power spectrum of a random signal, it is easy to calculate its correlation coefficient. Acoustic field spatial correlation and the signal angular power spectrum have a relationship that similar to Fourial transformation. Thus, the normalized vertical correlation coefficient ρ of sound propagation in shallow can be expressed by Eq.16 in Fig. 10:

Fig. 10

For reverberation coherence, we just use reverberation angular spectrum R_{asp} to replace sound propagation angular spectrum. Where d is a separation between two hydrophones. For the longitudinal correlation coefficient, what we need to do is to change $sin\theta$ into $cos\theta$.

In network theory, many signal processing problems become much simpler when they are changed from time domain into frequency domain. Based on the WKB approximation solution of the wave equation, and with the concept of the average angular power spectrum, some calculations for sound propagation, reverberation and their coherences are very simple and intuitive. Next, we would like to briefly give some results on range/depth dependences of average sound intensity, long-range reverberation and echo to reverberation ratio for four typical shallow water cases.

III. RANGE/DEPTH DEPENDENCE OF SOUND INTENSITY and ECHO TO REVERBERATION RATIO

(3.1) Bottom model

Fig. 11

First, we need a sea bottom model. For most seabeds, the reflection coefficient can approximately expressed by Eq. 17. Where θ_c is a critical angle. For small grazing angles, even if the bottom roughness and sediment inhomogeneity are considered, it is still a good approximation.

For the bottom backward scattering coefficient at low grazing angles and low frequencies, unfortunately, there is no general expression. It could be very complex function of bottom surface roughness, sediment type, inhomogeneity, frequency and so on. Here we introduce a phenomenological separable expression as Eq. 18. It has an arbitrary angle dependence, ignoring what is the main mechanism of bottom scattering. Here, we have made two assumptions: a) $M(\theta, \phi)$ slowly varies with angle; b) $M(\theta, \phi)$ is reciprocal, i.e., $M(\theta, \phi) = M(\phi, \theta)$. When the incident angle θ and scattering angle ϕ are exchanged, they are equal. Widely used Lambert's scattering law ($n = 2$) is a special case of Eq. 18.

(3.2) In Pekeris shallow water

Fig. 12

Average sound intensity expressions can be expressed by Eqs. 21–24 in Fig. 12. The results are same as that obtained by Weston. Eq. 23 expresses the famous three–half law region, first obtained by Russian scientist Brekhovskikh. For Eq.24, only the first normal mode left. We are most interested in regions expressed by Eq. 22 and Eq. 23. For these

regions, the reverberation intensity and echo–to–reverberation ratio can be expressed by Eqs. (25-28) (see Fig. 13.)

Fig. 13

Our results can explain Urick's report. At shot range, echo–to reverberation ratio deceases with increasing distance. In a very wide range, i.e., in the normal-mode stripping region (see Eq. 28), the range dependence of echo-to-reverberation ratio depends on the angular index of bottom scattering n. If bottom scattering index n is smaller than 2, echo–to–reverberation still decrease with increasing distance. But if the bottom scattering obeys Lambert's law ($n = 2$), Echo-to reverberation ratio remain constant, if n is grater than 2, echo-to-reverberation ratio would increase with increasing range.

(3.3) In wedged shallow water

Fig. 14

For a wedged homogeneous shallow water, the results are similar to that for a Pekeris model. In the most interested three–half law area, we have the average reverberation intensity and echo-to-reverberation ratio shown by Eq. 29 and Eq. 30. One of interesting results is that, the reverberation intensities obtained at two terminals with different depths would not be reciprocal. A sonar at shallower area is at the favorable position and will get the large echo-reverberation ratio, For example, if $H_1 = 50m \quad H_2 = 200m, \quad n = 2$, i.e., for Lambert's scattering law, then the reverberation interference at shallower area would be 12 dB less.

(3.4) In a linear negative gradient layer

Fig. 15

Fig. 15 shows the range/depth dependence of sound transmission in a linear negative gradient layer. Whole water column can be divided into 4 regions with different average sound intensity expressions by Eqs. 32-35. (if sound velocity gradient $a \longrightarrow 0$, all expressions reduce to ones for the pekeris model) At long-range, there is apparent depth dependence. We are most interested in Region D. For this region,

Fig. 16

the monostatic reverberation intensity can be expressed by Eq. 36 in Fig. 16, it strongly depends on the source depth z_0. The echo-to-reverberation ratio can be expressed by Eq. 37. Where $F(\widetilde{\alpha}, \widetilde{\beta})$ is a elliptic integral. M, N, reverberation and echo-to-reverberation ratio are strong function of source depth and target depth. Let us give a numerical example:

Fig. 17

Suppose water depth $H = 50m$, target depth $z = 15m$. If a sonar located at a depth of 40 m is raised to 15m, then echo-to-reverberation ratio would increase about 12.1 dB ! (for the widely used Lambert's scattering bottom model.).

(3.5) In strong thermocline shallow water

Fig. 18

Using a two-layer model to present a strong thermocline shallow water, we have derived analytical expressions of average transmission loss shown in Fig. 18. If both source and receiver are located bellow the thermocline, the transmission loss $TL_{bb}(r)$ is similar to that in a Pekeris model, changes from a spherical law to cylindrical, three–half law, at last only one mode left. But if a source is located above thermocline, and a receiver located below the thermoclines (or vice versa), the transmission loss TL_{ab} $(= TL_{ba})$ would be much larger than T_{bb}, and there is a r^{-3} dependence.

Fig. 19

Fig. 19 shows a set of experimental data (300 Hz and 1000 Hz) obtained from the Yellow Sea with a sharp strong thermocline. T_{ab} or T_{ba} in the middle range is close to the r^{-3} law. Then two-way transmission loss has r^{-6} dependence, the times the r^{+1} dependence of the scattering area. Thus, the monostatic reverberation obtained above the thermocline should have a r^{-5} dependence. This prediction has been approved by the Yellow sea reverberation data obtained at same region for transmission loss measurements. (see Fig. 19).

Fig. 20

For a strong thermoclines, the echo to reverberation ratio has very interesting range–depth dependence. (1) If sonar is located above the thermocline, a target located below thermoclines, the echo to reverberation ration decreases with increasing distance; (2) if both are located above thermoclines, the ratio is getting better, may increases with distance; (3) if a sonar is located below thermoclines, and target located above thermoclines, the active sonar performance becomes worst.

The conclusion from this section (III) is very general, that is, echo to reverberation ratio for a active Sonar in shallow water will strongly depend on environmental parameters, such as sound velocity profile, bottom scattering angular index, sonar location and target location, and so on. It is show that a depth-variable sonar has advantage in shallow water.

****

Next we would like to discuss the inversion problem of reverberation. First, let us introduce some at-sea experimental data.

IV. AT–SEA EXPERIMENTAL DATA ON REVERBERATION

(4.1) Reverberation intensities for three different sites

The experiments were conducted in the Yellow Sea and the East China Sea off China coast, by using explosive source with 1000 grams TNT charges. In order to offer possible simple test cases for numerical reverberation modeling, only three sets of experimental data obtained from the Pekeris shallow water models are presented in this report.

Fig. 21

Fig. 21 shows three sound velocity profiles. We choose three different sea areas with flat bottom and with very different sediments. From hard bottom, coarse sand to soft bottom, clay silt. In Fig. 21 m_d is mean grain diameter; k is porosity, and ρ is density.

Fig. 22–28

Figs. 22 shows average reverberation level obtained in Site I as a function of time for 200, 250, 315 and 400 Hz. For a possible test by numerical codes, here the reverberation

level, RL is already calibrated to the source level, i.e., Source Level is 0 dB. Equivalent pulse duration is 10 ms. Figs. (23-25) are data for 500 Hz– 3150 Hz. Putting different frequency data together, we get Fig. 26. The bottom at this area is a coarse–medium sand. The reverberation data obtained from Site II with find sand and silty sand bottom are shown in Fig. 27. Average reverberation levels on Site II are litter lower than that obtained from Site I. The data obtained from Site III with a soft bottom are shown in Fig. 28. The average reverberation levels at Site III are lowest. For this area (with a soft bottom), we find that at lower frequency range, reverberation has a stronger frequency dependence.

(4.2) Vertical coherence of long-range reverberation

For Site II (water depth $\sim$ 29 m), we measured the vertical coherence of reverberation. Let us show some results:

Fig. 29-31

Fig. 29-31 show the measured vertical cross-correlation coefficient for 800 Hz, 1250 Hz and 1600 Hz as a function of time (range) for different separations between two hydrophones. Solid lines are numerical results obtained from our model. We adjusted the bottom reflectivity to match theoretical prediction with data.

Figs. 32-34

Figs. 32-34 show the measured vertical cross-correlation coefficient at 800 Hz, 1250 Hz and 1600 Hz, plot against wavenumber k multiplied by hydrophone separation d. These data were obtained at 4s, 6s, 8s and 10s after the detonation of the explosive. All the

results from 12 explosive reverberation signals are shown in these figures. The big dark circles are average value. Dashed lines are numerical results obtained from our model with an averaged extracted bottom reflection parameters (Q = 0.3,0.6 and 0.88). They are in good agreement.

V. REVERBERATION-DERIVED BOTTOM SCATTERING STRENGTH AT SMALL-GRAZING ANGLES AND LOW-FREQUENCIES

In last part, we would like to discuss a little bit about the inverse problem of shallow water reverberation, and show some preliminary results. Fig.35 shows the "Inverse Technique Flow Chart" of our method.

Fig. 35

Numerical results show that in the three-half region of Pekeris model, the vertical coherence of reverberation more strongly depends on bottom reflection parameter Q than bottom scattering index n. First, using a trial scattering index n and inputting it to the theoretical vertical correlation model, and comparing with measured reverberation correlation coefficient, one can get an initial bottom reflection parameter Q (and equivalent scattering angle) . Then input this Q to the reverberation intensity model, compare the prediction with the measured reverberation levels to get a modified value of n. Then input a new value of n back to reverberation correlation model..... To continue iteration until numerical results match all measured reverberation levels and vertical correlation coefficients. In this way, we can get both bottom reflectivity and bottom scattering strength at small grazing angles and low frequencies from reverberation measurements.

For the first phase of this research, we assume that the bottom scattering index n is independent of the angle. Preliminary results are given in Fig. 36 and Fig. 37.

Fig. 36, 37

The bottom backscattering strength $S_b(\theta)$ is plotted against grazing angle from about 1.4° to 14.2° in Fig. 37. The reverberation to noise ratio is very important for extracting small angle scattering. For the reliability of these results, we only used those reverberation data that were about 8 dB higher than the environmental noise. For the comparison, the direct measurements for small angles in the deep sea by Merkliger are also shown in Fig. 37. His data are for 400–800 Hz, 800–1600 Hz and 1600–3200 Hz. It is only data that we can find in the publications for such small grazing angles and low frequencies.

In the past three decades, as we know, in JASA there are 3 papers on shallow–water reverberation-derived bottom scattering strength. Cole's data was derived from the 3.5 kHz long Island reverberation measurements under downward refraction condition. His result is reliable, but the downward refraction restricted the menservants to a very narrow angle range at the bottom. Urick's data were obtained from the Gulf of Mexico. But as he himself indicated the scattering angles are uncertain, data should be moved to some where. Another result obtained by Argentine scientists is wrong, because of wrong assumption on shallow water sound propagation loss.

Our preliminary results show that bottom scattering strength at small grazing angles and low frequencies is a strong function of frequency. For frequencies that are higher than (or equal to) 800 Hz, the bottom scattering indexes n are in a range between 1.6 and 2.0 (see Fig. 36), i.e., the bottom scattering is roughly close to the Lambert's scattering law.

There is an interesting phenomenon that must be mentioned. At site II (a Pekeris model), measured reverberation intensities have weak frequency dependence (see Fig. 27). However, inverse results derived simultaneously from both average reverberation intensity and vertical coherence, show that both the bottom reflection loss and bottom scattering

strength are strongly frequency dependent. If the wide-used Hamilton geo-acoustic model is used, the bottom attenuation has a linear frequency dependence, then bottom reflection parameter Q would be a constant. If someone uses the Hamilton geo-acoustic model and matches his numerical results using measured reverberation intensity data only, it might result in incorrectly weak frequency dependence for bottom scattering strength. Therefore, in order to test a theoretical bottom scattering model based on reverberation measurements in a given area, at least two types of information are required: reverberation intensity (decay curves) and either bottom reflection loss or reverberation spatial coherence.

Shallow-water Acoustic Reverberation and Its Inverse Problem

J.X. Zhou and X.Z. Zhang

(School of Mechanical Engineering, Georgia Institute of Technology)

I. Motivations

II. Angular power spectrum method
Sound propagation, reverberation and spatial coherence

III. Average sound intensity, reverberation, and echo to reverberation ratio in
(A) Pekeris model
(B) Wedged shallow water
(C) Linear negative gradient layer
(D) Strong thermocline shallow water

IV. At-sea experimental data on
Reverberation intensity, Vertical correlation coefficient

V. Inverse problems of shallow water reverberation
Reverberation – derived bottom scattering strength and bottom reflectivity at small grazing angles

Fig. 1

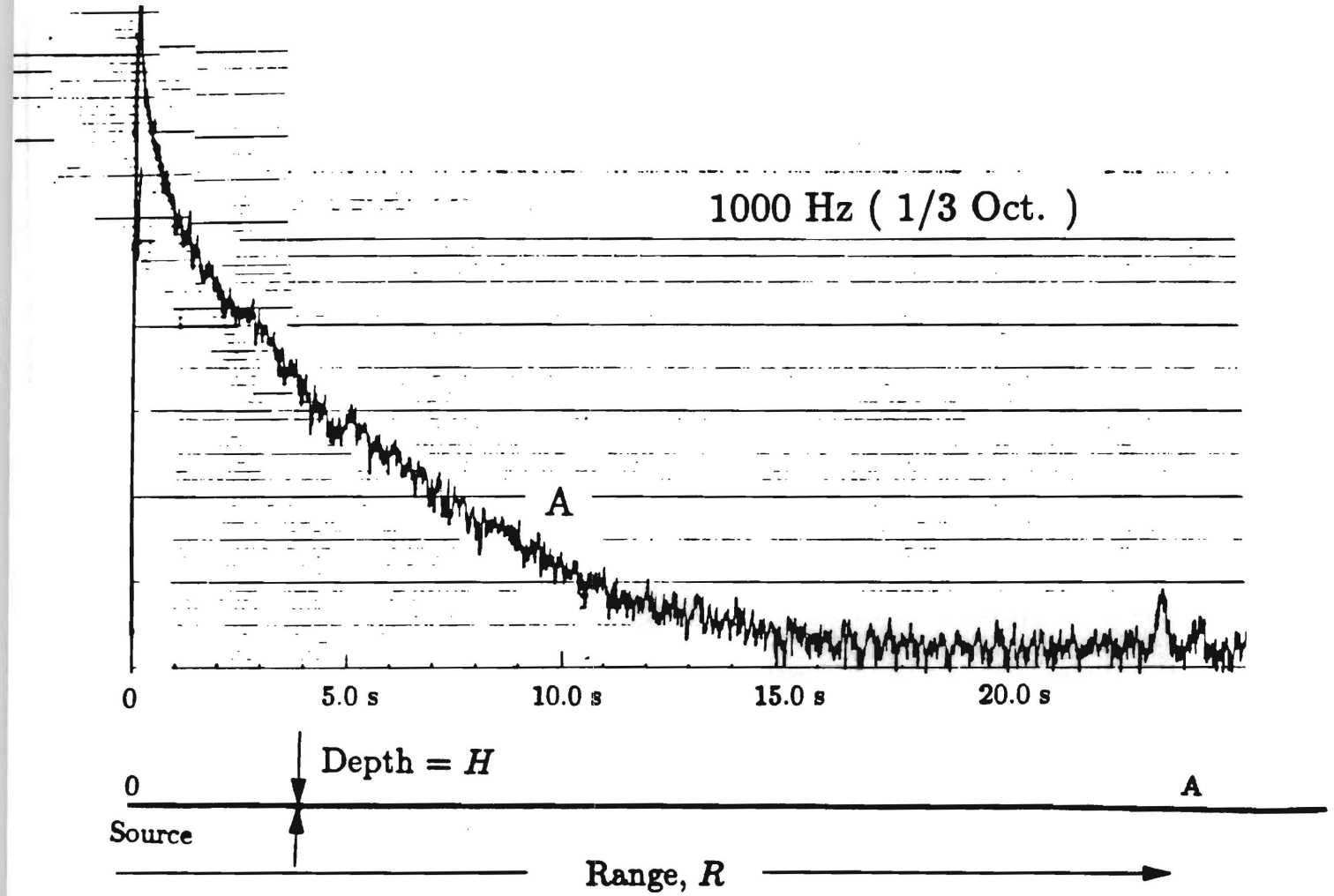

Fig. 2

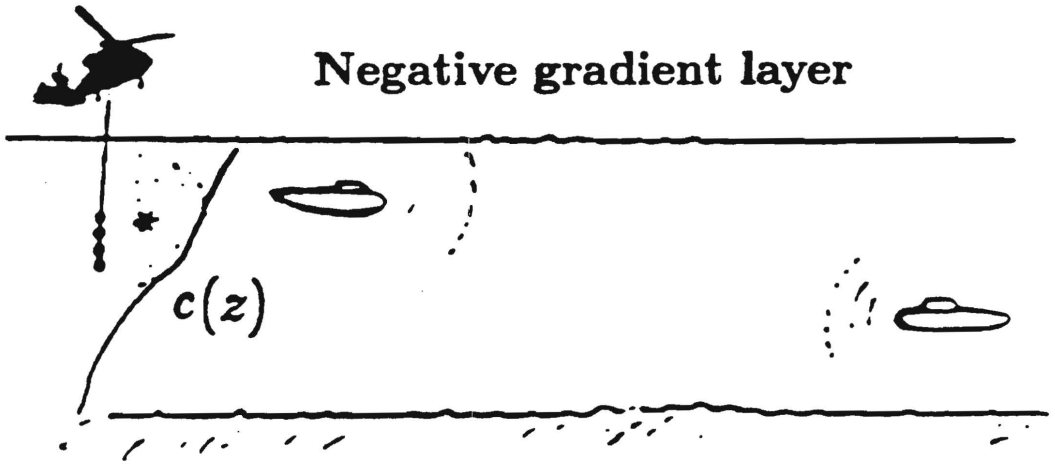

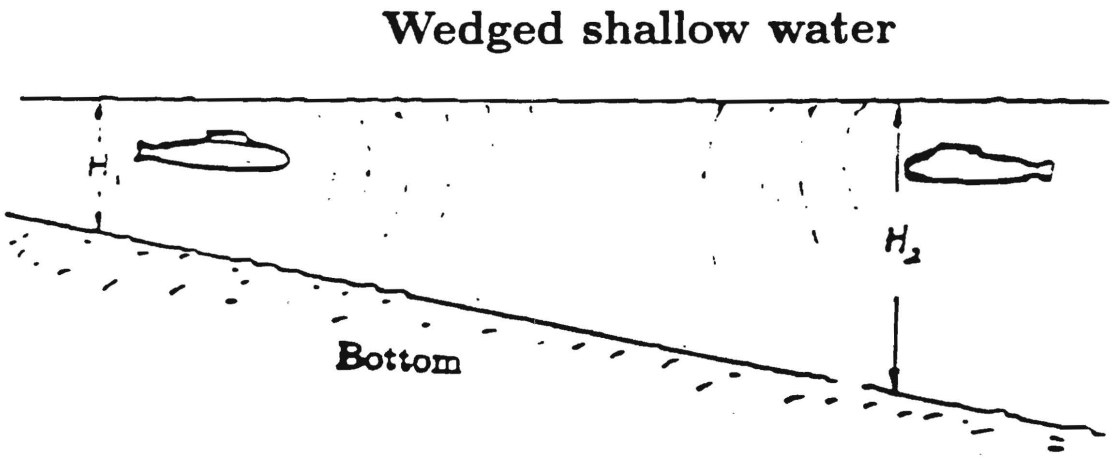

Which one is at the favorable position and will get the large echo-reverberation ratio? How much larger will it be? What depth of source dropped from a helicopter will yield the best echo-reverberation ratio for a negative gradient condition ?

Fig. 3

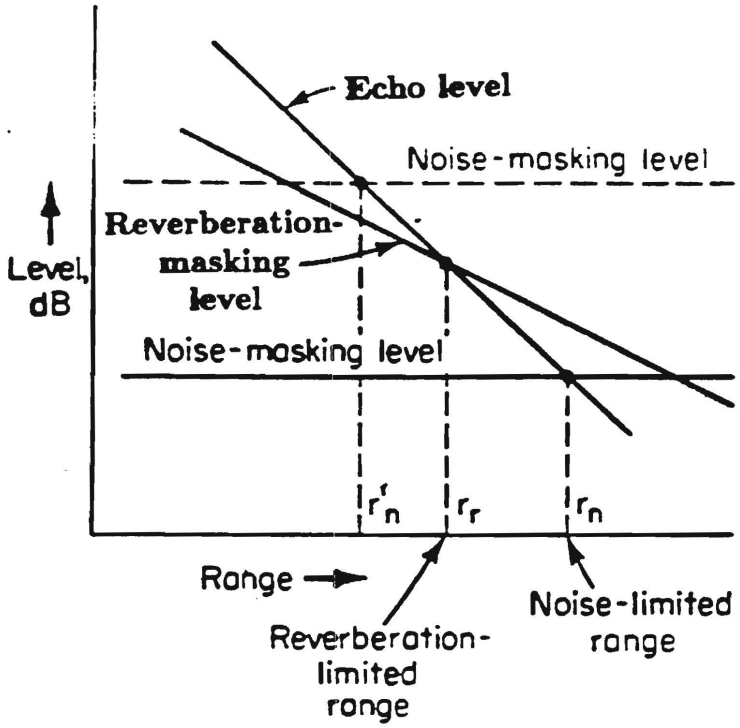

Echo, noise, and reverberation as functions of range.

Urick (JASA 48, 1970):

'A peculiarity sometimes observed with echo-ranging sonars in shallow water: an echo-to-reverberation ratio remains nearly constant, or even increases somewhat, with increasing range or time.'

Fig. 4

II. Average Angular Power Spectrum Method :

(2.1) Sound propagation Velocity potential:

$$\Psi(r,z;z_0) = (\frac{2\pi}{r})^{\frac{1}{2}} e^{-i\frac{\pi}{4}} \sum \frac{\Phi_l(z_0)\Phi_l(z)}{k_{rl}^{(1/2)} N_l} e^{ik_{rl}r} \tag{1}$$

$$N_l = \int_0^\infty \mid \Phi_l(z) \mid^2 dz \tag{2}$$

$$k_{rl} = k_l + i\,\beta_l \tag{3}$$

Sound field intensity:

$$\mid \Psi(r,z:z_0) \mid^2 = \frac{2\pi}{r} \sum \frac{\mid \Phi_l(z_0) \mid^2 \mid \Phi_l(z) \mid^2}{k_l N_l^2} e^{-2\beta_l r} + \frac{2\pi}{r} \sum\sum_{l \neq m} \frac{\Phi_l(z_0)\,\Phi_m^*(z_0)\,\Phi_l(z)\,\Phi_m^*(z)}{k_l^{1/2} k_m^{1/2*} N_l N_m^*} e^{i(k_l - k_m^*)r} \tag{4}$$

$$\mid \Psi(r,z;z_0) \mid^2 = \frac{2\pi}{r} \sum_l \frac{\mid \Phi_l(z_0) \mid^2 \mid \Phi_l(z) \mid^2}{k_l N_l^2} e^{-2\beta_l r} \tag{5}$$

Fig. 5

W.K.B approximation solution:

Mode energy depth distribution

$$|\Phi_l(z)|^2 = \frac{c_l}{k_l\, tan\theta(z)} \tag{6}$$

Mode-ray angle & eigenvalue

$$k(z)cos\theta_l(z) = k_l \tag{7}$$

$$2\int_{\xi_l}^{\eta_l} \sqrt{k^2(z) - k_l^2}\, d\, z + \epsilon_{\xi_l} + \epsilon_{\eta_l} = 2l\pi$$

$$l = 0, 1, 2, ...$$

Mode attenuation coefficient

$$\beta_l = \frac{-\, ln|\, V_b(\theta)\,|}{S_l + \delta_l} \tag{8}$$

($V(\theta)$ – reflection coefficient at the boundary.)

Cycle distance of mode-ray

$$S_l = 2\int_{\xi_l}^{\eta_l} \frac{k_{rl} d\, z}{\sqrt{k^2(z) - k_{rl}^2)}} = 2\int_{\xi_l}^{\eta_l} \frac{d\, z}{tan\theta_l(z)} \tag{9}$$

Fig. 6

$$|\Psi(r,z;z_0)|^2 = \frac{2\pi}{r}\sum_l \frac{|\Phi_l(z_0)|^2|\Phi_l(z)|^2}{k_l N_l^2} e^{-2\beta_l r} \qquad (10)$$

$$\frac{d}{dl}\int_{\xi_l}^{\eta_l} f(z,l)dz = \int_{\xi_l}^{\eta_l} f_l'(z,l)dz + f(\eta_l,l)\frac{d\eta_l}{dl} - f(\xi_l,l)\frac{d\xi_l}{dl} \qquad (11)$$

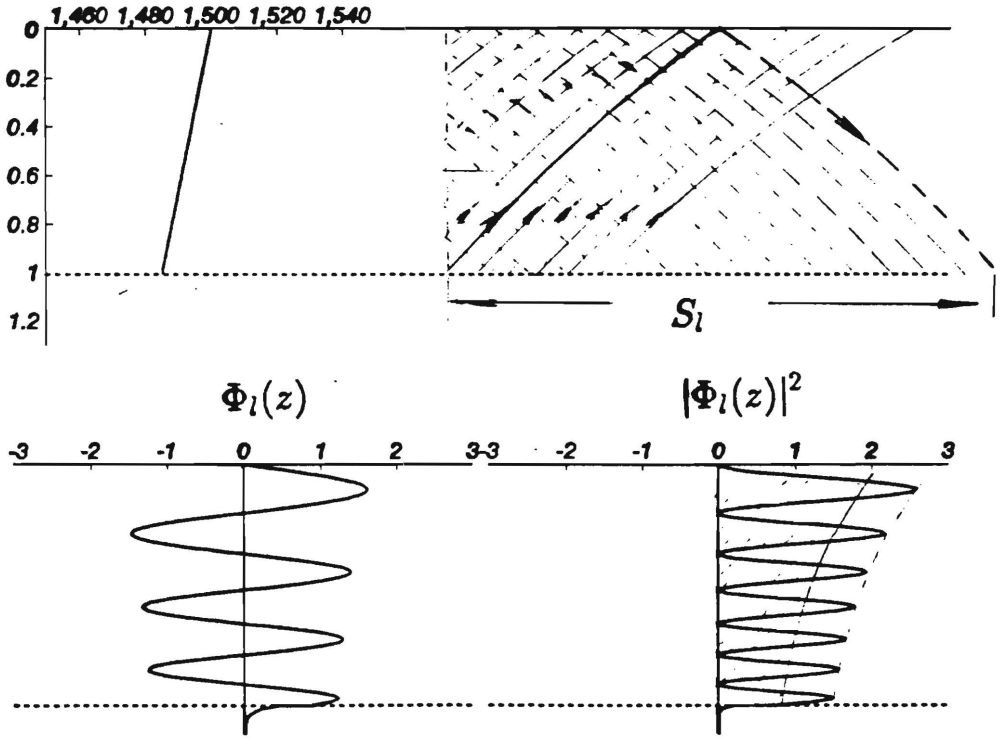

Use WKB solution envelope to present $|\Phi(z)|^2$

Neglect the energy in the exponential decay area

Use definite integral Eq. 11

change the summation into a integral with respect to θ

Fig. 7

Average Intensity:

$$I(r,z;z_0) = \frac{2}{r}e^{-\alpha r}\int \frac{2e^{\frac{2ln|V(\theta_b)|}{S_l(\theta)}r}}{S(\theta_l(z)) \times tan\theta(z)}d\theta(z_0) \qquad (12)$$
$$= \frac{2e^{-\alpha r}}{Hr}\int I_{aps}(\theta,r,z;z_0)d\theta$$

Average Angular Power Spectrum:

$$I_{aps}(\theta,r,z;z_0) = \frac{2H\, e^{\frac{2ln|V(\theta)|}{S(\theta_b)}r}}{S(\theta) \times tan\theta(z)} \qquad (13)$$

Same as one obtained by Brekhovskikh, Smith or Weston.

Where

α_v – water column absorption.

z_0, z – source (receiver) depth.

$\theta(z_)$ – grazing angle of mode-rays at the source *depth.*

$\theta(z)$ – grazing angle of mode-rays at the receiver *depth.*

Mode-ray are fuzzy everywhere in the space

Fig. 8

(2.2) Average shallow water reverberation

$$dI_s(\theta, \phi) = \mu I_i(\theta) M(\theta\,\phi) dA \tag{14}$$

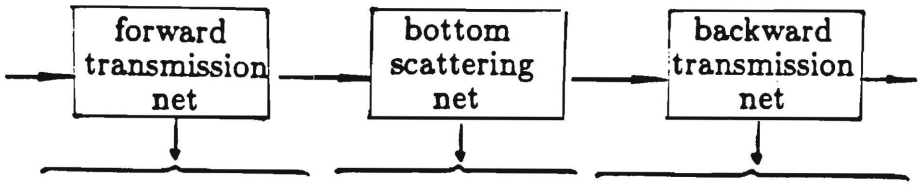

$$R(r, z; z_0) = \int\int \frac{e^{-\alpha r}}{Hr} I_{aps}(\theta, r, \tilde{H}; z_0) \times AM(\theta, \phi) \times \frac{e^{-\alpha r}}{Hr} I_{aps}(\phi, r, z; \tilde{H}) d\theta d\phi$$

$$= \frac{e^{-2\alpha r}}{(H\,r)^2} \int\int R_{aps}(r, z, z_0, \theta, \phi) d\theta d\phi \tag{15}$$

$R_{aps}(r, z, z_0, \theta, \phi)$ – angular power spectrum of average reverberation.

Fig. 9

(2.2) Sound field spatial correlation

Time signal $s(t)$

$\downarrow$

$$\rho(\tau) = \frac{\int |s(\omega)|^2 e^{-j\omega\tau} d\omega}{\int |s(\omega)|^2 d\omega}$$

Sound pressure field $P(r, z; z_0)$

$\downarrow$

$$\rho_z(d, r, z; z_0) = \frac{\int I_{aps}(\theta, r, z; z_0) e^{-jkdsin\theta} d\theta}{\int I_p(\theta, r, z; z_0) d\theta} \qquad (16)$$

For the longitudinal correlation coefficient: $sin\theta \longrightarrow cos\theta$.

Fig. 10

III. RANGE/DEPTH DEPENDENCE OF I and R

(3.1) Bottom model

Bottom reflection coefficient:

$$-ln|V(\theta)| = \begin{cases} Q\,\theta & \text{for} \quad 0 \le \theta \le \theta_c \\ -ln\,|V_0| \approx constant, & \text{for} \quad \theta_c \le \theta \le \frac{\pi}{2} \end{cases} \tag{17}$$

θ_c – crtical angle.

Bottom scattering model:

A phenomenological expression with an arbitrary angle dependence (no matter what is the scattering mechanism) :

$$M(\theta,\phi) = \left(\sum_i^N \sqrt{\mu_i}\Delta_i(\theta)\theta^{(\frac{n_i}{2})}\right) \times \left(\sum_i^N \sqrt{\mu_i}\Delta_i(\phi)\phi^{(\frac{n_i}{2})}\right) \tag{18}$$

where

$$\Delta_i(x) = \begin{cases} 1, & \text{if } x \in [x_{i-1}, x_i]; \\ 0, & \text{otherwise.} \end{cases} \tag{19}$$

Special case ($n = 2$, Lambert's law):

$$M(\theta,\phi) = \mu sin\theta \times sin\phi \tag{20}$$

Two assumptions: a) $M(\theta,\phi)$ slowly varies with angle; b) $M(\theta,\phi)$ is reciprocal, i.e., $M(\theta,\phi) = M(\phi,\theta)$.

Fig. 11

(3.2) In Pekeris Model

Sound field intensity:

$$I(r) = \begin{cases} \frac{4}{-ln|V_0|} \times r^{-2} & \text{for } r_1 > r \quad (21) \\ \frac{2\theta_c}{H} \times r^{-1} & \text{for } r_2 > r > r_1 \quad (22) \\ (\frac{\pi}{QH})^{1/2} \times r^{-\frac{3}{2}} & \text{for } r_3 > r > r_2 \quad (23) \\ \frac{2\pi}{kH^2} \times r^{-1} exp(-\frac{Q\pi^2}{k^2H^3}r) & \text{for } r > r_3 \quad (24) \end{cases}$$

where

$$r_1 = \frac{H}{-ln|V_0|\theta_c}$$

$$r_2 = \frac{H}{Q\theta_c^2}$$

$$r_3 = \frac{k^2H^3}{Q\pi^3}$$

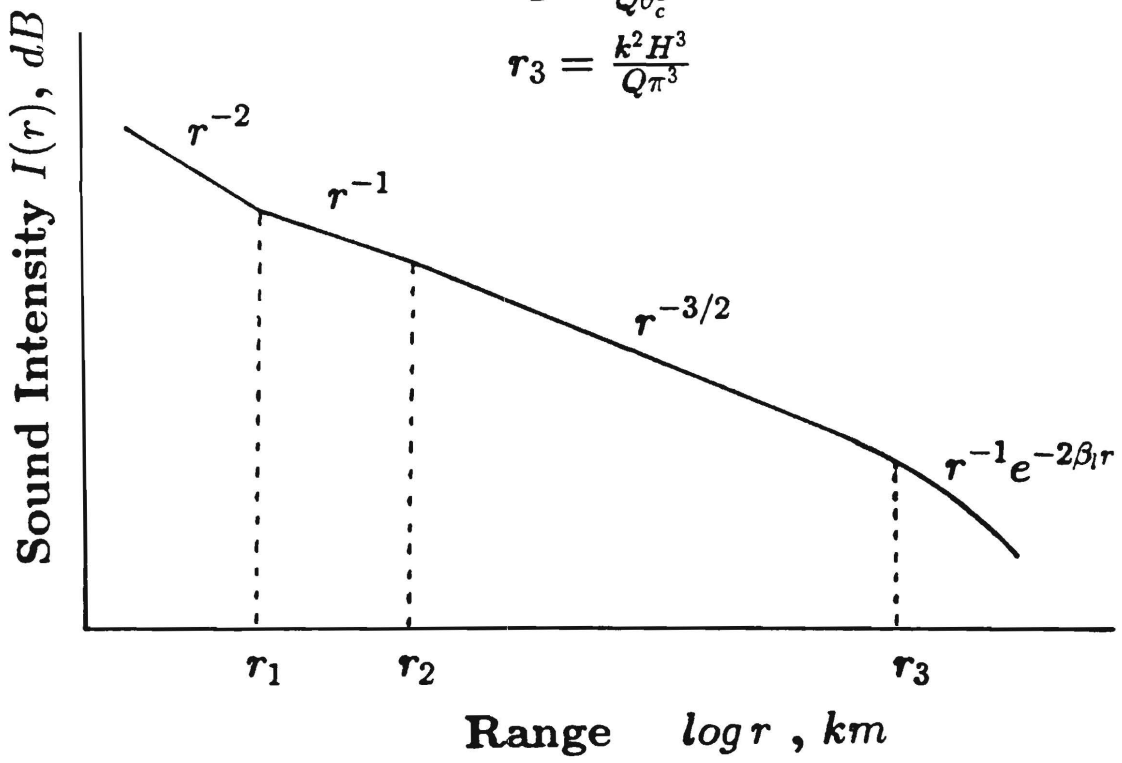

Fig. 12

(3.2) In Pekeris Model

Average reverberation intensity:

$$R(r) = \frac{\mu\pi c\tau\theta_c^{(2+n)}}{2^n H^2} \times r^{-1} \qquad for \quad r_2 > r > r_1 \qquad (25)$$

$$R(r) = \frac{\mu\pi^{(2-\pi/2)}c\tau}{4Q^{(1+n/2)}H^{(1-n/2)}} \times r^{-(2+n/2)} \quad for \quad r_3 > r > r_2 \quad (26)$$

Echo to reverberation ratio:

$$\frac{Ec}{R}(r) = K\frac{2^{(2+n)}}{\mu\pi c\tau\theta_c^n} \times r^{-1} \qquad for \quad r_2 > r > r_1 \qquad (27)$$

$$\frac{Ec}{R}(r) = K\frac{4\,Q^{n/2}}{\mu\pi^{(1-n/2)}c\tau H^{n/2}} \times r^{-(1-n/2)} \quad for \quad r_3 > r > r_2 \quad (28)$$

K – Target reflection coefficient.

$n = 2$, $\frac{\mathbf{Ec}}{\mathbf{R}} \longrightarrow$ *constant*

$n > 2$, $\frac{\mathbf{Ec}}{\mathbf{R}}$ increases with increasing range.

"A peculiarity sometimes observed with echo-ranging sonars in shallow water: an echo-to-reverberation ratio remains nearly constant, or even increases somewhat, with increasing range or time." (Urick, JASA 48, 1970).

Fig. 13

(3.3) In wedged shallow water

$$H(r) = H_0(1 + ar)$$

In three half law region

Average reverberation intensity:

$$R(r) = \frac{\mu\pi^{(2-\pi/2)}c\tau}{4Q^{(1+n/2)}} \times \frac{H_0^n}{[(H_0 + H_r)/2]^{(1+n/2)}} \times r^{-(2+n/2)} \quad (29)$$

Echo to reverberation ratio:

$$\frac{Ec}{R}(r) = K\frac{4\,Q^{n/2}}{\mu\pi^{(1-n/2)}c\tau} \times \frac{[(H_0 + H_r)/2]^{n/2}}{H_0^n} \times r^{-(1-n/2)} \quad (30)$$

$$\frac{R_{H_1}(r)}{R_{H_2}} = \left(\frac{H_1}{H_2}\right)^n$$

The reverberation intensities obtained at two terminals with different depths would not be reciprocal.

Example: $H_1 = 50m$, $H_2 = 200m$, $n = 2$ (Lambert's law), then the reverberation interference at shallower area would be 12 dB less.

Fig. 14

(3.4) In linear negative gradient layer

Sound intensity

$$c(z) = c_0(1 + az) \tag{31}$$

$$I_A(r, z; z_0) \approx \frac{4}{-ln|V_0|} \times r^{-2} \tag{32}$$

$$I_B(r, z; z_0) = \frac{2}{H}[\theta_c - \sqrt{2az_0} + M(z, z_0)] \times r^{-1} \tag{33}$$

$$\begin{aligned} I_C = {} & \frac{1}{2}\sqrt{\frac{\pi}{QH}} e^{-aQr(1-2z_0/H)}(e^{-aQr} + 1) \\ & \times [\Phi(\sqrt{\frac{Qr}{H}}\theta_c) - \Phi(\sqrt{\frac{2aQrz_0}{H}})] \times r^{-3/2} \end{aligned} \tag{34}$$

$$I_D(r, z; z_0) = 2M(z, z_0) \times r^{-r} e^{-aQr} \tag{35}$$

Range/depth dependence:

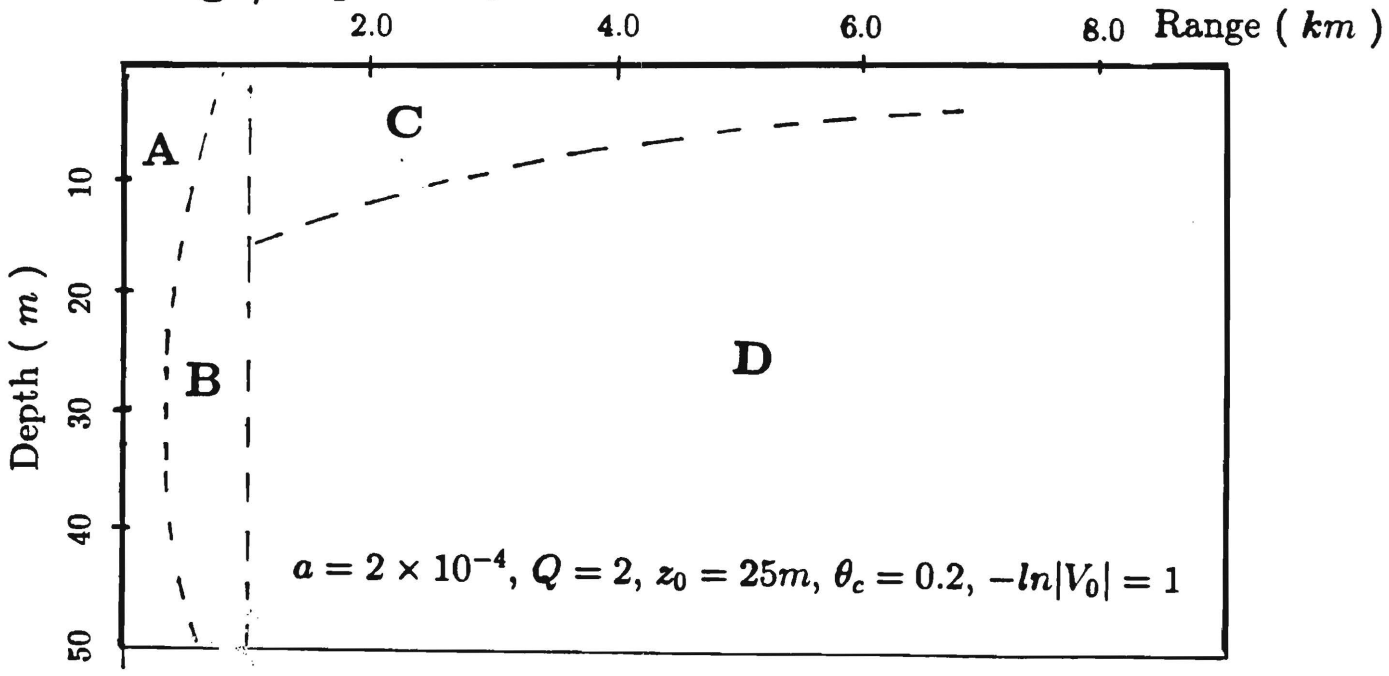

Fig. 15

(3.4) In linear negative gradient layer

(In field area D)

Average reverberation intensity:

$$R(r, z_0) = \mu\pi c\tau a^{(1+n/2)} N(z_0) \times r^{-1} e^{-2aQr} \qquad (36)$$

Echo-to-reverberation ratio:

$$\frac{Ec}{R}(r, z; z_0) = \frac{4K}{a^{(1+n/2)}\mu\pi c\tau} \times \frac{M^2(z; z_0)}{N(z_0)} \times r^{-1} \qquad (37)$$

where

$$N(z_0) = \frac{\left(cos^{-1}\sqrt{\frac{H-z_0}{H}}\right)^{2-n}\left(ln\frac{\sqrt{H}+\sqrt{z_0}}{\sqrt{H-z_0}}\right)^{n}}{[2(H-z_0)]^{(1-n/2)}}$$

$$M(z, z_0) = \sqrt{\frac{a}{2[H - min(z, z_0)]}} F\left(\widetilde{\alpha}, \widetilde{\beta}\right)$$

$$\widetilde{\alpha} = cos^{-1}\sqrt{\frac{|z - z_0|}{max(z, z_0)}}$$

$$\widetilde{\beta} = \sqrt{\frac{H - max(z, z_0)}{H - min(z, z_0)}}$$

$F(\widetilde{\alpha}, \widetilde{\beta})$ – elliptic integral.

Fig. 16

Example (in field area D):

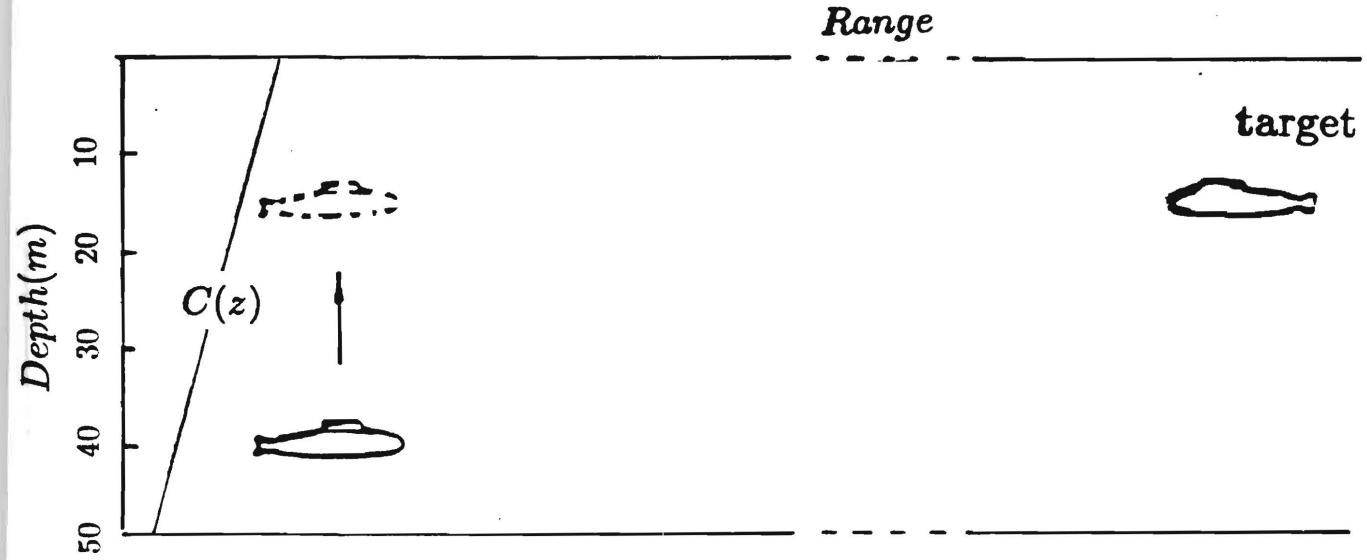

Suppose: $H = 50m$, target depth $z = 15m$.

If sonar depth (z_0) $40m \longrightarrow 15m$,

Echo-to-reverberation ratio would increase

12.1 dB for n = 2 (Lambert's scattering bottom)

14.0 dB for n = 1

15.8 dB for n = 0

A depth-variable sonar has advantage in shallow water.

Fig. 17

(3.5) In strong thermocline shallow water

(two-layer model)

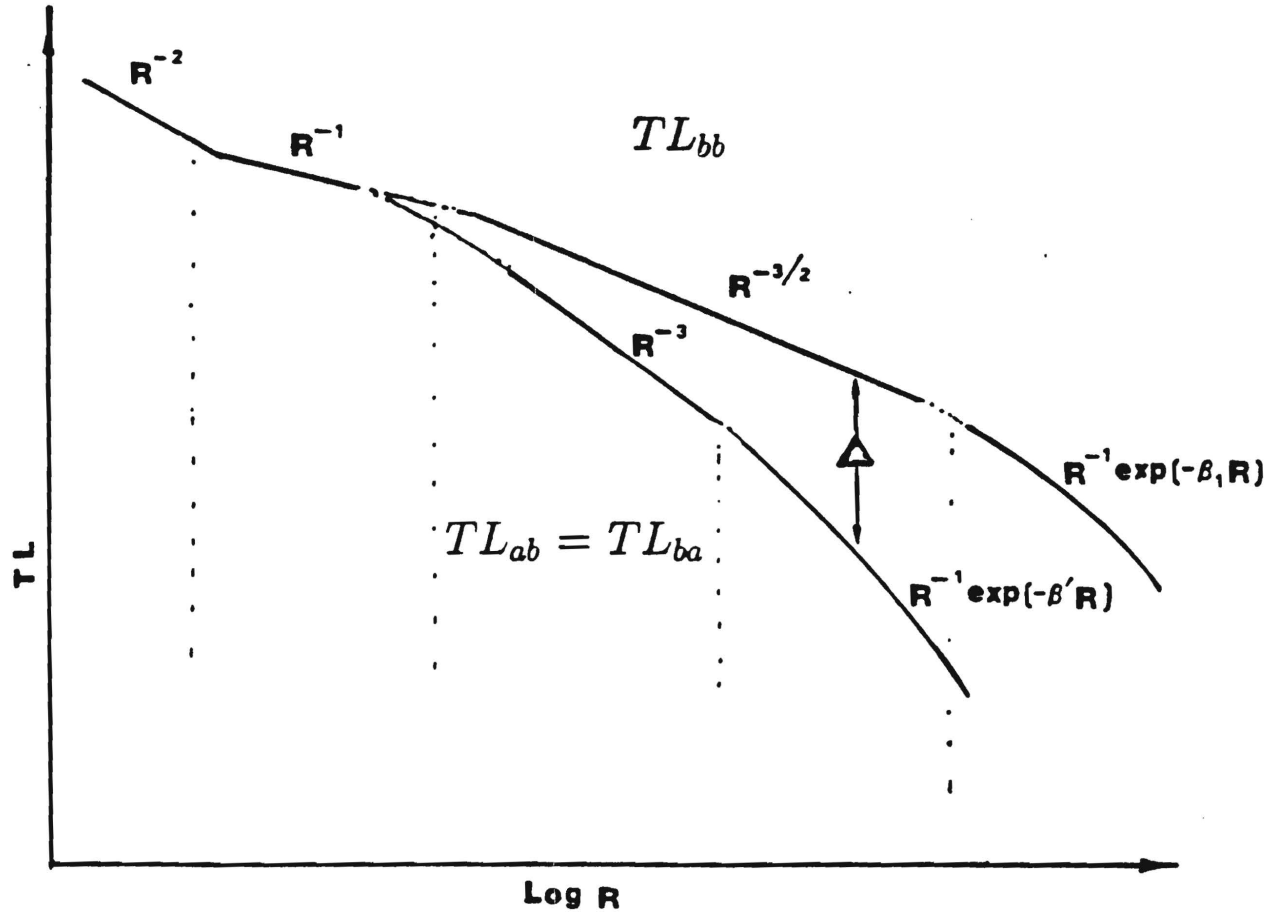

Fig. 18

Sound Transmission Loss

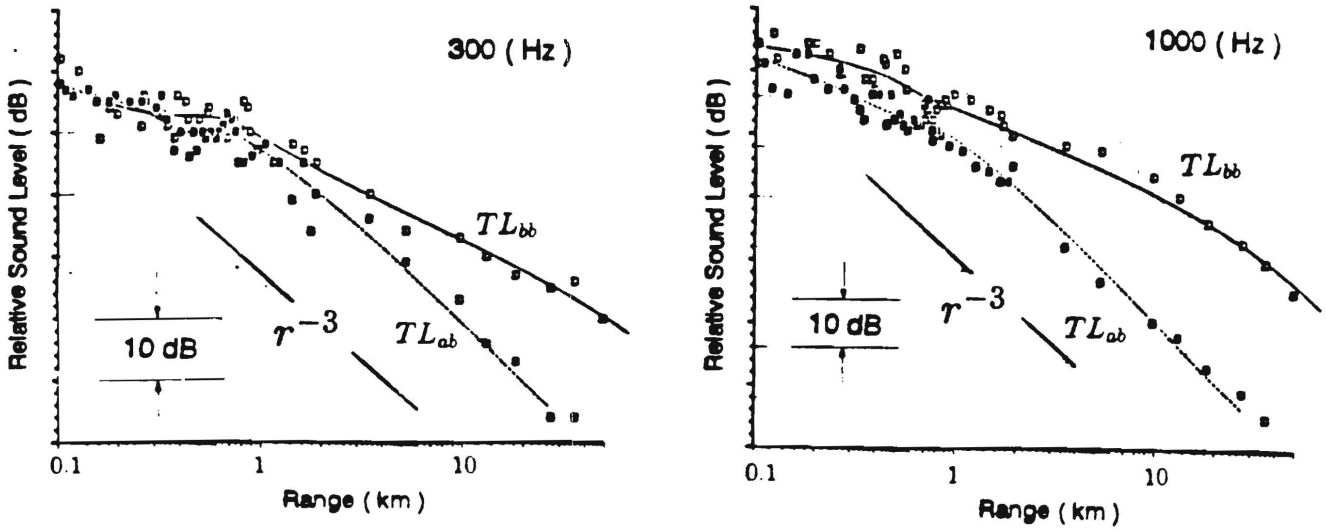

Reverberation Intensity

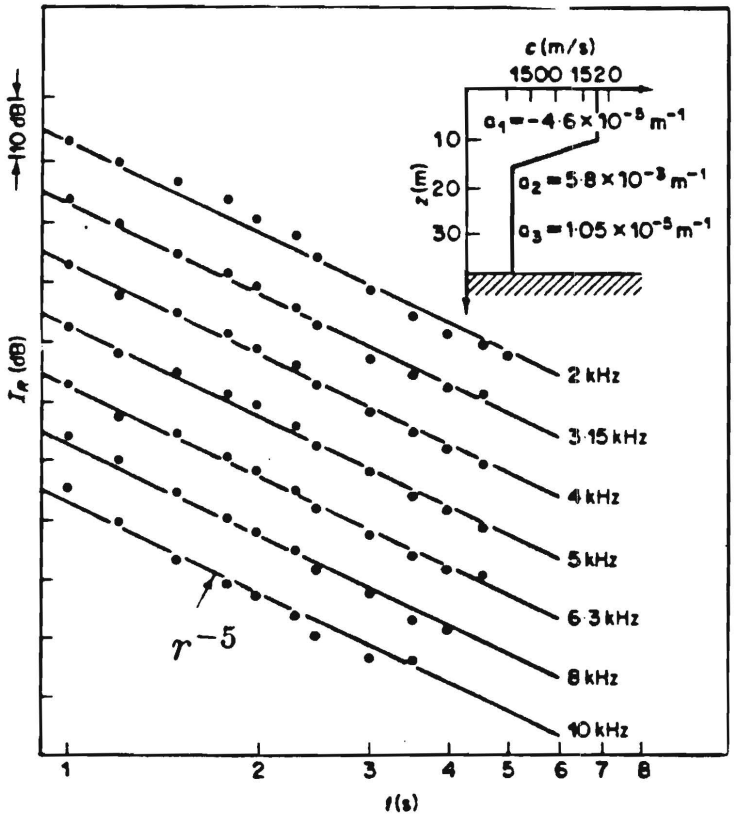

By Zhang and Jing
[J. Sound & Vib., 119 (1987)]

Fig. 19

Echo to Reverberation Ratio

(at the middle range in strong thermocline)

Sonar	Target	$Ec/R(r)$
a	b	$\propto r^{-1}$
a	a	Better ($\sim r^{+1}$)
b	a	Worst ($\sim r^{-3}$)
b	b	→ P. model

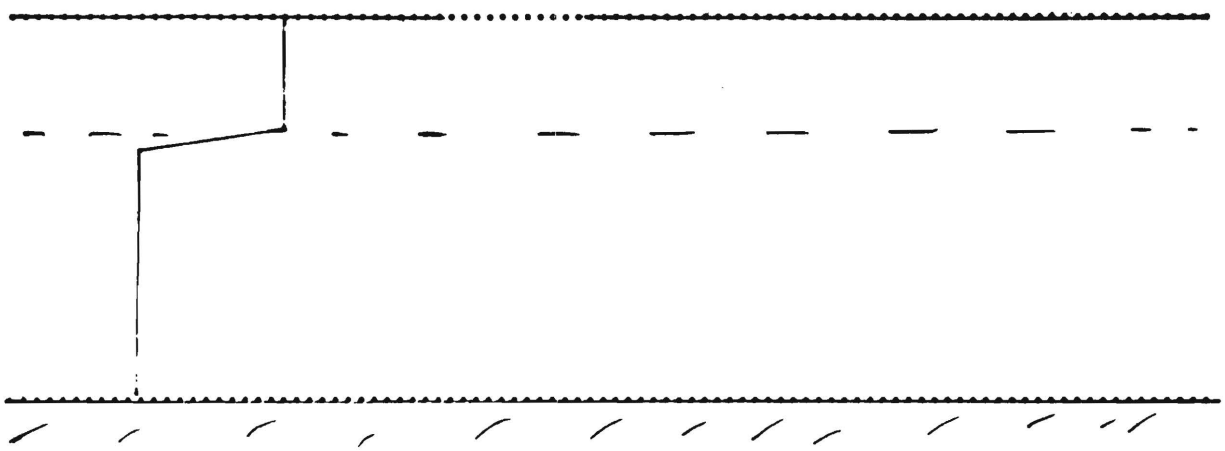

Conclusion

Echo to reverberation ratio for a active sonar in shallow water will strongly depend on environmental parameters, such as sound velocity profile, bottom reflection, bottom scattering angular index, sonar location and target location, and so on. A depth-variable sonar has advantage. To some degree, active sonar average performance can be predicted.

Fig. 20

(IV) At-sea experimental data on reverberation

(from three Pekeris models with different sediments)

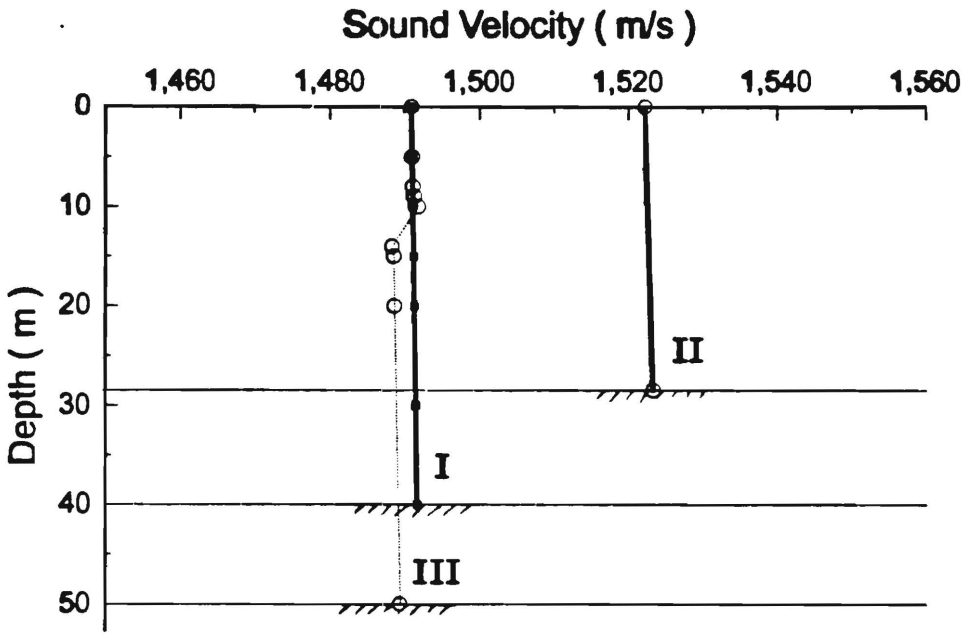

Area I: Coarse – medium sand

$M_d = 0.35mm \quad k = 35.5\% \quad \rho = 1.90g/cm^3$

Area II: Very find sand – silty sand – clay

$M_d = 0.07mm \quad k = 46.2\% \quad \rho = 1.85g/cm^3$

Area III: silt – clay silt

$M_d = 0.02mm \quad k = 56.1\% \quad \rho = 1.71g/cm^3$

m_d – mean grain diameter.; k – porosity; ρ – density.

Fig. 21

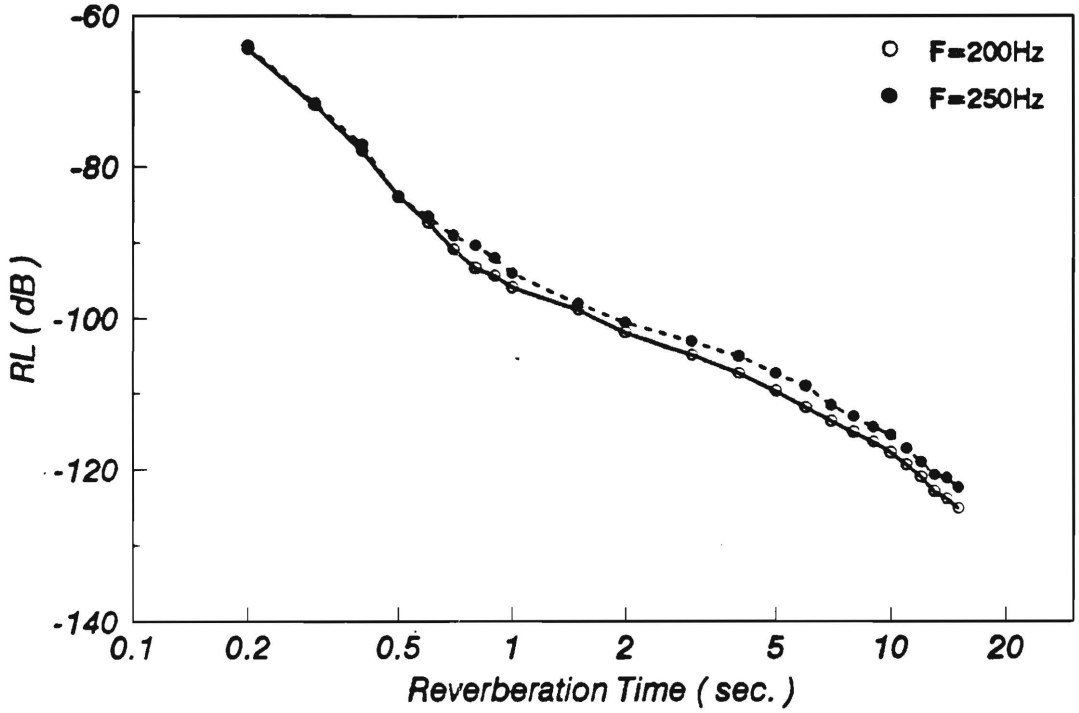
-60
-80
-100
-120
-140
RL (dB)
0.1
0.2
0.5
1
2
5
10
20
Reverberation Time (sec.)
F=200Hz
F=250Hz

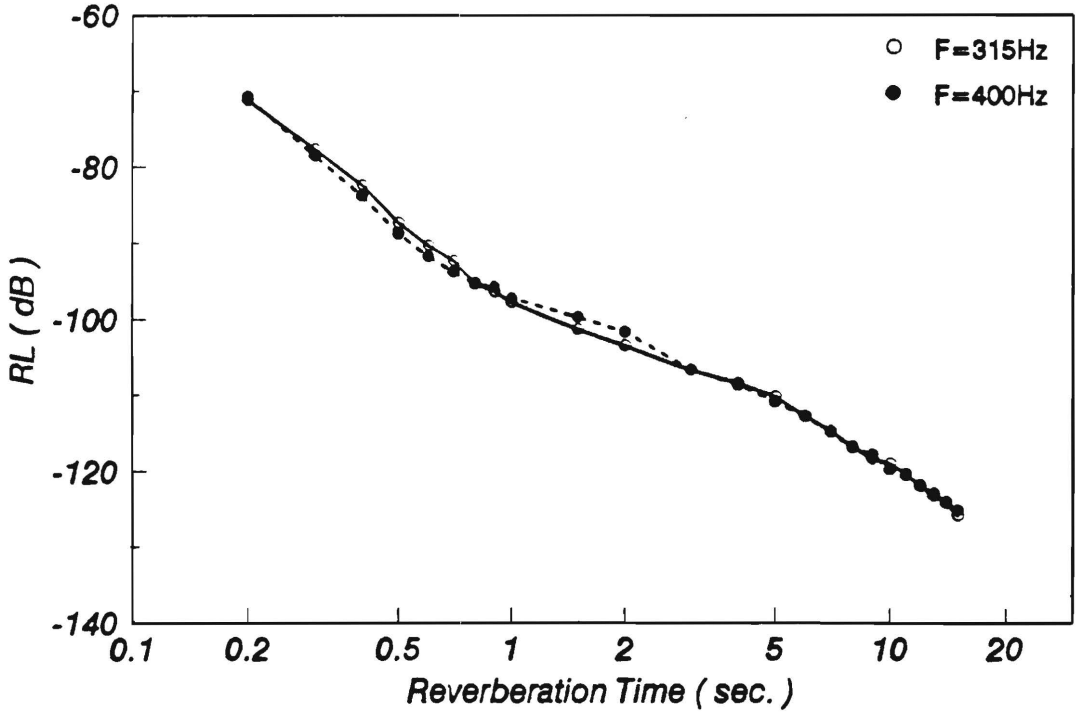
-60
-80
-100
-120
-140
RL (dB)
0.1
0.2
0.5
1
2
5
10
20
Reverberation Time (sec.)
F=315Hz
F=400Hz

Fig. 22

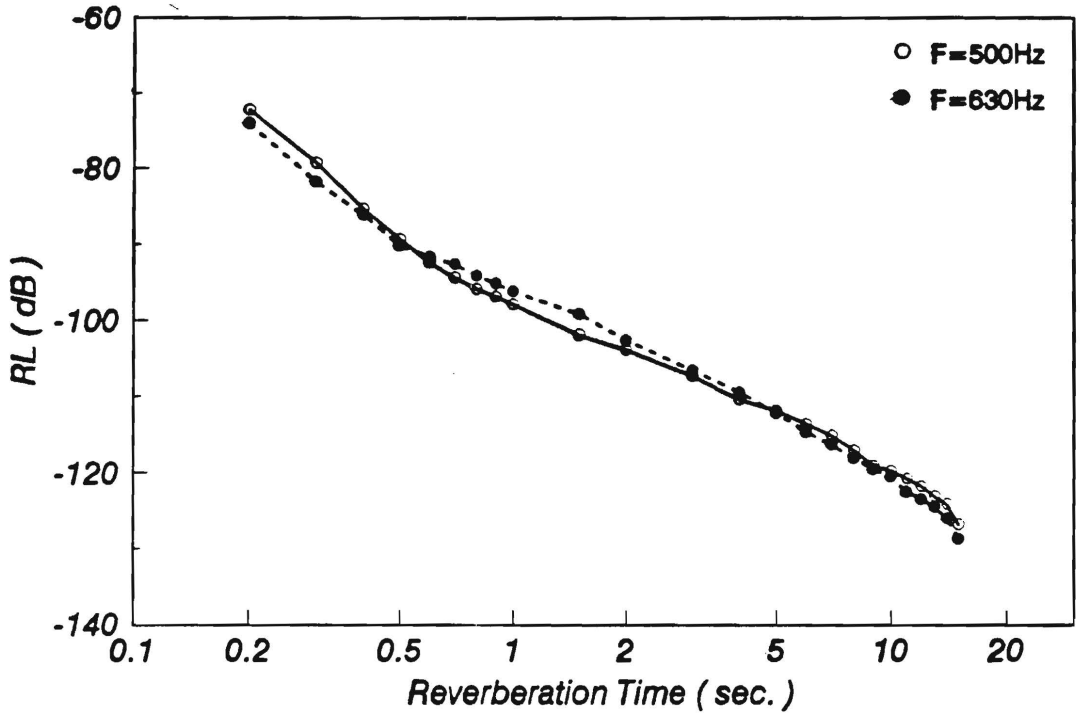
-60
-80
-100
-120
-140
RL (dB)
F=500Hz
F=630Hz
0.1
0.2
0.5
1
2
5
10
20
Reverberation Time (sec.)

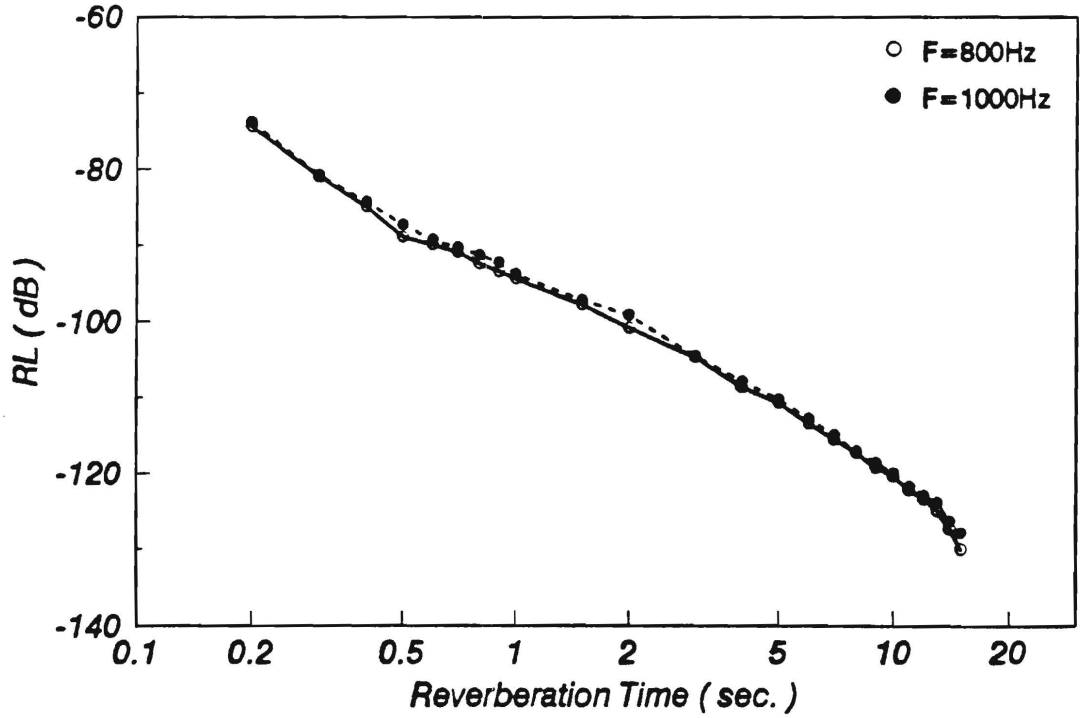
-60
-80
-100
-120
-140
RL (dB)
F=800Hz
F=1000Hz
0.1
0.2
0.5
1
2
5
10
20
Reverberation Time (sec.)

Fig. 23

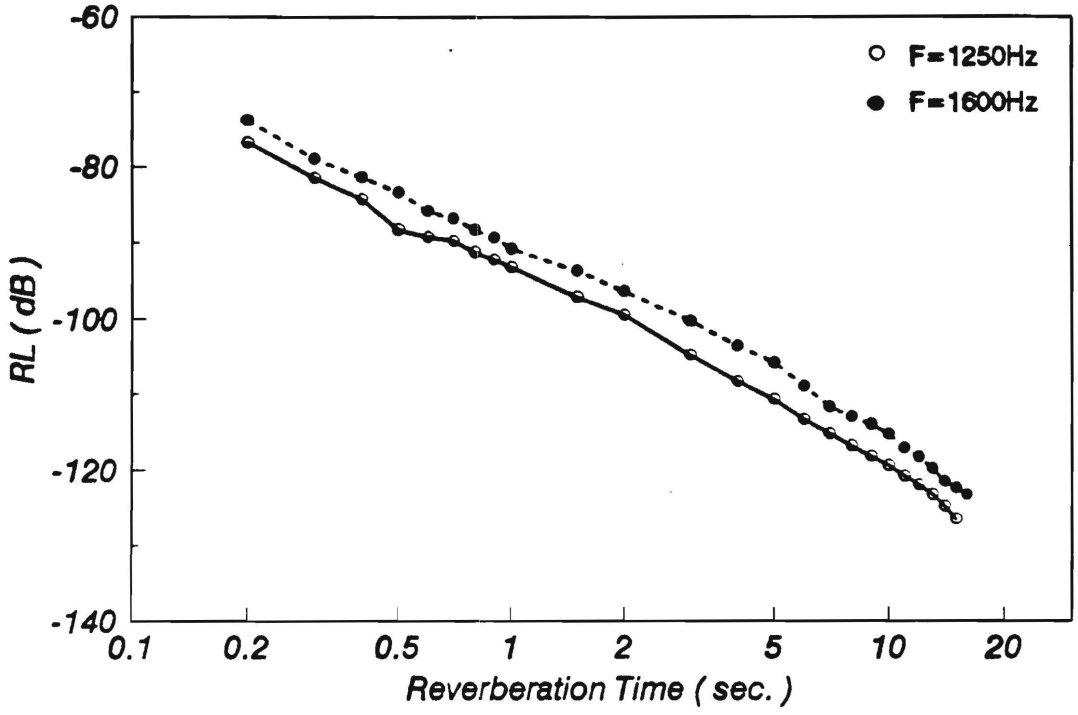
-60
-80
-100
-120
-140
RL (dB)
0.1
0.2
0.5
1
2
5
10
20
Reverberation Time (sec.)
F=1250Hz
F=1600Hz

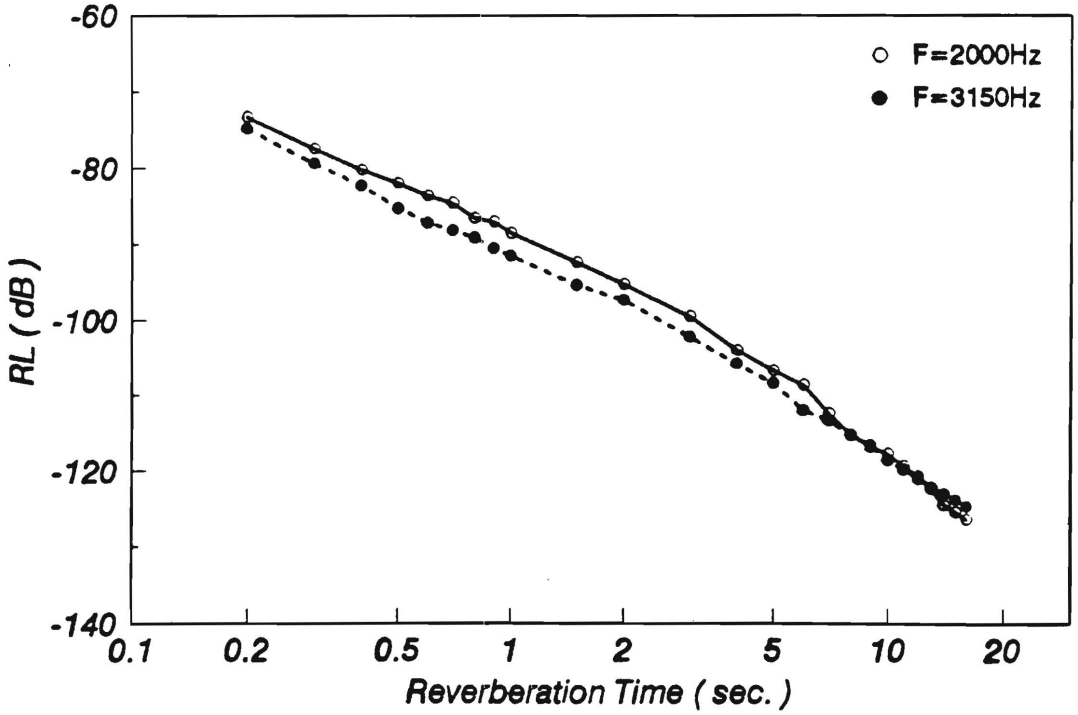
-60
-80
-100
-120
-140
RL (dB)
0.1
0.2
0.5
1
2
5
10
20
Reverberation Time (sec.)
F=2000Hz
F=3150Hz

Fig. 24

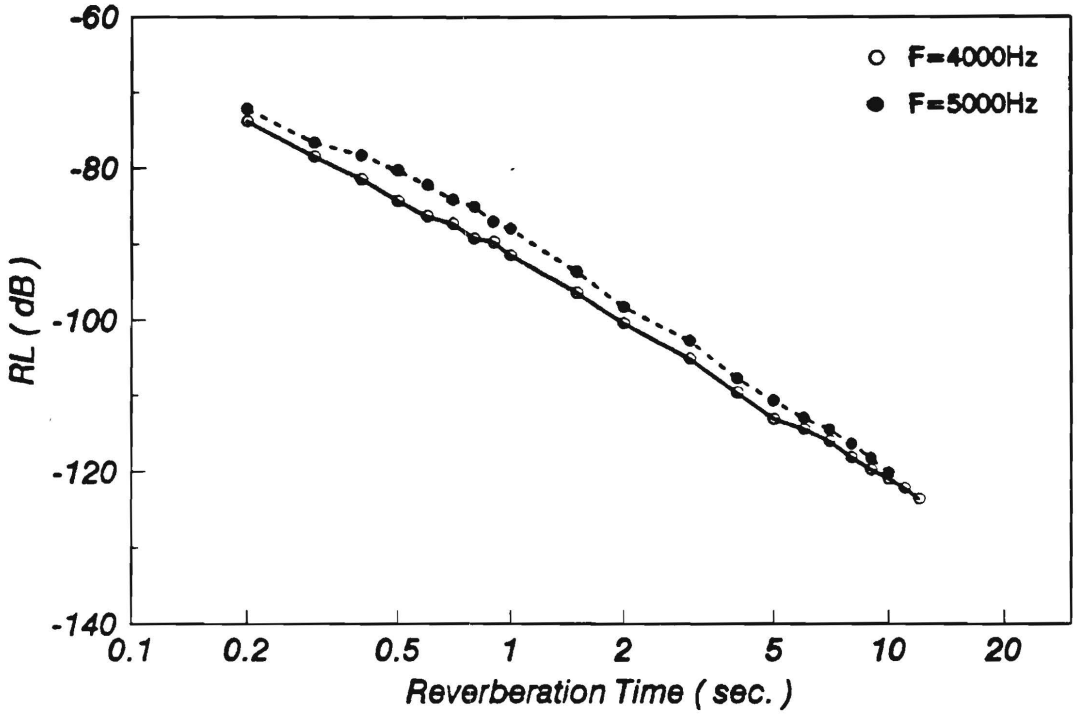
-60
-80
-100
-120
-140
RL (dB)
0.1
0.2
0.5
1
2
5
10
20
Reverberation Time (sec.)
F=4000Hz
F=5000Hz

Fig. 25

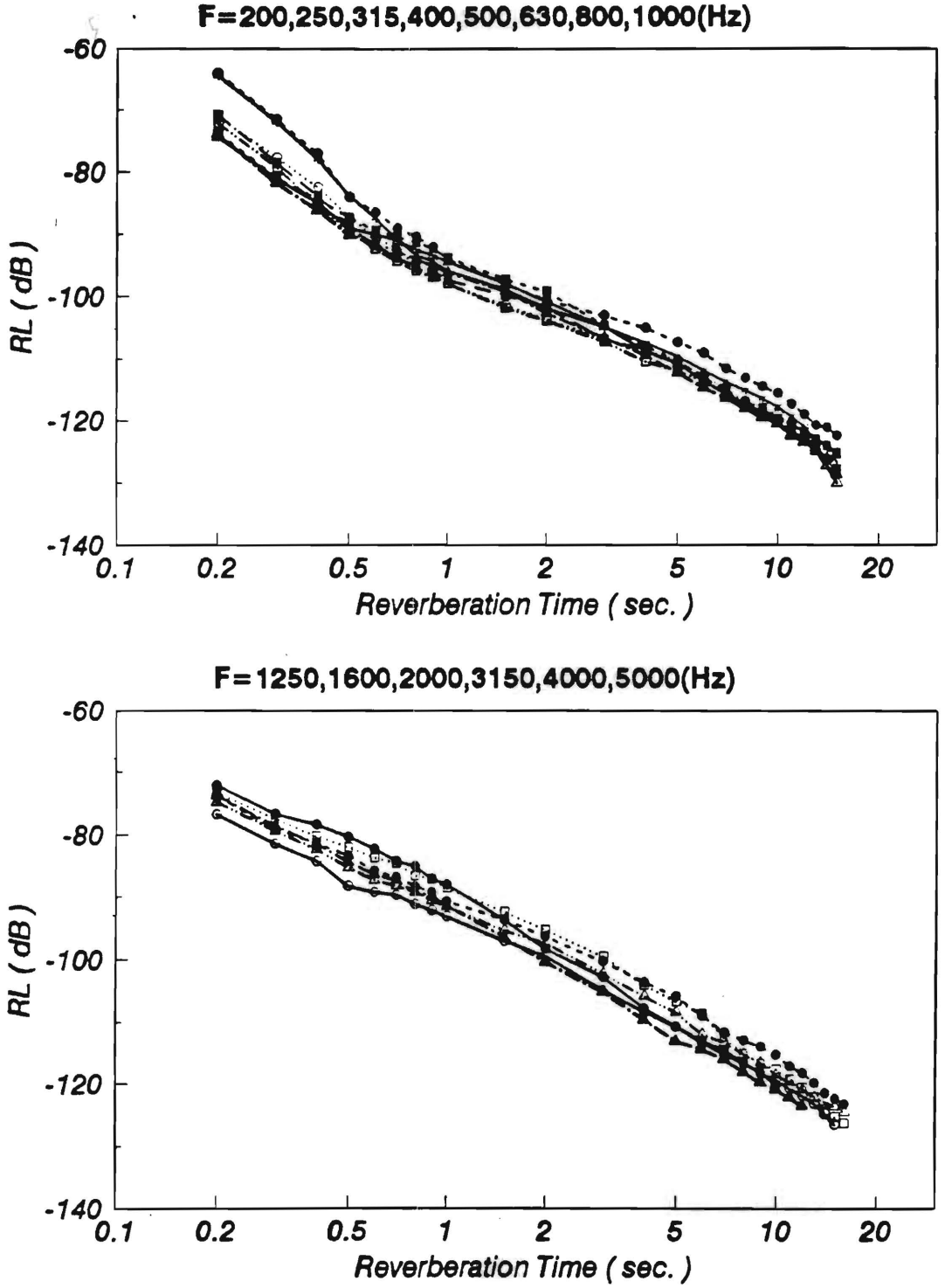
F=200,250,315,400,500,630,800,1000(Hz)
-60
-80
-100
-120
-140
RL (dB)
0.1
0.2
0.5
1
2
5
10
20
Reverberation Time (sec.)
F=1250,1600,2000,3150,4000,5000(Hz)
-60
-80
-100
-120
-140
RL (dB)
0.1
0.2
0.5
1
2
5
10
20
Reverberation Time (sec.)

Fig. 26

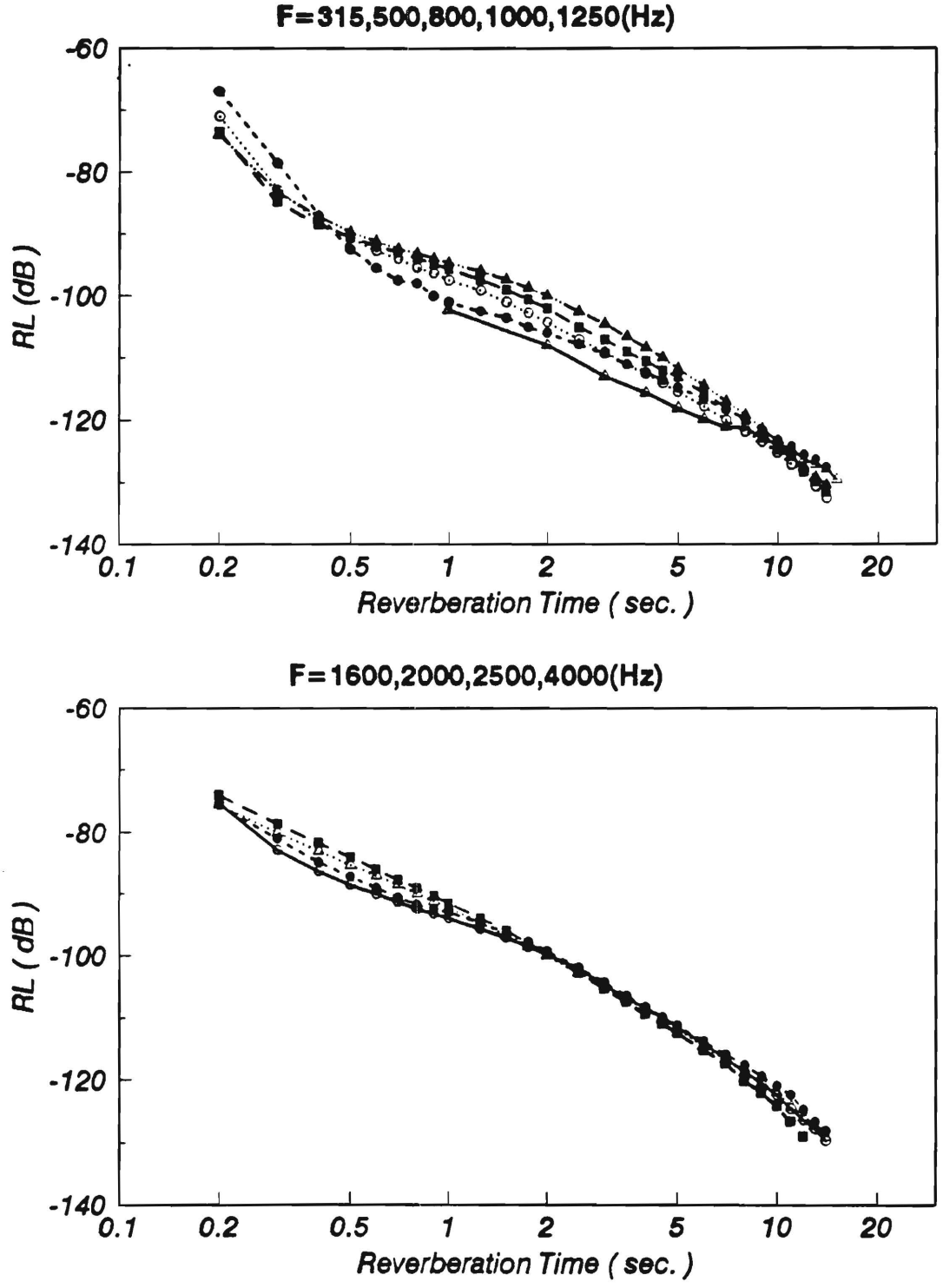
F=315,500,800,1000,1250(Hz)
-60
-80
-100
-120
-140
RL (dB)
0.1
0.2
0.5
1
2
5
10
20
Reverberation Time (sec.)
F=1600,2000,2500,4000(Hz)
-60
-80
-100
-120
-140
RL (dB)
0.1
0.2
0.5
1
2
5
10
20
Reverberation Time (sec.)

Fig. 27

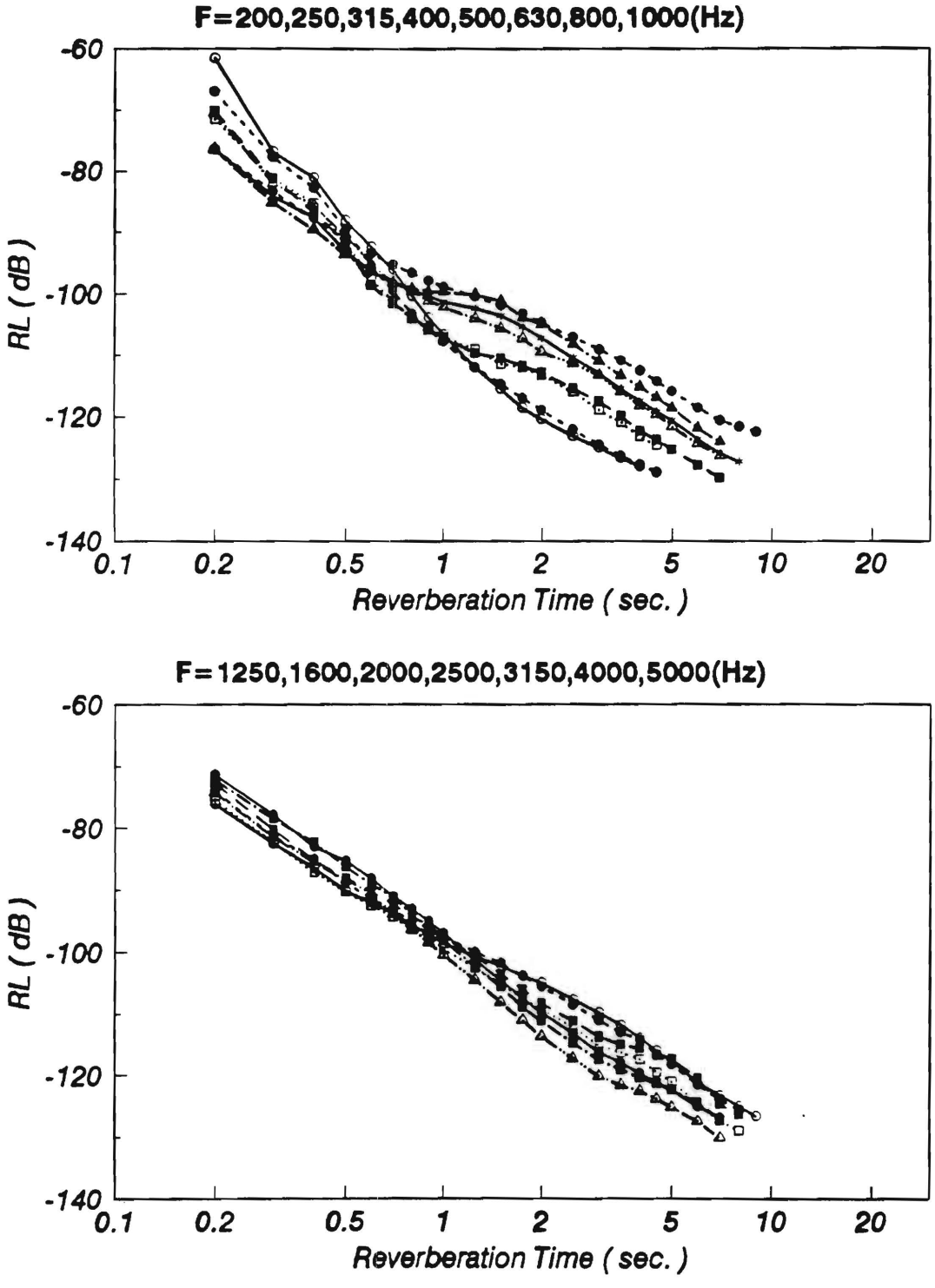
F=200,250,315,400,500,630,800,1000(Hz)
-60
-80
-100
-120
-140
RL (dB)
0.1
0.2
0.5
1
2
5
10
20
Reverberation Time (sec.)
F=1250,1600,2000,2500,3150,4000,5000(Hz)
-60
-80
-100
-120
-140
RL (dB)
0.1
0.2
0.5
1
2
5
10
20
Reverberation Time (sec.)

Fig. 28

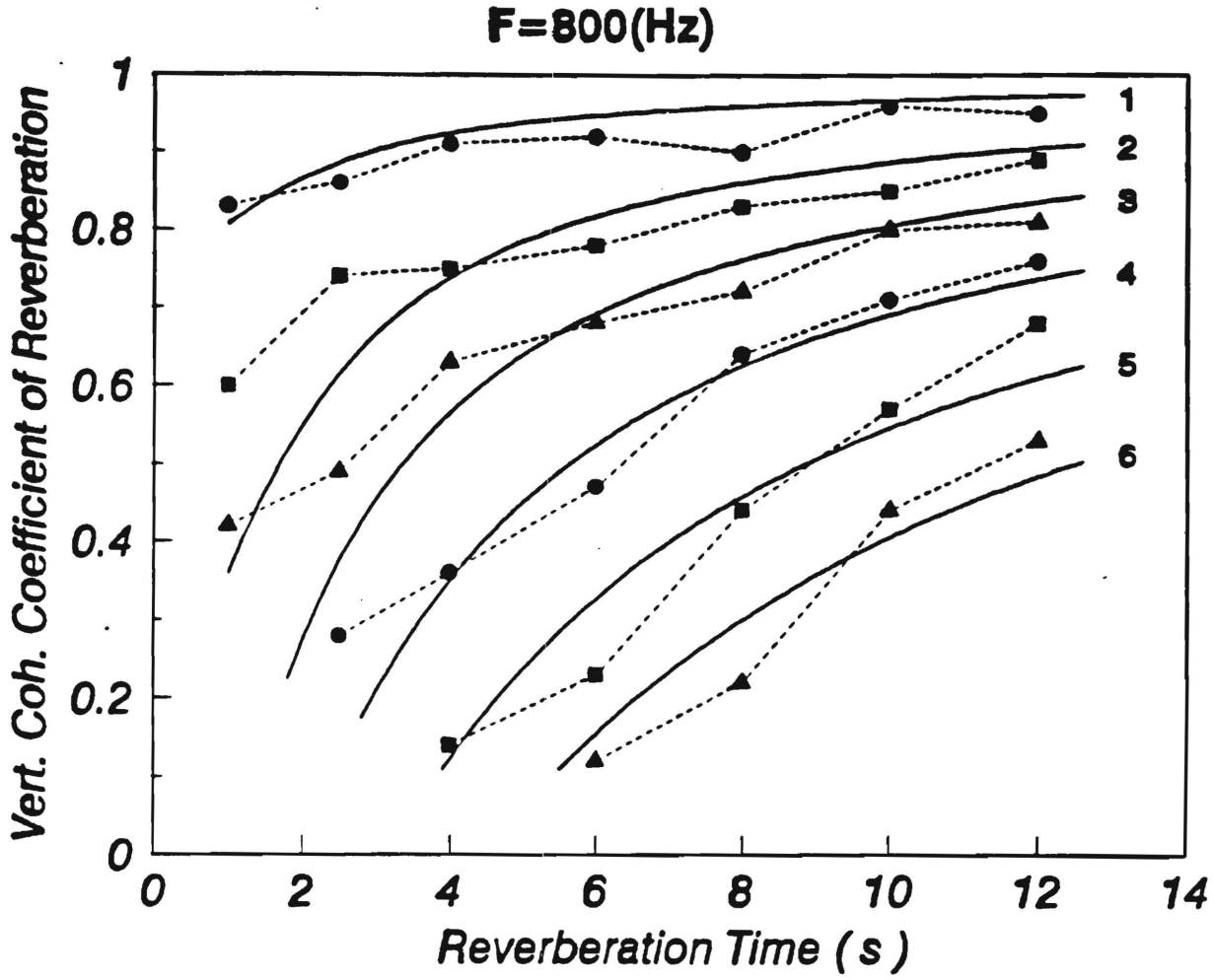

No.	1	2	3	4	5	6
d (m)	0.55	1.10	1.65	2.20	2.75	3.85
Q	0.20	0.22	0.28	0.30	0.30	0.42

Fig. 29

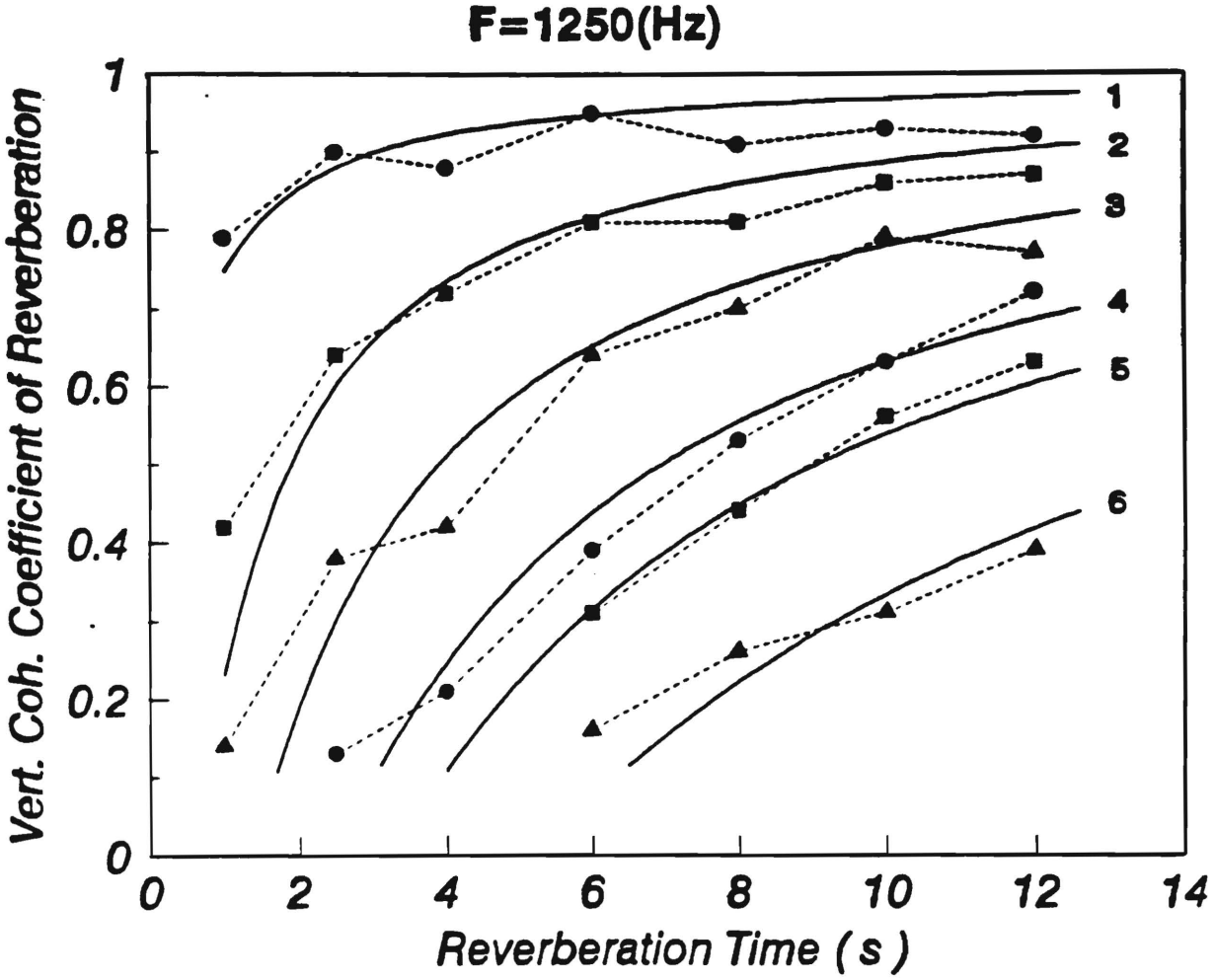

No.	1	2	3	4	5	6
d (m)	0.55	1.10	1.65	2.20	2.75	3.85
Q	0.50	0.54	0.60	0.60	0.72	0.88

Fig. 30

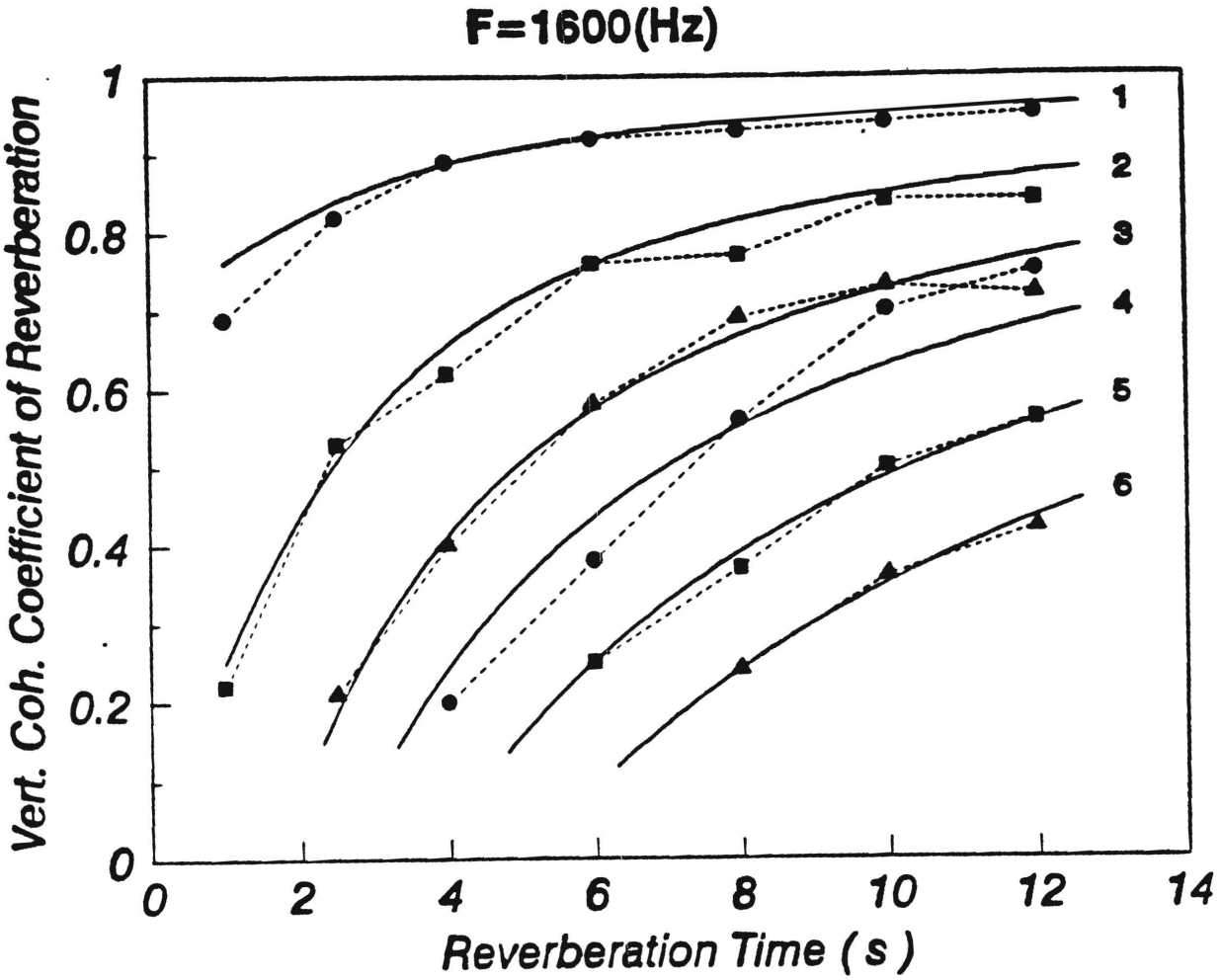

No.	1	2	3	4	5	6
d (m)	0.55	1.10	1.65	2.20	2.75	3.85
Q	0.54	0.66	0.78	0.98	1.04	1.50

Fig. 31

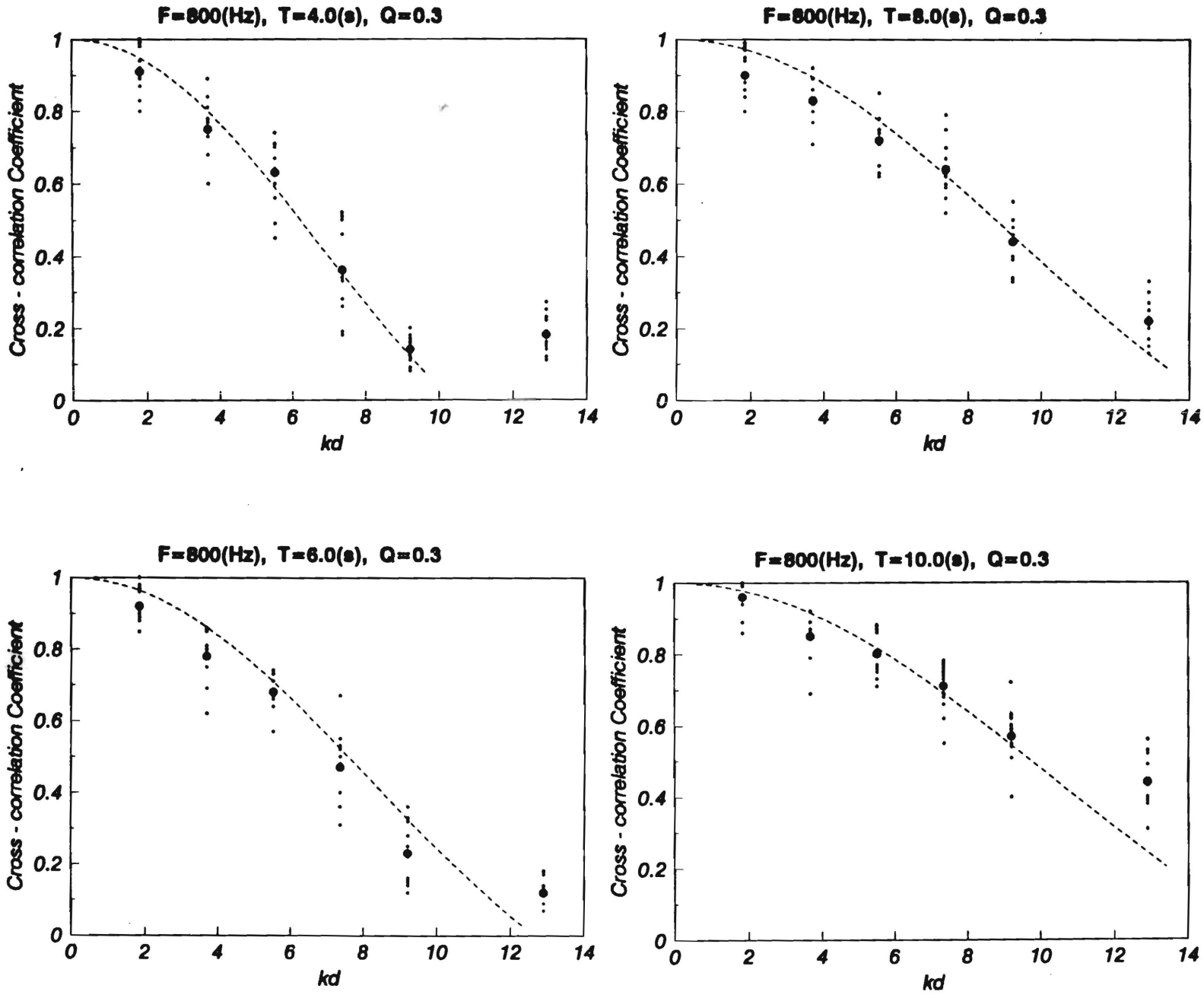
F=800(Hz), T=4.0(s), Q=0.3
F=800(Hz), T=8.0(s), Q=0.3
F=800(Hz), T=6.0(s), Q=0.3
F=800(Hz), T=10.0(s), Q=0.3
Cross - correlation Coefficient
kd
0
0.2
0.4
0.6
0.8
1
0
2
4
6
8
10
12
14

Fig. 32

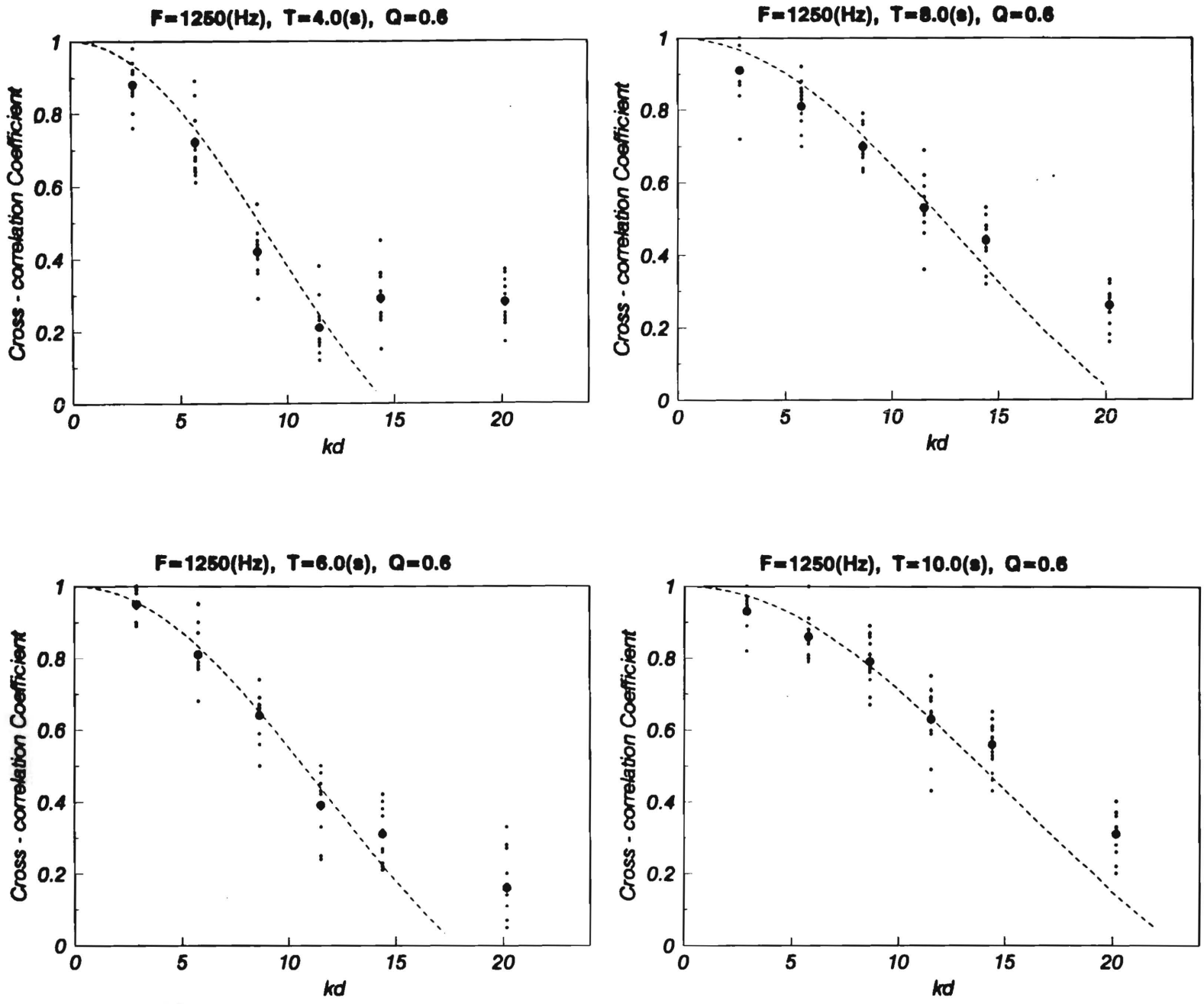
F=1250(Hz), T=4.0(s), Q=0.6
F=1250(Hz), T=8.0(s), Q=0.6
F=1250(Hz), T=6.0(s), Q=0.6
F=1250(Hz), T=10.0(s), Q=0.6
Cross - correlation Coefficient
kd
0
0.2
0.4
0.6
0.8
1
0
5
10
15
20

Fig. 33

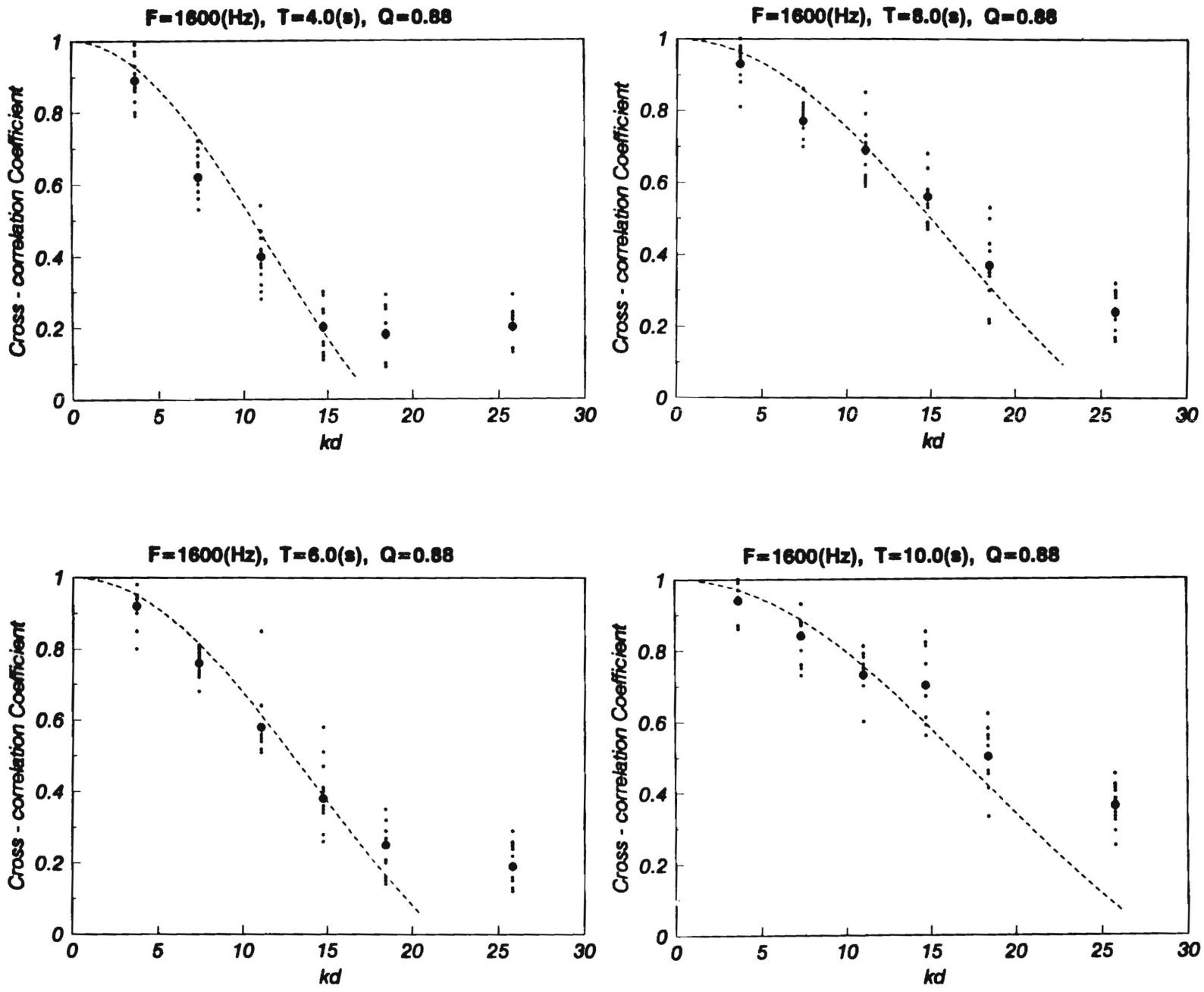
F=1600(Hz), T=4.0(s), Q=0.88
F=1600(Hz), T=8.0(s), Q=0.88
F=1600(Hz), T=6.0(s), Q=0.88
F=1600(Hz), T=10.0(s), Q=0.88
Cross - correlation Coefficient
kd
0
0.2
0.4
0.6
0.8
1
0
5
10
15
20
25
30

Fig. 34

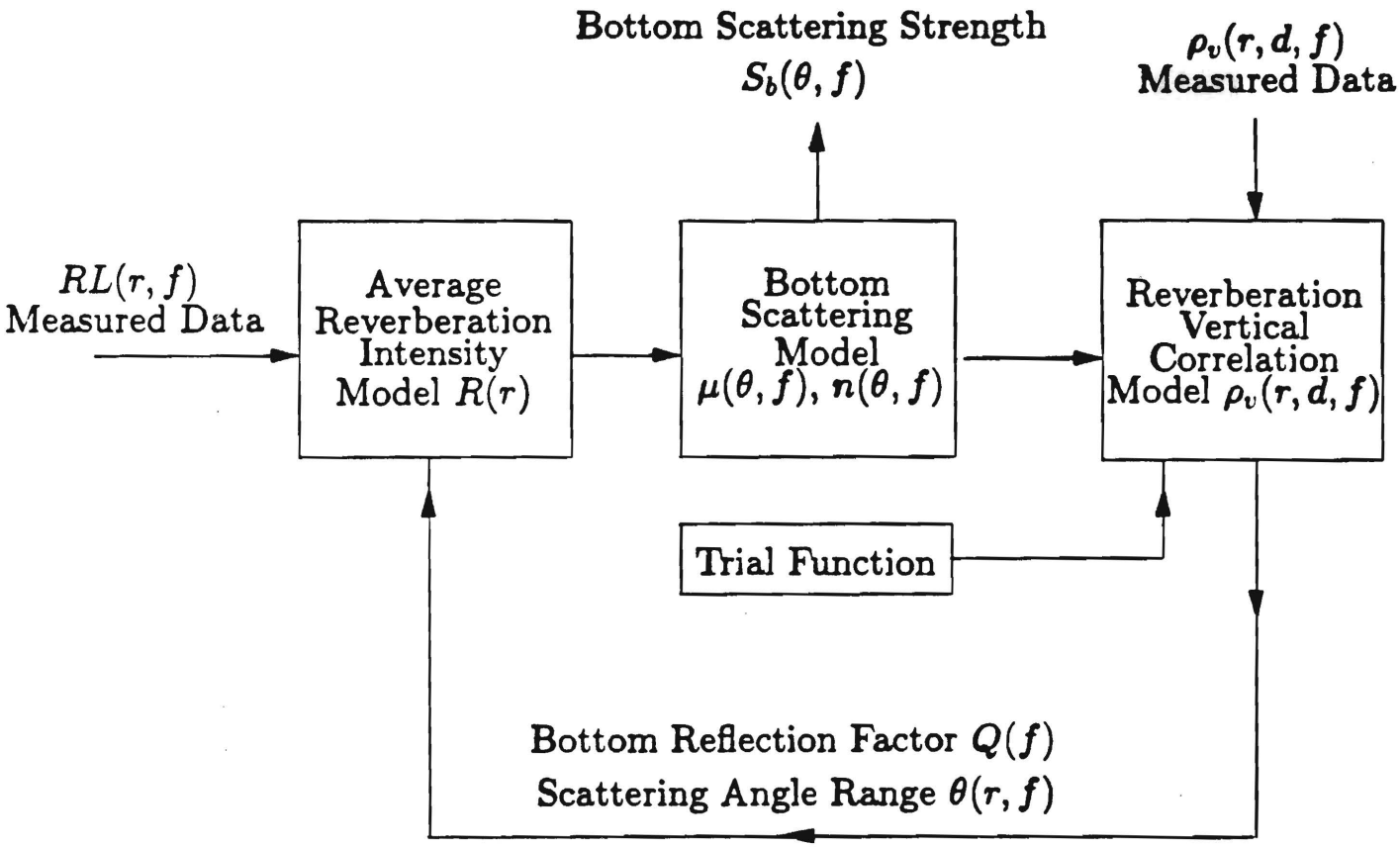

Inversion Technique Flow Chart

Fig. 35

Bottom reflection and scattering parameters:

$f\ (Hz)$	Q	n	$10log\mu\ (dB)$
500	0.20	1.1	-41.7
800	0.30	2.0	-30.5
1000	0.39	1.9	-27.8
1250	0.60	1.8	-24.6
1600	0.88	1.7	-22.1
2000	1.08	1.6	-20.9
2500	1.30	2.0	-14.3

Fig. 36

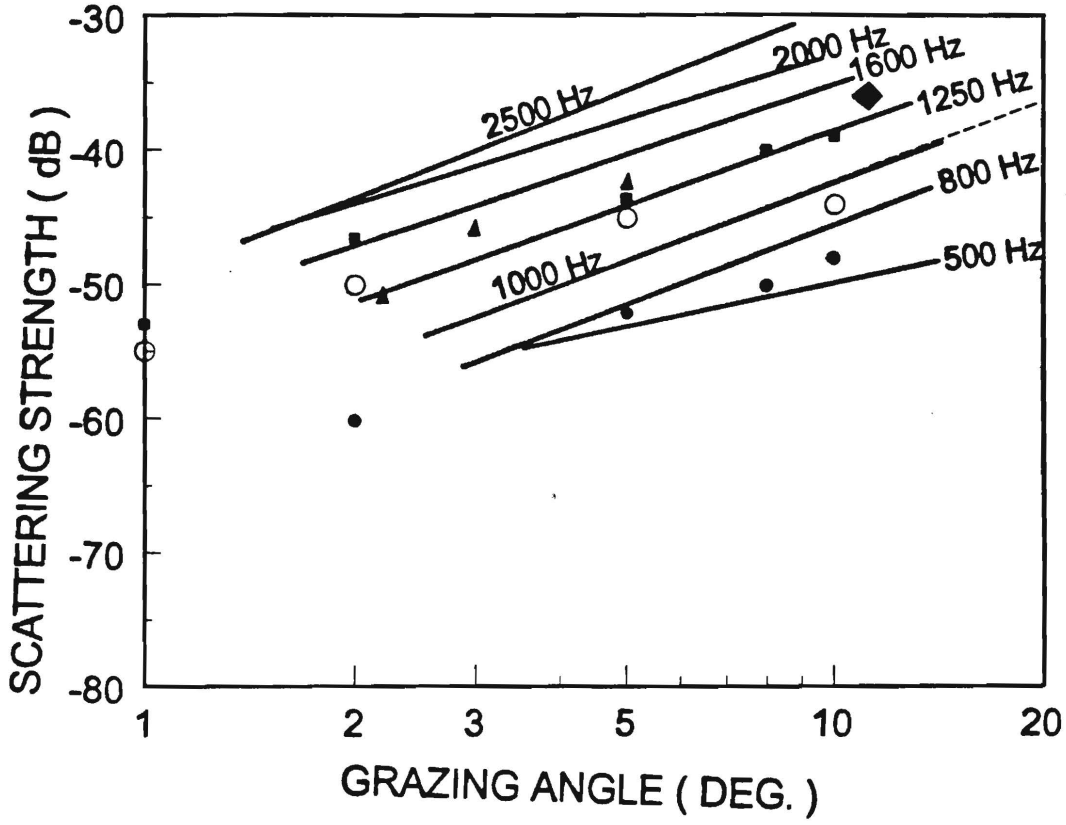

Merklinger (Sohm Abyssal Plain):

• • • 400 - 800 Hz

○ ○ ○ 800 -1600 Hz

▪ ▪ ▪ 1600 - 3200 Hz

Cole and Podeszwa (off Long Island):

◆ 3500 Hz

Urick (The Golf of Mexico):

▲ ▲ ▲ 1600 - 3200 Hz

MacKenzie

------ 530, 1030 Hz

Fig. 37